PROPERTIES OF ELECTRON CYCLOTRON RESONANCE PLASMA SOURCES

By

Aseem Kumar Srivastava

A DISSERTATION

VOLUME I

Submitted to

Michigan State University

in partial fulfillment of the requirements

for the degree of

DOCTOR OF PHILOSOPHY

Department of Electrical Engineering

1995

ABSTRACT

PROPERTIES OF ELECTRON CYCLOTRON RESONANCE PLASMA SOURCES

By

Aseem Kumar Srivastava

Over the past few decades, microwave electron cyclotron resonance (ECR) plasma/ion sources have found use in various divisions of physics and electrical engineering. The design and operating conditions of an ECR ion source is heavily dependent on its eventual application. Experiments in nuclear and atomic physics for example, rely on ECR ion sources (ECRIS) operating at extremely low pressures (about 10^{-7} Torr), and generating multiply charged ions. High energy ion beams are extracted from these ECRIS for injection into particle accelerators.

The emphasis for engineering plasma sources on the other hand, is on the generation of low energy, low charge state ions and reactive radical species. These plasma/free radical sources, operate at relatively high pressures (about 1 mTorr) and are used for substrate processing, like plasma assisted chemical vapor deposition, plasma assisted anisotropic etching, high T_c superconducting film deposition, etc. Such processes require low energy ions since the substrate could be damaged by energetic ion bombardment. ECRIS therefore, must be designed to produce the required plasma species in a wide range of parameters.

This dissertation evaluates several different ECR ion/plasma sources. The MPDR 610 - a commercially available compact, coaxial plasma/free radical

source is comprehensively characterized in terms of the plasma output (ion density, electron and ion energies, etc.) as the input variables (like microwave power, frequency of excitation, discharge pressure, gas type, etc.) are changed. The ion source generates high ion densities (10^{11} cm^{-3}) at sub-mTorr pressures, with low input power levels (less than 200 W).

The design, development and characterization of a 610 like source - the 610-*a* is then described. This source was useful in studying the electric field patterns inside the cavity structure of the MPDR 610. The normal electric field strength at the cavity wall of the 610 are about 30 to 40 kV/m. The existence of TEM standing waves in the coaxial section of the cavity is confirmed.

Another small source - the MPDR 5 is also characterized in this dissertation. While different from the 610, this source too is ECR based operating at 2.45 GHz with permanent magnets, and a tunable resonant cavity structure that sets up TE_{111} field pattern to couple power into the plasma.

The high energy sector of ECRIS is studied using the 6.4 GHz Superconducting ECR ion source (SCECR) at the National Superconducting Cyclotron Laboratory. Several mutual experiments between the Electrical Engineering and the Cyclotron ECR research groups had been identified, and the results are discussed in Volume Two of this dissertation. The performance of the SCECR at 2.45 GHz mimics other high frequency sources, like the 6.4 GHz RTECR. This unique modification of the SCECR has been the basis of an ongoing patent procedure at Michigan State University.

Copyright by
ASEEM KUMAR SRIVASTAVA
1995

।श्री।

For my parents,

Mrs. H. K. Srivastava and Dr. P. B. L. Srivastava,

without whose unceasing guidance and extreme sacrifices

this dissertation could never have been written.

Modern School in New Delhi, to the dozens of professors at Michigan State University who helped lay the foundation of my professional career. In that capacity, I also acknowledge Dr. J. Hopwood, Dr. M. Dahimene and Mr. D. Cole for their active help and support with my experiments when I needed it most.

Life extends of course, beyond the classrooms and laboratories, where society and experience don the garb of tutor and teacher. And in these extra-curricular moments, our friends influence us in uncountable ways. I have been blessed with wonderful friends like Flight Lieutenant Alok Sharma - my best friend in India, and the best pilot that ever flew a Mirage 2000. Mr. Sanjay Vazirani, now wasting his time away at a cushy job in California, has always been there to help and advice, even when the latter was not solicited. Dr. G. King - the best of friends, and colleagues. My good friend Mr. K. Medina - one of the most gracious people I know, and the best host in Chicago. Mr. J. Richards - my first friend in East Lansing has been through it all for the last nine years. And my friends Ms. N. Chaturvedi and Mr. M. Perrin whom I got to know well. Finally, my tennis partners Mr. J. Brocato, Mr. K. Weispfennig and Mr. M. Lorei - the past few years have been better with you around to beat up on the courts!

Ms. Mridvika - words alone cannot describe my friendship with you.

In closing once again, I acknowledge my family. My father - the first Ph.D. of the extended family, whose stellar example has inspired me to attain this goal, and others. My mother - the kindest and nicest person I know, who has profoundly influenced my way. My sister, Dr. Bhavna Srivastava - hope you know how good a sister you are, and the best doctor. And Amit - my brother, how well we connect. Your idealism is enriching, enlightening and a source of inspiration for us all.

ACKNOWLEDGEMENTS

The opportunity of working on cutting edge research rarely comes by ones way. It was therefore an auspicious day when Professor Jes Asmussen offered me a position to work with him. My deepest appreciations go to him for all the time, energy and effort that he has spent with me in the laboratory, in his offices, at the various conferences, and at his house. I have learned a lot from him, not just about our work, but through hours of discussions that covered a spectrum of political, historical and philosophical ideologies. My appreciations also go to Dr. Timothy A. Antaya, formerly of the National Superconducting Cyclotron Laboratory for providing me with the opportunity of working with him and the ECR group at the cyclotron. His efforts towards my continued education, in Plasma physics and other extra-curricular subjects, are very much appreciated. Thanks must also go to Dr. Donnie K. Reinhard and to Dr. Timothy A. Grotjohn, both of the Department of Electrical Engineering for providing valuable input during the course of the research and also during the writing of this dissertation. All have been a rich influence as my doctoral committee.

The attainment of knowledge goes well beyond a set of experiments, or a series of lectures and examinations. In my tradition, the teacher is esteemed beyond anyone else in the entire universe (...GUROOR SAAKSHAAT PARAM BRAHMA - Sanskrit for "...the teacher is Brahma himself..."). And so I salute all my teachers from the days of Saint Joseph's Academy in Dehra Dun, The

TABLE OF CONTENTS

Page No.

List of Tables xiii

List of Figures xiv

Chapter 1
Prelude to a Dissertation

1.1 Introduction 1
1.2 ECR Plasma Sources- an Introduction to Power Transfer 5
  1.2.1 "Pure" ECR 6
  1.2.2 Power transfer through Mechanisms Other than ECR 10
1.3 Microwave ECR Ion Sources - a Black Box Model 13
1.4 Organization and Motivation of this Research Effort 16

Chapter 2
Compact Plasma Sources - a Brief Review

2.1 Introduction 22
2.2 The Review Process 23
  2.2.1 The Kyoto University Microwave ECR Ion Beam Source 28
  2.2.2 The Hitachi non-ECR Microwave Ion Source 36
  2.2.3 Compact ECR Source of Ions and Radicals from Russia 39
  2.2.4 The Japanese ECR Radical Gun 43
  2.2.5 The Compact ECR Ion Source from RIKEN, Japan 47
  2.2.6 The N.C. State/ASTeX Inc. Compact ECR plasma Source 50
  2.2.7 The N.T.T. LSI Laboratories Compact ECR Ion Source 54
  2.2.8 The Oxford Applied Research Atom/Radical Beam Source 63
  2.2.9 A 2.45 GHz. Compact ECR Ion Source from France 66

2.2.10 Microscience, Inc. Ion Beam Source ---------- 70
2.3 Discussion - Ion/Ion Beam/Plasma Sources ---------- 76
2.4 Discussion - Figures of Merit ---------- 82
2.5 Concluding Remarks ---------- 85

Chapter 3
Characterization Principles

3.1 Introduction ---------- 88
3.2 Theory of Langmuir Probes ---------- 90
3.2.1 Assumptions of a Simplified Probe Theory ---------- 92
3.2.2 Single Langmuir Probes ---------- 94
3.2.3 Double Langmuir Probes ---------- 102
3.2.4 Limitations of Probe Analysis ---------- 108
3.2.5 Data Acquisition using Langmuir Probes ---------- 110
3.3 Multi-Grid Ion Energy Analyzer ---------- 121
3.3.1 Theory of the Ion Energy Analyzer ---------- 122
3.3.2 Design of the Ion Energy Analyzer ---------- 124
3.3.3 Limitations of the Ion Energy Analyzer ---------- 126
3.3.4 Data Acquisition using the Ion Energy Analyzer ---------- 129
3.4 Energy Distributions - Proposal for a New Method ---------- 134
3.5 Micro-coaxial Probes ---------- 136
3.5.1 Theory and Design of the Micro-coaxial Probes ---------- 137
3.5.2 Sources of Error with the Micro-coaxial Probes ---------- 141
3.6 Ion Beam Characterization ---------- 142
3.6.1 Charge State Distribution of the Ion Beam ---------- 143
3.6.2 Emittance of the Ion Beam ---------- 144
3.6.3 Emittance Measurement Techniques ---------- 148
3.7 Concluding Remarks ---------- 152

Chapter 4
Evaluation: The MPDR 610 at 2.45 GHz

4.1 Introduction ---------- 154
4.2 Description of the Plasma Source - the MPDR 610 ---------- 156
4.3 Description of the Vacuum System - the Yorktown T ---------- 163
4.4 Description of the Microwave Apparatus ---------- 170
4.5 Discharge Ignition in the 610 ---------- 171
4.6 Operational Performance of the 610 - ARGON ---------- 176
4.6.1 Argon Density Analysis ---------- 177
4.6.2 Argon Electron and Ion Energy Analysis ---------- 191
4.6.3 Comparison of Measured Data with Theoretical Predictions ---------- 199
4.6.4 Discussion of Theoretical and Measured Data ---------- 205
4.7 Operational Performance of the 610 - NITROGEN ---------- 207
4.7.1 Nitrogen Electron Energy Analysis ---------- 208

4.7.2 Nitrogen Ion Energy Analysis ---------- 212
4.7.3 A Summary of the Anomalies of a Nitrogen Discharge ---------- 222
4.8 Operational Performance of the 610 - HELIUM ---------- 223
4.9 Concluding Remarks ---------- 225

Chapter 5
Evaluation: The MPDR 610 at 915 MHz versus 2.45 Ghz

5.1 Introduction ---------- 229
5.2 Experimental Description. ---------- 233
5.3 Operational Performance: Temperature and Density Comparisons ---------- 235
5.4 Operational Performance: Ion Energy Comparisons ---------- 249
5.5 Concluding Remarks ---------- 257
Errata

Chapter 6
Evaluation: 610-a and the Electric Fields of the MPDR 610

6.1 Introduction ---------- 262
6.2 Description of Experimental Configuration ---------- 265
6.2.1 Description of the 610-a ---------- 266
6.2.2 Description of the Micro-coaxial Probes ---------- 279
6.3 Operational Performance - Plasma Loaded Measurements ---------- 281
6.4 Operational Performance - Empty Cavity Measurements ---------- 290
6.5 Operational Performance - Wall Losses, Plasma Loaded Q and Coupling Efficiency Estimates ---------- 296
6.6 Summary of Results ---------- 301
6.7 Concluding Remarks ---------- 305
Errata

Chapter 7
Evaluation: The MPDR 5 - a Multipolar ECR Plasma Source

7.1 Introduction ---------- 307
7.2 Description of the Source - the MPDR 5 ---------- 309
7.2.1 Source Design ---------- 310
7.2.2 Microwave Cavity Design Considerations ---------- 315
7.3 Operational Performance of the MPDR 5 ---------- 317
7.3.1 Previous Characterization of the MPDR 5 - a Synopsis ---------- 317
7.3.2 Further Characterization of the MPDR 5 ---------- 327
7.4 Concluding Remarks ---------- 334

Chapter 8
Application: The 610 as an Injector to the SCECR

8.1 Introduction 337
8.2 Multiply Charged ECRIS - a Brief Introduction 340
8.3 Multiply Charged ECRIS - a Black Box Model 345
8.4 The Superconducting ECR Ion Source (SCECR) 349
8.5 Experimental Hardware Description 353
8.6 Operation of the Hybrid Source 362
8.7 Operational Performance - 610 on, SCECR off 364
8.8 Operational Performance - 610 on, SCECR on 372
8.9 Summary of Results 380
8.10 Concluding Remarks 382

Chapter 9
Evaluation: Beam Extraction from the MPDR 610

9.1 Introduction 383
9.2 Ion beams - a Brief Introduction 385
    9.2.1 Space Charge Effects 388
9.3 Beam Extraction from the MPDR 610 - Initial Trials 389
9.4 Further Beam Development - the MPDR 610 on the Beam Line of the SCECR 392
9.5 Operational Performance of the Two Electrode Extraction Apparatus on the MPDR 610 396
    9.5.1 Emittance Measurements for the Two Electrode System 400
    9.5.2 Beam Current Measurements for the Two Electrode System 403
    9.5.3 Photographic Confirmation of the "Meniscus Effect" 406
    9.5.4 Discussion of the Meniscus Effect 415
9.6 Further Beam Development - the Pierce Type "Accel-Decel" Extraction System for the MPDR 610 419
    9.6.1 The Test Stand 420
    9.6.2 The New Extraction System 423
9.7 Operational Performance of the Improved Three Electrode Extraction System 432
9.8 Concluding Remarks 436

Chapter 10
Evaluation: The 2.45 GHz Excitation of the SCECR

10.1 Introduction 442
10.2 Theoretical Background of ECRIS Design 444

10.2.1 The Frequency Squared Scaling Law 445
10.2.2 The SCECR, and its "High-B" Mode of Operation 448
10.3 The 2.45 GHz Operation of the SCECR 452
10.3.1 Experimental Hardware Description 453
10.4 Operational Performance of the SCECR at 2.45 GHz 459
10.4.1 Operational Performance - OXYGEN 462
10.4.2 Operational Performance - ARGON 468
10.5 Discussion of Results 472
10.5.1 Problems with Conventional ECRIS for Multiply Charged Ions 477
10.5.2 Benefits of this "New Source" 478
10.6 Concluding remarks 481

Chapter 11
Epilogue to a dissertation

11.1 Introduction 485
11.2 Review of the Sub-studies 486
11.3 Proposals for Future Research 501

APPENDIX

References 506

LIST OF TABLES

Page No.

Chapter 2

Table 1: A comparison of compact ion/plasma/ion beam sources 77

Chapter 4

Table 1: Comparison of theory and measured data 206

Chapter 8

Table 1: Particle currents of oxygen charge states in the hybrid source 375

Chapter 9

Table 1: Variation of drain current versus applied bias on the MPDR 610 404

Chapter 10

Table 1: High-B magnet current scaling for the 2.45 GHz operation of the SCECR 460

Table 2: Tuning effects on oxygen production from the 2.45 GHz SCECR 465

Table 3: Tuning effects on argon production from the 2.45 GHz SCECR 470

LIST OF FIGURES

Page No.

Chapter 2

Fig. 2.1 Kyoto University Microwave ECR Ion Beam Source 29

Fig. 2.2 Hitachi Non ECR Microwave Ion Source 37

Fig. 2.3 Compact ECR Source of Ions/Radicals from Russia 40

Fig. 2.4 Japanese Radical Gun 44

Fig. 2.5 Compact Ion Source from RIKEN 48

Fig. 2.6 N.C. State/ASTeX Compact ECR Plasma Source 51

Fig. 2.7 NTT LSI Laboratories Compact ECR Ion Source 55

Fig. 2.8 NTT LSI Laboratories Compact ECR Ion Source with Permanent Magnets 56

Fig. 2.9 Oxford Applied Research Atom/Radical Beam Source 64

Fig. 2.10 Compact ECR Ion Beam Source from France 67

Fig. 2.11 Microscience, Inc. Compact ECR Ion Beam Source 71

Chapter 3

Fig. 3.1 An I-V characteristics of a Single Langmuir Probe 96

Fig. 3.2 The Single Langmuir Probe circuit 99

Fig. 3.3 A typical EEDF of the MPDR 5 101

Fig. 3.4(a) A DC isolated Double Langmuir Probe circuit 103

Fig. 3.4(b) Recessed Langmuir Probe 103

Fig. 3.5(a) Potential drops across the Double Langmuir Probes 105

Fig. 3.5(b) An I-V characteristics of a Double Langmuir Probe 105

Fig. 3.6 Double Langmuir Probe data acquisition circuitry 113

Fig. 3.7 A fully automated GPIB controlled single Langmuir probe circuit 117

Fig 3.8 The ion energy analyzer with three grids 127

Fig. 3.9(a) The potential drops for a three grid IEA 128

Fig. 3.9(b) The potential drops for the IEA with a fourth grid 128

Fig. 3.10 Ion energy analyzer measurement circuitry 131

Fig. 3.11 Fully automated GPIB controlled IEDF measurement technique 132

Fig. 3.12 Typical IEDFs for the MPDR 5 133

Fig. 3.13 Design of the two micro-coaxial probes 139

Fig. 3.14 Charge state distribution measurement 145

Fig. 3.15 A typical charge state distribution of the SCECR at the NSCL 146

Fig. 3.16 The dynamic emittance measurement technique 150

Fig. 3.17 Typical emittance diagram of the SCECR+610 151

Chapter 4

Fig. 4.1 MPDR 610 158

Fig. 4.2(a) The magnet design of the MPDR 610 (original) 160

Fig. 4.2(b) Other magnet and quartz designs that were also tested 160

Fig. 4.3 Description of the "Yorktown T" ....

Fig. 4.4 Top view of the vacuum chamber 165

Fig. 4.5(a) Gas flow system for the Yorktown T vacuum station 168

Fig. 4.5(b) Microwave apparatus for the ion source characterization 168

Fig. 4.6 Sliding short and center conductor assembly (argon plasma) 174

Fig. 4.7 Transient analysis of an argon discharge in the 610 178

Fig. 4.8 Argon ion density variation with pressure 179

Fig. 4.9 Ion density dependence for argon and oxygen pressure 182

Fig. 4.10 Electron temperature variation with pressure 184

Fig. 4.11 Ion saturation current variation with pressure 187

Fig. 4.12 Ion saturation current variation with radial position 188

Fig. 4.13 Ion saturation current variation with position downstream 189

Fig. 4.14 Ion saturation current variation with position downstream for four different discharge gases 190

Fig. 4.15 A typical EEDF for an argon discharge 192

Fig. 4.16 Argon plasma potential variation with pressure 194

Fig. 4.17 Argon IEDF variation with power 196

Fig. 4.18 Argon IEDF variation with pressure 198

Fig. 4.19 A typical EEDF for a nitrogen discharge 209

Fig. 4.20 Nitrogen electron energy and plasma potential variation with pressure 210

Fig. 4.21 Nitrogen electron energy and plasma potential variation with input power 211

Fig. 4.22 Nitrogen electron energy and plasma potential variation with position downstream 213

Fig. 4.23 Nitrogen ion energy distribution variation with input power 214

Fig. 4.24 Nitrogen average ion energy variation with input power 215

Fig. 4.25 Nitrogen ion energy distribution variation with pressure 217

Fig. 4.26 Nitrogen average ion energy variation with pressure 218

Fig. 4.27 Nitrogen ion energy distribution variation with downstream distance 219

Fig. 4.28 Nitrogen average ion energy variation with downstream distance 221

Fig. 4.29 Helium ion density variation with input power 224

Fig. 4.30 Helium ion density variation with pressure 226

Chapter 5

Fig. 5.1 Electron temperature variation for the two frequencies 236

Fig. 5.2 Ion density variation with pressure for the two frequencies 240

Fig. 5.3 Saturation current density variation with pressure for the two frequencies 241

Fig. 5.4 Ion density and saturation current density variation with input power for the two frequencies 243

Fig. 5.5 Ion density and saturation current density variation with distance downstream for the two frequencies 244

Fig. 5.6 Ion density and current density variation with radial position at the two frequencies 3 cm downstream 245

Fig. 5.7 Ion density and current density variation with radial position at the two frequencies 5 cm downstream 247

Fig. 5.8 Ion energy distribution function variation with input power at 915 MHz 250

Fig. 5.9 Ion energy distribution function variation with input power at 2.45 GHz 251

Fig. 5.10 Average ion energy variation with input power for the two frequencies 252

Fig. 5.11 Ion energy distribution function variation with discharge pressure at 2.45 GHz 254

Fig. 5.12 Ion energy distribution function variation with discharge pressure at 915 MHz 255

Fig. 5.13 Average ion energy variation with discharge pressure for the two frequencies 256

Chapter 6

Fig 6.1 Cross section of the MPDR 610-a (not to scale) 267

Fig. 6.2 Outer wall of the 610-a 268

Fig. 6.3(a) Quartz plasma chamber 269

Fig. 6.3(b) Quartz chimney of the 610-a 270

Fig. 6.4 Base plate for the 610-a 271

Fig. 6.5 Magnets for the 610-a 273

Fig. 6.6(a) and (b) The two magnet holder sections for the 610-a 275

Fig. 6.6 (c) The assembled magnet holder for the 610-a 276

Fig. 6.7 The MPDR 610 and 610-a on the vacuum chamber 278

Fig. 6.8 Typical measured radial electric field curve versus length of the 610-a 283

Fig. 6.9 Electric field versus cavity length showing argon pressure dependence 286

Fig. 6.10 Electric field versus cavity length showing argon power dependence 288

Fig. 6.11 Electric field versus cavity length showing nitrogen pressure dependence 289

Fig. 6.12 Empty cavity measurements on the 610-a 293

Fig. 6.13 Topology of the coaxial section of the 610-a 295

Fig. 6.14 Equivalent circuit for the ECR microwave plasma source 302

Chapter 7

Fig. 7.1 The MPDR 5 311

Fig. 7.2 The MPDR 5 mounted on the vacuum chamber 312

Fig. 7.3 The octapolar magnetic field configuration for the MPDR 5 314

Fig. 7.4 Variations in plasma density with downstream distance 320

Fig. 7.5 Radial distribution of plasma density at different downstream positions 321

Fig. 7.6 Radial distribution of plasma density at different discharge conditions 322

Fig. 7.7 Typical EEDF for the MPDR 5 324

Fig. 7.8 Radial and downstream variation of plasma potential 325

Fig. 7.9 Electric field pattern measurements for the MPDR 5 329

Fig. 7.10 Vertical variation of the electric fields in the MPDR 5 330

Fig. 7.11 IEDF variation with power for the MPDR 5 331

Fig. 7.12 IEDF variation with discharge pressure 333

Chapter 8

Fig. 8.1 Schematic of a typical ECRIS for multiply charged ions 346

Fig. 8.2 Schematic of the SCECR 350

Fig. 8.3 Schematic of the SCECR+610 "Hybrid Source" 355

Fig. 8.4 Schematic of the quarter wave transformer 356

Fig. 8.5 The high voltage isolation joint on the waveguide bidirectional coupler 360

Fig. 8.6 CSD of 610 on, SCECR off 365

Fig. 8.7 Details of the CSD in Figure 8.6 367

Fig. 8.8 Emittance plot of the 610 (SCECR off) 369

Fig. 8.9 Emittance plot of the 610 (SCECR off) 370

Fig. 8.10 Ar^{1+} current versus pressure in the injection stage 371

Fig. 8.11 Current versus charge states (610 on, SCECR on) for various 610 biases with respect to the SCECR 376

Fig. 8.12 CSD, 610 on, SCECR on, +1 kV relative bias on 610 377

Fig. 8.13 CSD, 610 on, SCECR on, 0 relative bias on 610 378

Fig. 8.14 CSD, 610 on, SCECR on, - 1 kV relative bias on 610 379

Chapter 9

Fig. 9.1 Initial beam extraction from the 610 393

Fig. 9.2 PANDIRA simulations for electric fields on the 610 395

Fig. 9.3 CSD of the MPDR 610 399

Fig. 9.4 Typical emittance diagram of the 610 402

Fig. 9.5 Variation of beam current with extraction bias 405

Fig 9.6(a) through (l) Biases on the 610 - from 0 kV to 10 kV 407

Fig. 9.7 The test stand for autonomous beam characterization of the 610 421

Fig. 9.8(a) Composite of the three grid accel-decel extraction system 427

Fig. 9.8(b) and (c) Side view of the two types of plasma electrodes 428

Fig. 9.8 (d) Top view of the plasma electrode 428

FIg. 9.8(e) Side view of the acceleration electrode 429

Fig. 9.8(f) Decelerating electrode (normally grounded 430

Fig. 9.8(g) The Maycor ring that isolates the accelerating electrode from the decelerating electrode 430

Fig. 9.9(a) Plasma electrode at 6 kV, accel-decel electrodes grounded 434

Fig. 9.9(b) Plasma electrode at 3 kV, accel electrode at -3 kV, decel electrode grounded 434

Fig. 9.10 3 electrode system at 10.0 kV, 0.84 cm separation 437

Fig. 9.10(b) 2 electrode system, 10.0 kV, 0.84 cm separation 437

Chapter 10

Fig. 10.1 The modified first stage of the SCECR for 2.45 GHz operation 456

Fig. 10.2 Front view (top) and side view (bottom) of the 2.45 GHz quarter wave transformer 457

Fig. 10.3 Comparison of the "normal" magnetic field (top) and the "High-B" field (bottom) at 2.45 GHz for the SCECR 461

Fig. 10.4 The first oxygen CSD from the 2.45 GHz SCECR 464

Fig. 10.5 The final oxygen/helium CSD from the 2.45 GHz SCECR 467

Fig. 10.6 The first argon/oxygen CSD from the 2.45 GHz SCECR 469

Fig. 10.7 The final argon/oxygen CSD from the 2.45 GHz SCECR 471

Fig. 10.8 Comparison of current production (in eμA) of five ECRIS - argon 473

Fig. 10.9 Comparison of current production (in eμA) of five ECRIS - oxygen 474

Fig. 10.10 Comparison of the ORNL source at 2.45 GHz and 6.4 GHz with the SCECR at 2.45 GHz 476

Chapter 1

Prologue to a Dissertation

1.1 Introduction

1.2 ECR - an Introduction to Power Transfer

1.2.1 "Pure" ECR

1.2.2 Power Transfer Through Mechanisms Other than ECR

1.3 Microwave ECR Ion Sources - a Black Box Model

1.4 Organization and Motivation of this Research Effort

Chapter 1

Prologue to a Dissertation

1.1 Introduction

The word "plasma" is derived from the Greek language for "something molded." It was first applied by Tonks and Langmuir in 1929 to the inner region, away from the boundaries, of a glowing ionized gas produced by an electrical discharge in a tube [Bit-86, Nic-83]. The term is now used to describe any concentration of charged and neutral particles that has a zero net space charge and is internally field free, and where interactions between each charged species are governed by long range Coulomb forces [Bit-86]. For practical purposes, a plasma may in fact be treated as a conductor because of its large population of energetic charged particles (both negative and positive), with its conductivity being defined by the charge density and electron mobility.

If enough energy is imparted to a solid, its internal kinetic energy increases to the point where its binding potential is overcome, converting the solid to a liquid. The solid is then said to have undergone a phase transition. Another such transition occurs when the liquid is heated up to the level beyond

which it changes to a gas. A plasma is often called the fourth state of matter, since it is a superheated, and ionized gas [Nic-83]. This is somewhat misleading, since the phase transitions from solid to liquid, and from liquid to gas occur at a temperature known as the latent heat of that phase transition. For a given pressure the latent heat of these phase transitions is constant. However, the transition from a gas to a plasma is not a phase transition in this thermodynamic sense, because this transition occurs gradually with increasing plasma temperatures.

A plasma discharge is created when sufficient energy is imparted to the neutral discharge gas such that a significant number of the gas molecules (or atoms) lose one or more of their valence shell electrons. Hence the plasma is a mixture of a very large number of neutral gas atoms (or molecules), and individual charged, energetic, metastable and unstable species, with complex interactions occurring between them. Note that the ions generated in the discharge may be singly, or multiply ionized depending on the operating conditions of the discharge. Plasma discharges occur naturally in the universe in many shapes and sizes - the sun's corona, the earth's ionosphere and the Van Allen belts, lightning bolts, etc. Most of intergalactic space is presumed to be a (very low density) plasma where the charged species are spread out over vast volumes. It is in fact estimated that about 99% of the universe is a plasma and cold planets like the earth are rare areas where natural plasmas (like lightening bolts) exist only under severe circumstances.

While there are many artificially generated plasma discharges on earth that are used in everyday life, like fluorescent lighting, a plasma cannot be created on earth at atmospheric pressures except for electrical discharges, or

combustion. Stringent requirements of pressure (or lack thereof) and energy transfer to individual constituents of the plasma need to be satisfied before these artificial discharges can be sustained under the normal atmospheric conditions. These requirements are met through the use of complex systems that incorporate vacuum technology, theory of electromagnetic energy transport, often cryogenics and superconductivity, and many other branches of physics and engineering. Appropriately, the machine that actually generates and sustains a plasma is known as an ion source, or a plasma source. The two terms may in general be used interchangeably (except when an ion beam is extracted from the source, in which case the machine is specifically referred to as an ion, or an ion beam source).

There are many different ways through which energy may be transferred into the plasma, both artificial and natural. The ionosphere of the earth, for example, is sustained due to naturally occurring photo-ionization. A plasma on the earth's surface is generally a gas discharge that has been generated by transfer of electrical power into the gas. For weakly ionized plasma discharges (less than 5% ionization), the neutral (un-ionized) gas is the largest constituent. However, the identification of all the plasma species is a very complicated pursuit, and even the simplest plasma discharges have not yet been completely characterized (other than the exhaustive work done on fluorescent lights by companies like General Electric and GTE).

Initial research into plasma theory in the fifties and sixties was done mainly to satisfy the demands of the controlled thermonuclear fusion program and the magnetohydrodynamic (MHD) conversion of thermal power into electrical energy [Gal-83]. Also about that time, plasma discharges in outer

space and around the hulls of space vehicles were studied by NASA. In recent times, a number of spin off technologies have been spawned, mainly due to the improvements in the ability to create the required plasma species with relative ease, and also due to a better understanding of the plasma chemistry. The success of plasma processing technology for integrated circuit fabrication, plasma assisted chemical vapor deposition, and other applications utilizing some kind of plasma discharge has been amply demonstrated both in the research and industrial environments.

Due to this success, there has been a concerted effort in ion/plasma source research and development. A variety of plasma sources with innovative designs have been developed with their dimensions and characteristics being defined by the end process and application, and by the engineering talents of the designers. To do batch processing of silicon wafers for example, a low energy broad beam ion/free radical source is necessary [Kau-85, Har-89]. Initial research into such a broad beam ion source was actually conducted at NASA for space (electric) engine design. On the other hand, narrow, energetic slit shaped ion beams are extracted from specially designed sources, and these ion beams are rastered over the substrate in ion implantation machines [Ste-92, Kel-89]. Yet other applications require smaller ion sources that can adapt to pre-existing apparatus, or be able to produce the requisite plasma species in the appropriate abundance close to the substrate surface.

This dissertation documents a comprehensive study of a number of plasma and ion beam sources that were designed at the Department of Electrical Engineering (EE) at Michigan State University (MSU). Joint experiments on ion sources with the ion source research group at the National Superconducting

Cyclotron Laboratory (NSCL) at MSU are also detailed. The research detailed in the forthcoming chapters was performed at the EE and the NSCL laboratories at MSU, and encompassed the last five years. In this chapter a brief introduction into the energy transfer techniques from the impressed electric fields to the plasma discharge is presented. A simple black-box model of a generic microwave ion source is also presented, to lay a foundation for understanding concepts developed here, and in later chapters. This is followed by a chapter-wise breakdown of the rest of this dissertation, that will also explain the motivation behind the efforts of the past five years. Individual ion sources that were experimentally evaluated, and all their peripheral systems (like the vacuum stations, the microwave apparatus, etc.) will be introduced and described in detail in the appropriate chapter, along with the results of each sub-study.

1.2 ECR Plasma Sources - an Introduction to Power Transfer

There are several ways of creating an electrical discharge - the simplest of them being a glow discharge in an evacuated tube between two biased electrodes. Ion source construction of course varies in complexity with each new and unique design, the design itself predicated by the end user demands. Probably the most important aspect of ion source design is the method(s) of energy transfer to the plasma load from the impressed electromagnetic fields. One of these methods of power transfer is electron cyclotron resonance (ECR) and the ion sources employing this technique are appropriately known as ECR ion sources (ECRIS). As will be seen, ECR is a very efficient method of power transfer, and takes advantage of the natural cyclotronic resonance of electrons

(hence the name ECR) to selectively transfer power from the impressed electric fields and into the electron gas. From this heated electron gas, the energy is transferred to the other constituents of the plasma through collisions. While the theory of "pure" ECR is simple to understand and a basic ECRIS is not too complicated to design and develop, the actual picture of power transfer to the plasma is much more complex. In the following sub-sections a simplified ECR theory is presented, after which a more complete analysis of microwave power absorption in ECR plasma sources is discussed. This analysis is based on a monograph by Popov [Pop-94a].

1.2.1 "Pure" ECR

In the presence of a static magnetic field, a charged particle resonates around magnetic lines of force at a particular frequency, known as its rotation or cyclotron frequency. For an electron, this is given by $\omega_{ce} = qB/m$, where ω_{ce} is the cyclotron frequency, B is the necessary static magnetic field, and q and m are the electronic charge and mass respectively. While in this static magnetic field, if the particle is then subjected to a time harmonic AC electric field oscillating at the cyclotron frequency of the particle, and a component of the impressed electric field is perpendicular to the static magnetic field, the charged particle will rapidly absorb power from the impressed electric field. This phenomenon of electron cyclotron resonance (ECR) is used to couple energy into the electron gas that constitutes a plasma. A complete analysis of ECR heating (ECRH) is available in several references [Bit-86, Nic-83, Kel-89, Asm-89a, Eld-72, Lie-94], and only a brief introduction is now presented to aid in development

of the forthcoming chapters.

In an ECRIS, neutral discharge gas is incrementally injected into a confined structure (like a quartz, alumina or copper tube) under high vacuum conditions. A static (time constant) magnetic field of specific strength and orientation exists such that all, or part, of the confinement structure is immersed in this field. As mentioned earlier, in the presence of this static magnetic field, the charged particle follows a helical path gyrating about the magnetic field lines. Now if a time harmonic electric field with frequency equal to the cyclotron frequency of the charged particle ($\omega = \omega_{ce}$) is impressed on the confinement structure, if the appropriate magnetic field strength is present at some point, and if there exists a component of the impressed electric field that is perpendicular to this static magnetic field, the charged particle will absorb energy from this impressed electric field.

Based on several assumptions (some of which are actually inaccurate, used only to generate a closed form solution from a complex set of equations - see Reference Pop-94a), this energy absorption by the electron gas may be modelled by the following equation [Asm-89a, Pop-94a]:

$$P = Re(J \times E) = \frac{eN_e E_r^2}{4m} \left\{ \frac{\nu_e^2}{\nu_e^2 + \left(\omega - \omega_{ce}\right)^2} + \frac{\nu_e^2}{\nu_e^2 + \left(\omega + \omega_{ce}\right)^2} \right\} \qquad (1.1)$$

Here E_r is the component of the electric field that is perpendicular to the static magnetic field and ν_e is the electron-neutral elastic collision frequency. As can be seen, the first term in the right hand part of the equation (curly brackets)

denotes a resonance between the impressed microwave and the electron cyclotron frequencies where the electron rotates around the static magnetic field line in the same direction as the vector of the microwave electric field. Such an electromagnetic wave is called the right hand circularly polarized (RHCP) wave. The second term in the curly brackets denotes an electric field whose vector rotates in a direction opposite to that of the electron rotation in the magnetic field. This is known as the left hand circularly polarized (LHCP) wave. Note that any electric field may be represented as a linear superposition of the RHCP and the LHCP wave.

The energy absorption by the gyrating electron results in an increasing radius of the electron's helical path about the magnetic field line (see Figure 3, Reference Asm-89a). The regions inside the plasma confinement structure that have the required magnetic field strength and the appropriate electric field orientation for ECRH are known as the "ECR zones." For example, the required B field strength for the operating microwave frequency of 2.45 GHz, is 875 gauss, and ECRH of the electron gas would occur in regions of the plasma confinement structure where B = 875 gauss, and the electric field has a component perpendicular to this B field. The energetic, or "hot" electrons then transfer this energy to valence electrons of neutral atoms (or molecules) of the working gas through inelastic collisions.

Note that this process involves using the hot electron's kinetic energy to increase the potential energy of the bound electron. Ionization occurs when sufficient energy is transferred from the hot electrons (usually by single, sometimes by multiple collisions) to the valence electron of the discharge gas, such that the valence electron is stripped away from the atom (or molecule). An

ion-electron pair is then formed. Once the loss mechanisms (diffusion and recombination) are balanced by ionization in a steady state, a discharge can be sustained. ECRH is, therefore, a low pressure (m-Torr or lower) phenomenon that relies on collision frequencies that are high enough to sustain the discharge, yet sufficiently low such that the electron gas may gain substantial energy from the high frequency impressed electric field before transferring this energy to the other constituents of the discharge. Typically the electric fields are launched with frequencies in the microwave range - several hundred MHz to about 100 GHz, although some (non-ECR) plasma/free radical sources (notably the inductively coupled devices) operate at the lower radio frequency (rf) of 13.56 MHz.

It has been shown by Popov [Pop-94a] and others (see Figure 13.5, page 418, Reference Lie-94) that real ECR heating occurs only through absorption of the energy from RHCP waves by the discharge. This may happen, however, for a very limited set of circumstances - at microwave breakdown and for very low power absorption levels that generates an over dense (ion density greater than the critical density for that excitation frequency) magnetoactive plasma. (More discussions of critical density, and over dense discharges will be taken up later.) For most ion sources that are used in industrial applications, the external plasma conditions (for example, input power levels, gas flow rates, discharge pressure etc.) vary significantly from this, and mechanisms other than pure ECR for electron momentum transfer are needed to explain the power transfer that occurs in these discharges. Some of these alternate energy transfer techniques are now presented.

1.2.2 Power Transfer Through Mechanisms Other than ECR

Many ion sources currently in use employ electron cyclotron resonance for heating the electron gas which then indirectly heats and ionizes the neutral gas through inelastic collisions. This, of course is not the only method of power transfer to sustain a discharge. A similar phenomenon for ion cyclotron resonance (ICR) also exists that directly couples energy to the ion gas. ICR however, is not a practical method of power transfer for most ion sources. Since the magnetic field requirement scales linearly with the mass of resonating particle, the static magnetic field strength for ICR heating is approximately 1840 times that of the electrons for a given excitation frequency. The only machines that may utilize ICRH in a practical manner are the large toroidal tokamaks used in controlled thermonuclear fusion that have plasma chambers up to two meters high.

There is another, less known method of energy transfer for the generation of a stable discharge - the Penning effect [Ste-92] based on multiple collisions of a discharge species with the other constituents of the plasma. In this case, an energetic atom (or molecule) collides with an atom that is in a metastable state due to energy absorption from prior electron-atom (or molecule) collisions. If the ionization potential of the atom in the metastable state is only slightly higher than its metastable state, even a small amount of energy transfer from the second collision to the metastable atom leads to ionizing the latter. Rare gases, like neon can utilize this effect to sustain a discharge. For instance, neon has a metastable state at 16.5 eV with a long lifetime, while its ionization energy is 21.6 eV. If an atom-metastable collision transfers about 5 eV of energy from the

atom to the metastable, the latter will ionize. Since atoms have large collision cross sections, energy can more easily be transferred through elastic, or inelastic collisions between atoms and/or ions. Hence, for specific rare earth gases that can take advantage of this phenomenon, this seems to be an efficient method of energy transfer.

If the excitation frequency of the impressed electric field is different from the cyclotron frequencies, power transfer can still occur from the electric field to the plasma if the discharge pressure is high enough. This is known as Joule, or collisional, or Ohmic heating. The effective collision frequency at high pressures goes up, and this allows for significant energy transfer to the discharge constituents through these collisions. Many high pressure ion sources (100 mTorr to several tens of Torrs) in the EE Plasma Sciences Laboratories of MSU involved with chemical vapor deposition of diamond and diamond-like thin films employ the principle of Joule heating to create and sustain a plasma.

In his monograph, Popov [Pop-94a] presents an excellent discussion of at least nine mechanisms of microwave absorption in ECR plasma sources, other than "pure" ECRH. These are: (1) Doppler shifted ECR, (2) Whistler waves absorption in overdense magnetoactive plasmas, (3) LHCP wave absorption, (4) Upper hybrid resonance (UHR), (5) Higher harmonic resonance, specifically second (SHR) and third harmonics, (6) Plasma geometrical resonances, (7) Stochastic heating, (8) Non-linear power absorption at high microwave electric fields, and (9) Non-resonant collisional absorption of LHCP waves. Appropriate references in his monograph actively supplement each subtopic.

It is not the purpose here to detail every such method of microwave power transfer, but the point being made is that in general, while designing ECRIS,

only conditions satisfying ECR heating (for example, whether ECR zones exist somewhere in the plasma generation region, or whether the impressed electric field has a component that is perpendicular to the static magnetic field in these ECR zones) are accounted for. However, the actual mechanism of power transfer is very much more complex, and this transfer can occur under conditions that vary significantly from ECR specifications. For example, a high level of microwave power absorption of transverse electromagnetic waves at 2.45 GHz can occur at magnetic field strengths much less than 875 Gauss, as well as for field strengths much greater than 875 Gauss provided the plasma density is not lower than the critical density at that frequency of operation. This power absorption, probably due to Landau damping of whistler waves, was experimentally verified by Musil et al. [Mus-75]. Another method of energy transfer - second harmonic resonance (SHR) has in fact been considered in the near past as a prime candidate for powering the next generation of microwave plasma sources.

Several such deviations from the pure ECRH of microwave plasmas are listed by Popov, leading to an inescapable conclusion: while the design of microwave ECRIS is usually based on satisfying electron cyclotron resonance conditions alone, power absorption into the plasma load is significantly diverse and can occur under conditions atypical for ECR. A total reliance on Eqn. (1.1) is therefore inappropriate. This equation was derived using several assumptions (like the cold plasma approximation, homogeneous plasma density and homogeneous magnetic field, linear electrodynamics [Pop-94a], etc.) which simplify the complex equations and produce a closed form solution. However, over-simplification of the problem may also result in loss of information.

Perhaps that is why ECRIS are generally very robust and characteristically forgiving - even poorly designed ECRIS manage to perform well.

All four plasma sources that are experimentally evaluated in this dissertation are microwave ECRIS. The MPDR 610, the 610-a, and the MPDR 5 were designed at the EE Plasma Sciences Laboratory at MSU, while the Superconducting ECR Ion Source (SCECR) was designed, and is under continuous operation at the NSCL. While all the sources are indeed ECRIS, the differences between the design, the external operating conditions (like frequency of operation, input power levels, discharge pressure, etc.) and the final source output (like ion density, ion beam energy, etc.) will become apparent as this dissertation progresses. For example, the frequency of excitation ranges from 915 MHz to 6.4 GHz for the various ion sources, while the operating discharge pressure ranges from 10^{-7} Torr for the SCECR, to 10^{-4} Torr more typically found in the EE sources.

To enhance the importance of ECR effects, and also to serve as a basis for the review of several ECR (and some non-ECR) plasma sources in the next chapter, a generic model of an electron cyclotron resonance ion source is now presented. It will be seen that this model accounts for satisfying pure ECR conditions only.

1.3 Microwave ECR Ion Sources - a Black Box Model

In practice, an ECR ion source consists of a discharge confinement structure that may be made of quartz, alumina, boron-nitride, stainless steel, or copper. This quartz tube, or copper vessel is surrounded by permanent magnets,

or electromagnetic coils (which might be superconducting) that generate the static magnetic field topology for ECR, and also to control (or restrict) the flow of charged species within, and outside the source. The discharge vessel is sealed to a vacuum system which ensures sufficiently low base pressures (usually of the order of 10^{-8} Torr). These low pressures are created with one or a combination of several types of pumps - diffusion, cryogenic, turbo-molecular, titanium sublimation and the regular mechanical backing pump. Discharge gas (or a mixture of several gases) is fed into the plasma vessel through a controlled leak. Electromagnetic energy at the appropriate AC frequency is impressed on the neutral gas, generally through an applicator that ensures maximum possible power transfer to the gas.

Somewhere inside the discharge confinement structure, the static magnetic field is designed such that it has the correct orientation and strength (with respect to the impressed electric field). ECR zones are thereby formed where the power absorbed by the electron gas is enhanced. Subsequent ionizing collisions between the hot electrons and atoms (or molecules) create and sustain the discharge. In general, some sort of cooling (either air, or water) is necessary for the ion source due to the heat generated from the wall losses of the electromagnetic fields, and also from the energy dissipated by collisions and recombinations on the plasma containment vessel walls. Once the discharge is in a steady state, plasma constituents can diffuse out freely from the generation region and into the processing chamber, or a specific subspecies from the quasi-neutral plasma may be selectively extracted using an appropriate extraction apparatus.

ECR technology has several outstanding advantages over previously

established ion source technologies (like Penning gauges that typically have cathodes, or filaments that generate the hot electrons). Filaments (or cathodes) that are present in the discharge region are bombarded by high energy ions and are liable to degrade over time. This leads to short lifetimes, and also contamination from the sputtered material off the electrodes. ECR sources do not require any electrodes, or filaments to ignite or sustain the discharge. Although there are some ion sources reviewed in the next chapter that do have antennae within the discharge zone, ECR ion sources are typically electrodeless in nature. Hence there is no question of contamination from an electrode, or a filament (although wall collisions might lead to sputtering of the wall material). Also, in a well designed source, the only material that needs continuous replenishment is the working gas - all other components should be relatively unharmed after extended use. There are sources that can operate up to 200 hours without problems - ECR ion sources have long lifetimes, which ultimately leads to lower operational costs.

Another advantage of ECR technology is that the plasma electrons are preferentially heated by the impressed electric field. This contains the thermal ion energy to extremely low levels. Low thermal energy of ions is extremely good for several reasons - ion bombardment of substrates does not cause prohibitive damage if the ion energies are low. Hence the performance of ECR plasma sources is dominated by low plasma temperature chemistry. Also, for ion beam sources, one of the factors that leads to beam divergence is high thermal energy of the ions, which generates radially directed space charge fields and increases the repulsive force between the ions constituting the beam, ultimately causing prohibitive beam divergence.

The purpose of an ion source is therefore two fold. First, the discharge confinement structure isolates the (low pressure) plasma generation region from external atmospheric (high pressure) contamination and from the downstream processing region, while delivering the plasma constituents at a steady rate. And second, energy from the power supply (at an appropriate AC frequency), is normally coupled into the plasma through a specially designed applicator that enables maximum power transfer. The ion sources designed in the EE labs, for example, have a resonant microwave cavity structure that acts as an applicator, in which power resonates before being absorbed by the plasma. More details about these ion source and the plasma applicators are presented in the forthcoming chapters as the ion sources experimentally evaluated for this study are introduced and described.

1.4 Organization and Motivation of this Research Effort

No study is complete without an attempt at relating the obtained results to previous and current developments of the technology. This is best accomplished through a survey of the existing literature. Chapter Two of this dissertation is a review of several compact microwave and radio frequency (rf) ion sources. Practically, it is very difficult to compare and contrast each ion source reviewed in Chapter Two due to the many different figures of merit that researchers employ to characterize their ion sources. This also makes it difficult to compare the experimentally measured results of the various ion sources studied in this dissertation, with the results of the reviewed source of Chapter Two. However, where possible, this comparison is made. It is expected that a

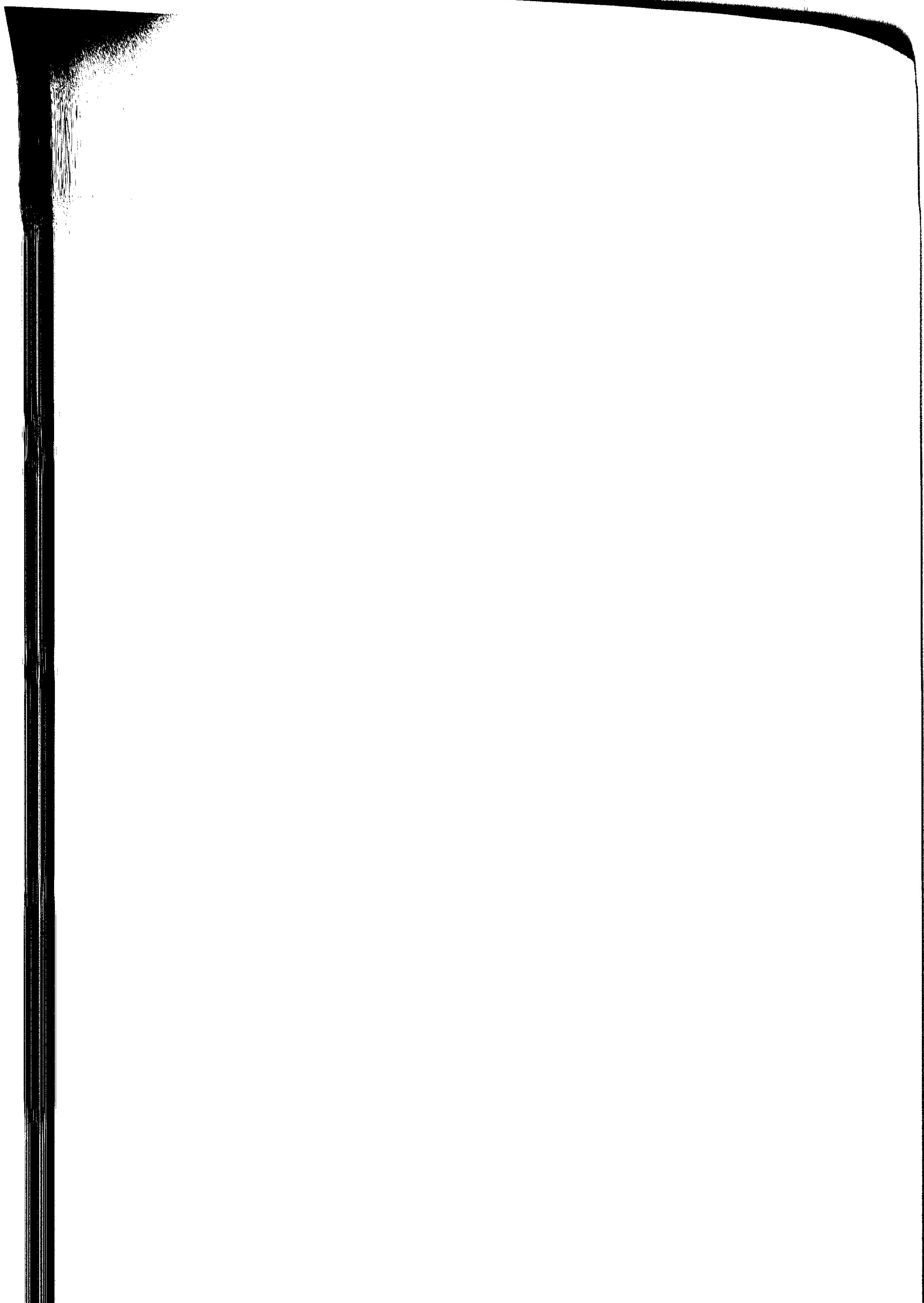

scrutiny of the current technology performed in Chapter Two will also help in understanding the experimental results of the sources that are experimentally evaluated in this dissertation.

Chapter Three explains the various characterization principles and experimental techniques that were used to evaluate the ion sources of this study. This chapter is not meant to provide exhaustive details of each characterization technique, but instead to lay a foundation for a basic understanding of each technique, along with its shortcomings, and exact data acquisition methodology. Several pertinent references for each technique are provided if further study is required. For measurement of some parameters (like the ion energy distribution function), new - and possibly next generation methods of data acquisition are also described.

Chapter Four begins the experimental section of this dissertation. The microwave plasma disc reactor 610 (MPDR 610™) is introduced and described. (Note that during the course of this dissertation, the terms "MPDR 610" and "610" may be used interchangeably, and neither is to be confused with the "610-*a*," which is a modification of the 610, and will be introduced in Chapter Six.) While the characterization of the 610 was conducted on several vacuum systems, the "Yorktown-T" that was used for a majority of the experiments is described in this chapter. Other vacuum systems that were used will be described in the appropriate chapters. Characterization results of operating the MPDR 610 at 2.45 GHz microwave frequency are presented. These results include measurements of ion density, electron temperature, plasma potential, electron and ion energy distribution functions, as these output parameters vary with input pressure, power levels and position downstream from the 610. The

results discussed in this chapter were presented at several conferences, including the International Conference on Ion Sources (ICIS-91) in Bensheim, Germany and subsequently published in the proceedings.

The 610 is a unique ion source that can operate at any of a large band of microwave frequencies due to its coaxial structure (refer to Chapter Four for further explanations). The results of exciting the 610 at 915 MHz are presented in Chapter Five. Similar experiments as those done for Chapter Four were also conducted at the operating frequency of 915 MHz, and the results (similarities and differences) of the two frequencies of excitation are compared in Chapter Five. These results were presented at the American Vacuum Society symposium (AVS-92) in Chicago, USA and subsequently published in the proceedings.

Further characterization of the MPDR 610 necessitated the development of the 610-*a*. As will be inferred from Chapters Four and Five, the MPDR 610 was designed to be inserted deep into vacuum systems to generate a plasma close to the substrate surface, and away from the vacuum seal. The 610-*a* does not extend inside the vacuum chamber as does the MPDR 610. Instead, in the 610-*a*, the plasma is generated close to the vacuum seal. This allows for the entire body of the 610-*a* to stay outside of vacuum. Micro-coaxial probes can then be used to determine the electric field patterns, and the absolute (calibrated) electric field strength on the inner surface of the 610-*a*. All internal dimensions of the 610-*a* are similar to those of the original 610, and the sliding short/center conductor assembly of the latter was interchangeably used for both sources. Chapter Six explores these electric fields that exist inside the 610-*a*, and by inference inside the 610, and how these fields change as the pressure, power and gas type are varied. This chapter also brings together concepts of

loaded, and empty cavity quality factors to determine the coupling efficiency of the "cavity applicator" of the 610. Power loss to the walls is calculated based on the measured absolute electric field strengths, and this provides further information on the coupling efficiency of the MPDR 610 cavity structure. Finally, a lumped circuit model for the 610 emerges, based on the calculation of coupling efficiency. Results of this chapter were presented at the IEEE Conference on Plasma Sciences (ICOPS-94) in Santa Fe, New Mexico, USA and subsequently published in a refereed journal.

Chapter Seven shifts gears slightly when attention is moved from the 610 (and 610-*a*) to another compact ECR microwave ion source that was developed at the EE laboratory several years ago - the MPDR 5. While this source has been evaluated earlier, there were significant gaps in its characterization. Further experimentation on this source was therefore conduced for this chapter in terms of its ion energy distribution functions, ion density, etc. as the usual parameters of pressure, power and position were varied. Results of this chapter were incorporated with prior studies by other researchers, and presented at the International Conference on Ion Sources (ICIS-93) in Beijing, China and subsequently co-published in the proceedings.

Chapters Eight, Nine and Ten depart from the EE Plasma Science laboratory and to the ion source facility of the NSCL, where several interesting joint experiments were conducted. The Superconducting ECR ion source (SCECR) produces multiply charged ions for injection into the two particle accelerators (cyclotrons) at the NSCL. ECRIS that are used to create multiply charged ion beams generally have two stages. The first stage was normally thought to pre-ionize the discharge gas before injection into the main stage of

the multiply charge state ECRIS. Chapter Eight is an applications oriented study of the 610 as an injector stage for the 6.4 GHz SCECR to study the exact effects of the first stage on the performance of the SCECR. The 610 could be positively biased relative to the main stage for ion injection, or negatively biased (again, relative to the main stage) for electron injection into the main stage. Or it could be floated for neutral plasma injection. Hence it could be determined with one set of experiments whether the main stage of the multiply charged ion source requires negative, positive or neutral injection from the first stage. Results of this study were presented at the International Conference on Ion Sources (ICIS-93) in Beijing, China and subsequently published in the proceedings.

Chapter Nine is a study of the 610 as an ion beam source, where the source is set up on a test stand (another vacuum system) at the NSCL, and an ion beam is extracted from it. Description of the new vacuum station is followed by the results of beam extraction from the MPDR 610. The first known photographs of the effects of increasing extraction voltage on the plasma meniscus (the ion emitting surface) are presented. Prior results of the 610 on the analysis magnet of the SCECR beamline are also presented, along with charge state distribution spectra, and emittance measurement results. Results of this study were presented as a late entry to the IEEE Conference on Plasma Sciences (ICOPS-94) in Santa Fe, New Mexico, USA.

Chapter Ten is an analysis of the performance of the SCECR when it is excited at a lower microwave frequency of 2.45 GHz. This rather interesting set of experiments indicated that while the SCECR performance in it's "High-B" mode at 2.45 GHz is not as impressive as the SCECR High-B performance at 6.4 GHz, it is perfectly feasible to design a multiply charged state ion source at the

more abundantly available (and therefore much cheaper) frequency of 2.45 GHz. The surprising results of this chapter also call into question the dependence of the designers of multiply charge state ECRIS on the often quoted "law of frequency squared scaling of the ion density." An invention disclosure for the design of this new multiply charged ECRIS at 2.45 GHz has been submitted to the Office of Intellectual Property of MSU, and an international and US patent is currently pending. Also, results of this study will be presented at the forthcoming International Conference on Ion Sources (ICIS-95) in Whistler, Canada, and subsequently published in the proceedings.

Chapter Eleven then brings to a closure the efforts of the past five years with a recapitulation of the conclusions about the MPDR 610, the 610-*a*, and the collaborative experiments at the NSCL. No experimental work is ever quite complete however, and proposals for further research on this set of ion sources are cited at the culmination of this dissertation as a guide for future researchers.

Chapter 2

Compact Plasma Sources - a Brief Review

2.1 Introduction

2.2 The Review Process

- 2.2.1 The Kyoto University Microwave ECR Ion Beam Source
- 2.2.2 The Hitachi non-ECR Microwave Ion Source
- 2.2.3 Compact ECR Source of Ions and Radicals from Russia
- 2.2.4 The Japanese ECR Radical Gun
- 2.2.5 The Compact ECR Ion Source from RIKEN, Japan
- 2.2.6 The N.C. State/ASTeX Inc. Compact ECR Plasma Source
- 2.2.7 The N.T.T. LSI laboratories Compact ECR Ion source
- 2.2.8 The Oxford Applied Research Atom/Radical Beam source
- 2.2.9 A 2.45 GHz. Compact ECR Source from France
- 2.2.10 The Microscience, Inc. Ion Beam Source

2.3 Discussion - Ion/Ion Beam/Plasma Sources

2.4 Discussion - Figures of Merit

2.5 Concluding Remarks

Chapter 2

Compact Plasma Sources: A brief review

2.1 Introduction

With the advent of plasma processing technology in the industrial environment, there has been a concerted effort in ion and free radical source research and development stemming from the demands of a varied field of research - including plasma physics, atomic physics, ion accelerators, but most specifically from the semiconductor industry. A variety of innovative plasma source designs have been developed with their dimensions and characteristics being predicated by the process and the application. Plasma sources have been designed to work through a vast range of power (few tens of watts to few hundreds of kWatts), pressure (several atmospheres to sub milli Torr) and for cracking several types of gases or metal vapors.

Of the vast variety of plasma sources that have been developed, one subset consists of the compact microwave ion/plasma sources. Some of these are used as a source of ions, while others as reactive free radical sources, and yet others have energetic ion beams extracted from them. Applications of these

plasma sources range from molecular beam epitaxy (MBE) nitriding of GaN and InN, high T_c superconducting thin film deposition using reactive oxygen radicals, free radical pre-cleaning of GaAs wafers using reactive atomic hydrogen, low temperature etching, oxygen implantation using an energetic oxygen beam among other uses. Plasma technology, and ion source development continues to exert its strong influence on the semiconductor and materials processing industry.

2.2 The Review Process

For a basic understanding of the state of the art in ion source design, and also to provide a platform of comparative information (like source dimensions, diagnostics data, etc.), this chapter reviews several compact plasma sources currently used in the semiconductor industry. While the definition of "compact" is rather subjective, an inner source diameter of about 10 cm or less is considered to be compact in this study. However, the adherence to this "cutoff" criterion during this review process is loose at best, so as to study a variety of interesting and unique compact ion/plasma sources. Based on this somewhat flexible criterion, ten compact plasma sources are reviewed in this chapter. To further specialize this review, the frequency of excitation for these sources is in the S band - the microwave range (several hundred MHz up to 100 GHz) in most ion sources, while one of the sources is excited at radio frequency (rf - some tens of MHz).

Each source is individually described in terms of its physical design, assisted by detailed (though not to scale) figures. These figures are

reproductions from the published literature on that ion/plasma source. During the source description, numbers in parentheses indicate the labelled parts in the accompanying figure. An important aspect that defines each source is the method of power transfer into the discharge gas from the source's power coupling structure. While the specific power coupling structure is relatively easy to describe, the actual mechanism of power transfer is usually not that easy to explain. Where possible, the power coupling mechanisms for each source are discussed, or speculated if suitable information is not specifically provided in the source literature.

Performance characteristics of the source are then presented. While different researchers perform different characterization experiments, certain figures of merit for each ion source are commonly measured, like ion/electron density (in cm^{-3}), electron temperature (in degree Kelvin, or eV; 1eV=11,604.4 K), average ion/electron energy (in eV) and the ion/electron energy distribution functions, and ion saturation current density (in $mA\text{-}cm^{-2}$). Free radical sources are generally characterized in terms of their atomic flux (in $mA\text{-}cm^{-2}\text{-}s^{-1}$) and film growth analyses, measured indirectly by XPS, reflection high energy electron diffraction (RHEED), or quartz crystal microbalance (QCM) studies of the film. Optical emission spectroscopy (OES) data are also provided by some researchers to identify individual species within the plasma. Ion beam data are generally provided as the total beam current (in mA or μA, assuming 100% beam acceptance by a shielded Faraday cup), or beam current density (in $mA\text{-}cm^{-2}$) that accounts for the Faraday cup's collection area. The emittance (in mm-mRad), or the normalized emittance where relativistic effects of the beam are taken into account (also in mm-mRad), and brightness (in $A\text{-}m^{-2}\text{-}rad^{-2}$) of the

beam are also characteristic of the ion beam source and its extraction apparatus. These two measurements of the ion beam indicate the efficiency of the extraction apparatus, and the transmission properties of the beam transport system. Mass spectrometry of a discharge, typically using a quadrupole mass spectrometer (QMS), can produce a charge state distribution (CSD) that gives the relative current intensity for each charge state present in the beam. Details of several characterization techniques mentioned above are presented in Chapter Three - these techniques were utilized to evaluate the performance of the four major ECR plasma/ion beam sources studied during the course of this dissertation.

Input power, in all cases implies the net power being absorbed by the discharge and/or the ion source. It is the difference of the total incident power and the reflected power from the plasma source, taking into account all attenuation factors pertaining to power loss in the cables, connectors, source walls, etc.

This review process concludes with a general discussion of compact microwave ion sources that are studied in this chapter, with a brief comparison, where possible, of the figures of merit that define these sources. A discussion of the necessity to standardize certain figures of merit also follows. Many of the sources discussed here have commercial versions available, and all are used for processing applications, or as tools for fundamental plasma physics and chemistry investigations. Where reported in literature, the various applications of the plasma/ion/ion beam sources are detailed.

This review confines itself to compact plasma sources and some ion beam sources used in materials processing and semiconductor applications. A

significant omission from this study, therefore, is the family of microwave ion beam sources used in accelerator laboratories throughout the world. While most of these ion sources used in atomic and particle physics research (including particle accelerators) are large and bulky, some may be classified as "compact." The main difference between accelerator ion beam sources and those used in processing applications is that the former are designed to produce highly charged species with multiply stripped ions, which are then extracted as a very energetic beam (up to several tens of kV extraction potential), and injected into the accelerators for further energy gain. The latter variety on the other hand (the plasma/ion sources used in substrate processing applications), require only singly charged ions to prevent substrate damage from energetic ion bombardment. (The higher the charge state of the ion, the more energy it gains while being accelerated through an extraction potential, or even while falling through the plasma potential within the discharge.) Note that while ion beam sources used in ion implanters do produce multiply charged species (like O^{2+}) to reduce the required acceleration potential, the beam energies and most other operating conditions of ion implanter sources are still very different from high charge state producing ion sources.

While each plasma source discussed in this chapter varies from the other, they have many things in common. Most are electron cyclotron resonance (ECR) based ion sources that require a static magnetic field to create resonant conditions for the electron gas, while some are off resonance devices (non ECR). Non ECR sources employ essentially Joule heating and other mechanisms of power transfer such as stochastic (non collisional) heating - as discussed in Chapter One - to create and sustain the plasma. There are usually some

magnets even in non ECR plasma sources to confine and control the diffusion of charged species out of the source. Some sources use permanent magnets, mainly to simplify the design and reduce overall size and peripheral apparatus costs, while others rely on current coils for better control of field strength while sacrificing some of the simplicity and cost benefits of permanent magnets (current coils require water cooling, and peripheral power supplies to control the magnetic flux).

An important point needs to be made about resonance - a topic that will come up while describing several sources. There are two types of "resonant sources" that will be discussed. The microwave plasma disk reactors (MPDRs) designed at MSU in the EE laboratories have tunable resonant cavities that set up specific electromagnetic resonant modes within the adjustable cavities. This type of resonance has to be differentiated from the electron cyclotron resonance, which all ECR based sources incorporate. Hence, a "resonant cavity" may simply be the source's reliance on ECR, or it may mean that the source has adjustable dimensions that are tunable to appropriate EM modes, as in the case of the MPDR family of sources. This distinction will be pointed out when the sources are discussed during the appropriate sections.

It is expected that once this review is completed, it will provide a better understanding of ion sources (both ECR and non-ECR) in terms of their design parameters, optimal operating conditions and performance characteristics. Also, as awareness grows about these various plasma sources, a basis will be formed to more thoroughly understand and compare the evaluative results obtained during the past five years of research on the four primary plasma sources that are detailed in Chapters Four through Ten of this dissertation.

2.2.1 The Kyoto University Microwave ECR Ion Beam Source

In 1983, Ishikawa et al. at Kyoto University in Japan reported the development of a low power compact ECR microwave ion source with a non resonant cavity structure [Ish-84, Sak-89]. Shown in Figure 2.1 (not to scale), the source has an overall diameter of 5.0 cm, and height of 6.5 cm. The plasma chamber is 1.6 cm in diameter and 5 mm in effective height, ending in a 2 mm non ferro-magnetic aperture. The gap between this aperture and the extraction electrode (5) is 3 mm. The base flange is water cooled, allowing the use of a Viton O-ring for sealing this flange to the rest of the source, although the source itself uses a copper gasket to seal to the vacuum chamber. A sheath heater (2) is wound around the ion source to raise the temperature of the source when a metal vapor is to be ionized.

Design of the axial magnetic field structure is critical to this ion source, and numerical simulation of the beam extraction and magnetic lines of force was used to optimize this magnetic field configuration. The Sm-Co permanent magnet (3) used in this source is donut shaped measuring 50 mm outer diameter, 40 mm inner diameter and 15 mm high. The extraction electrode (5), the magnet and a connecting flange made of ferro-magnetic material forms a closed magnetic circuit from the bottom of the discharge region to the top of the source. This effectively creates a magnetic field residual flux density of about 0.97 kiloGauss, with the field strength varying from 800 G to 1200 G between the antenna (7) and the extraction electrode. The "ECR zones" therefore fall well within the plasma generation region of the source. The field lines are also arranged to enhance ion divergence.

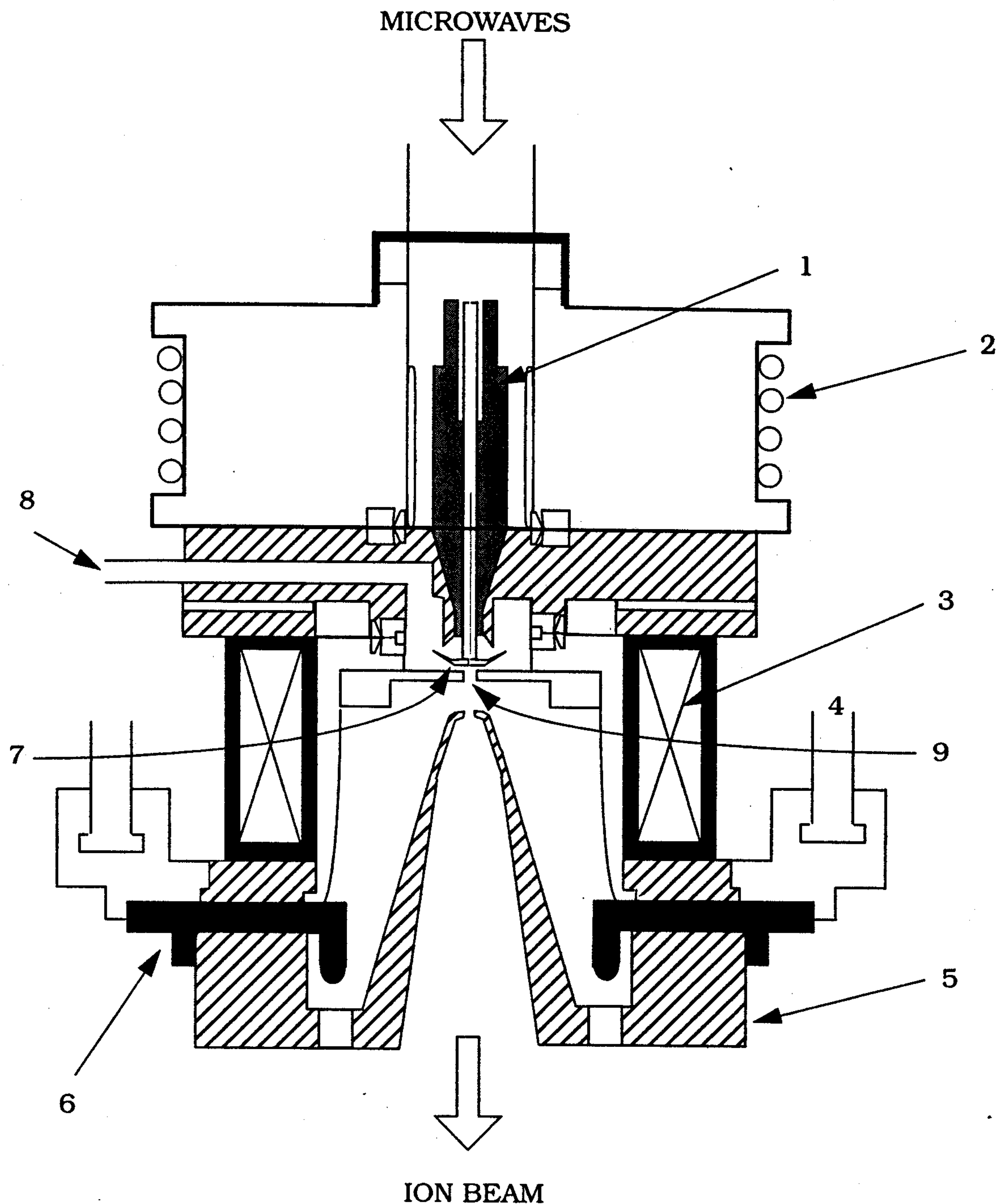

Figure 2.1 Kyoto University Microwave ECR Ion Beam Source

1. Boron Nitride Plug
2. Sheath Heater
3. Permanent Magnets
4. Coolant
5. Extraction Electrode
6. Maycor Insulator
7. Antenna
8. Gas Inlet
9. Aperture

Microwaves at 2.45 GHz are fed through a flexible coaxial cable, to a sealed coaxial connector and into the discharge chamber via a "T" shaped antenna (7). This antenna, made of molybdenum or stainless steel wire of 1.5 mm diameter, protrudes into the plasma production chamber. The unique shape of the antenna maintains a high electric field within the chamber walls, and this electric field is able to sustain a stable discharge even at low pressures (few mTorr). A boron nitride (BN) plug (1) prevents plasma generation near the antenna shank. For input power (incident minus reflected) of about 20 to 30 W, the power coupling has a reflection ratio of about 30-40% for metal vapor, and about 30% for argon, nitrogen, and other gaseous discharges. This reflection ratio is somewhat high, and should be expected because of lack of any tuning mechanism to counteract the changing load impedance as the discharge approaches steady state. It is, therefore, impossible to match the microwaves to the plasma for all operating conditions. However, the high reflection coefficient does not affect the ion source performance.

The performance characteristics of the source were measured using a multi-grid Faraday cup placed 6 cm downstream from the plasma generation region [Ish-84]. Also, mass spectra were analyzed, and emittance measurements were made. The electron suppressor voltage on the first grid of the Faraday cup was kept sufficiently high (negative 150 V) to prevent high energy electrons from entering the cup and polluting the readings with secondary electron emissions. At low input power levels of about 20 - 30 W, and an extraction voltage of 15 kV, the argon ion current density at a relatively low pressure of 1 mTorr is almost 100 mA-cm^{-2}. The ion beam current variation with extraction voltage is less than the maximum current predicted by the classical Child-Langmuir law - a linear

relation between the extraction voltage and the beam current on the log-log scale (assuming a specific ion density in the generation region). The current-voltage characteristics of the source indicate an initial linear increase in beam current with increasing potential, leading to a saturation beyond a certain voltage. Typically, the linear region is ion density limited, while the saturation region is said to be space charge limited.

Similar high current densities are observed for nitrogen, carbon dioxide and oxygen gas, and also for Cs and Rb metal vapors. For a metal vapor (like cesium) at about 20 watts input power and 15 kV extraction voltage, the current density was over 80 mA-cm^{-2}, the total current being 2.7 mA. Plasma density can be controlled by pressure and power variation. QMS analysis showed a high ratio of about 95:5 for the Ar^{1+}:Ar^{2+} ions, possibly due to the divergent and non-confining structure of the magnetic field. The ratio of doubly charged ions does increase as the pressure decreases, in part due to the increased lifetime of hot electrons with the falling electron-neutral collision frequency with reduced discharge pressure. Theoretical estimations of the ion density, based on the assumption that the average electron temperature in the plasma is 5 eV are made to be in the low 10^{12} cm^{-3} - note that ion density and electron temperature is not directly measured.

A plasma density of 10^{12} cm^{-3} for a 2.45 GHz discharge at about 1 mTorr pressure is relatively high. This may be explained by the efficient power transfer from the EM fields to the discharge as claimed by the authors. The skin depth, which is defined as the depth at which the attenuating electric field is exp(-1) of its amplitude before being attenuated by the discharge, is given by the following equation [Ish-84]:

$$\delta = \frac{c}{\left(\omega_p^2 - \omega^2\right)} \tag{2.1}$$

where δ is the skin depth, c is the speed of light, ω_p is the plasma angular frequency, and ω is the frequency of excitation. At 2.45 GHz and with an estimated ion density of 10^{12} cm^{-3}, δ is calculated to be about 5.5 mm; the height of the plasma generation region is 5 mm. Hence, the authors speculate that such high density is probably due to effective penetration of the right hand circularly polarized (RHCP) up to the skin depth in the magnetized plasma.

Emittance calculations were done to characterize the beam extraction and transport for this ion source. The measurement system consisted of a plate with a series of 0.5 mm diameter holes; this plate is separated from the mobile wire detector of 25 μm diameter by a distance of 16.5 cm. With 86.5% of the total ion beam current covered by the fitted emittance contour, the normalized emittance of the beam was estimated to be 3.7 X 10^{-8} m-rad, or 3.7 X 10^{-2} mm-mRad. The normalized brightness is calculated to be about 1.8 X 10^{11} A-$m^{-2}rad^{-2}$. Both the emittance and brightness were a function of input power. The ion beam divergence angle measured with the emittance apparatus was estimated to be about 5°. This divergence is relatively high presumably because of the inadequacies of the double grid extraction system and should decrease with the use of a proper accel-decel system.

The ion source can therefore work at extremely low power and low pressure conditions, and can effectively absorb microwave power even though it does not have a resonant cavity structure. Potential applications of the ion source are postulated to be in accelerators, sputtering and ion beam assisted

etching machines. A similar source is currently under construction at the cyclotron laboratory of Catania, Sicily for possible beam injection into the main stage of a multiply charged state ion source [Gam-94].

A scaled up variation of the above source was introduced in 1989 [Tsu-89]. Although not a compact source any more (outer diameter is 22 cm, and height is 10 cm), it is a significant modification - there are three similar helical molybdenum (or stainless steel) antennae instead of one. The scaling is done therefore, by effectively stacking three sources together. The plasma production region is larger - 1.6 X 6.6 X 0.5 cm^3. Each antenna is fed via a quasi coaxial line, as in the previous version, using a BN plug as an insulator that prevents plasma from being generated near the antennae shanks. Even with this larger area the source is not a resonant cavity structure. 10 small Sm-Co permanent magnets (3.0 X 0.8 X 2.0 cm^3) are circularly arranged and, along with the ferromagnetic materials of the bottom plate, provided the axially divergent magnetic fields for ECR and ion transport requirements.

Two microwave power sources at 2.45 GHz were used to power the three input lines - one supplying power for the center antenna, and the other source for the two outer antennae. Typical microwave power was about 40 W, with a total of about 27 W reflected. About 80% of the input power from each antenna was absorbed by the plasma, a fact confirmed by alternately switching on individual antenna while keeping the other antennae off. This also indicated that the EM fields from any antenna did not adversely affect the fields of the other antennae. A "sheet beam" was extracted from the ion exit slit (0.6 X 60 mm^2), with a 4 X 70 mm^2 long extraction aperture. An enizel lens (three pairs of plate electrodes with an opening area of 3.0 X 9.0 cm^2) was used to focus the sheet

beam. Such a sheet beam is typically used in ion implanters.

Performance characteristics were measured using a multigrid Faraday cup placed 27 cm away from the ion exit aperture. An electron suppressor voltage of 1.2 kV is applied to the top grid to prevent contamination of collected current data from secondary electrons. As for the previous version of the source, the plasma density generated within the source is estimated to be about 10^{12} cm^{-3}. At an extraction voltage of 20-25 kV and 100 W input power, a 10-20 mTorr argon discharge produces a total current of 12.5 mA. Note that this is a relatively high pressure discharge, specially if the pressure measurement is conducted downstream - the discharge pressure in that case may be several times higher than the processing chamber pressure. For the same pressure and power conditions, a nitrogen discharge produced an ion current of about 13.5 mA, while the oxygen current was 5.6 mA for an oxygen plasma - a marked increase in the total current production over the previous source design. This modified source, therefore, operates at higher pressure and power levels, while providing higher beam currents.

As can be seen, a major advantage of this source is that for more intense ion currents, or a larger beam area, the plasma source can be easily scaled up because of its quasi-modular design, and also because it is not a resonant cavity structure despite being an "ECR source". Addition of similar antennae and extraction apparatus is possible without sacrificing the source performance in any way. While resonant cavity based plasma sources like the microwave plasma disk reactors (MPDRs) that will be discussed later in the dissertation, may also be scaled up, factors like choice of resonance at specific electromagnetic modes might affect the scaling process. The different "stacking together" method of

scaling used in this source ensures that such problems are not an issue, specifically because the source is not based on a resonating any specific mode in the cavity structure.

Yet another version of this compact ion source was presented at the International Conference on Ion Sources in 1991 in Beijing, China by a research group at the Peking University, PRC [Son-92]. The source design remained essentially the same as the original single antenna source of Ishikawa et al. The total source diameter is 4.6 cm, and its height is 5.0 cm. The copper discharge chamber has a diameter of 2 cm, and is equipped with a 2 mm extraction hole in the bottom stainless steel plate. The ferromagnetic extraction electrode is 3-7 mm away from the ion exit plane, and has a 4 mm diameter hole. A similar annular axial permanent magnet is used create the magnetic fields inside the discharge chamber. The "T" shaped antenna is made of stainless steel with a diameter of 2 mm.

Initial performance characterization of this version of the plasma source has indicated a similar tendency of a high reflection coefficient - about 40% of the power is reflected back. With less than 60% of the power coupling into the plasma, the authors conclude that further research into the plasma impedance matching mechanism needs to be done. A nitrogen discharge was used to obtain preliminary ion extraction data. At a pressure of 10 mTorr, and about 50 watts of power absorbed, the nitrogen discharge produced a total beam current of about 1.2 mA with an extraction voltage of 10 kV. Further experiments to characterize the ion source, and also to improve its design and performance are currently under way.

2.2.2 The Hitachi non-ECR Microwave Ion Source

Another off resonance microwave ion source was developed by Sakudo and associates in the Tokyo laboratories of Hitachi Limited in 1977 [Sak-77] and further reviewed later [Sak-87, Sak-89]. The source, which is shown in Figure 2.2 (not to scale), has a discharge chamber diameter of about 6 cm. The plasma chamber is essentially an extension of the 50 Ohm circular coaxial waveguide (2). Microwaves at 2.45 GHz are fed through a rectangular waveguide (1) - this is intersected by the coaxial waveguide, terminating in a water cooled antenna (4) that extends into the chamber. The discharge chamber is also water cooled so as to prevent the ceramic vacuum window (9) from being over heated, and/or destroyed by particulate bombardment.

A magnetic mirror ratio of about two is created by three electromagnet coils (3). The magnetic field configuration thus generated helps in preventing backstreaming of energetic particles. The main purpose, however, of the magnetic mirror, is to gradually vary the resistivity of the plasma load. The intensity of the field generated by the coils throughout the source length is higher than that required for ECR at 2.45 GHz. Assuming that the plasma is a resistive (lossy) dielectric, a mirror ratio helps in creating a plasma source that terminates in a gradually varying resistive load, which in turn helps in microwave coupling into the plasma for all discharge conditions. With no external tuning mechanisms, this gradually varying resistive load auto-tunes the resistive component of the plasma load to the 2.45 GHz waveguide impedance. This was demonstrated by a test in which the absorption of microwave energy increased from about 60% to over 90% as the magnetic fiend

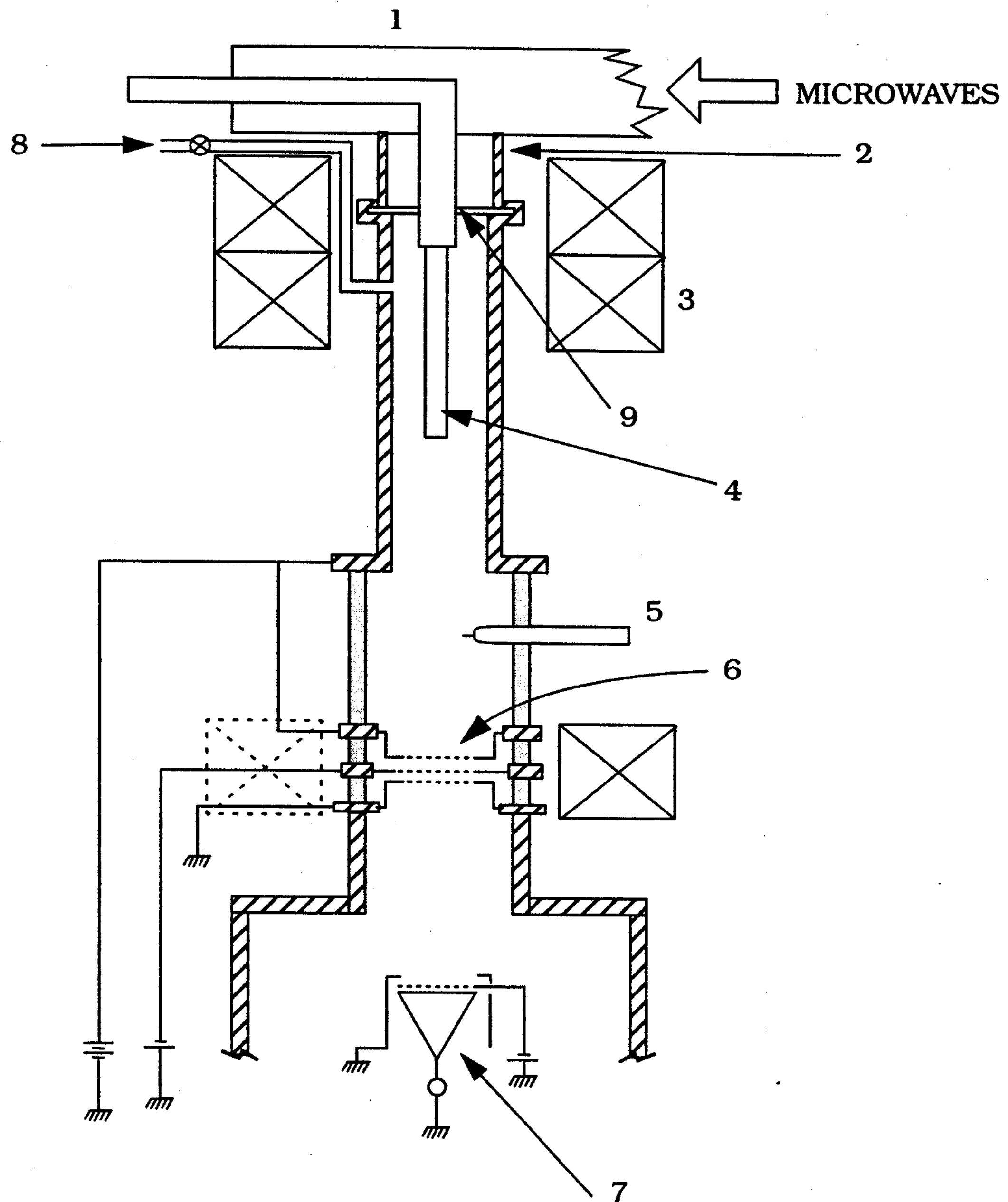

Figure 2.2 Hitachi Non ECR Microwave Ion Source

1. Rectangular Waveguide
2. Circular Waveguide
3. Magnet Coils
4. Antenna
5. Movable Langmuir Probe
6. Multi-aperture Lens
7. Multi-grid Faraday Cup
8. Gas Inlet
9. Ceramic Window

intensity was increased from 40% to 100%.

Note that although there might be regions where the magnetic field conforms to the requirements of ECR, this is not an ECR based source - specifically, the source produces a type of "wave heated" discharge (as discussed in Reference Lie-94). It works on the principle that if the magnetic field inside the source is higher than that required for electron cyclotron resonance, but lower than that for ion cyclotron resonance (ICR), a plasma discharge may be ignited and sustained without relying on ECR [Mus-74]. A three grid (with multiple apertures - 124 holes, each 3 mm in diameter) accel-decel extraction system (6) is used to extract the energetic particle beams, with a negative 300 V suppressor voltage on the middle grid.

Performance characteristics of this source were measured using a cone shaped multigrid Faraday cup (7) placed 15 cm from the extraction grids, and a movable Langmuir probe (5). Electron temperatures for both hydrogen and argon discharges increased slightly with increasing input power ranging from 3 - 4 eV at 200 W, to 5 - 6 eV at 1 kW input power. At 1 mTorr pressure, the argon ion density increased from 10^{12} cm^{-3} to 10^{13} cm^{-3} as input power was raised from 400 W to 1 kW - this source generates densities about 10 to 100 times those in a source that relies on ECR for plasma generation. The source therefore has a very high ionization efficiency. Ion density in hydrogen were typically seen to be a little less than those in an argon discharge. Since the source does not rely on ECR, it need not conform to the critical density development that, theoretically, limits the maximum density of a 2.45 GHz plasma to 7.4×10^{10} cm^{-3}. Over the entire pressure range, the power absorption was noted to be about 75%, which may be increased to 90% by using an external EH stub tuner

between the directional coupler and the ion source. At a pressure of 1.3 mTorr and with 1 kW incident power, a maximum hydrogen ion current of about 380 mA at 4.5 kV extraction voltage, and a maximum argon ion current of about 200 mA at 5 kV extraction voltage was measured with the multi-grid Faraday cup (7) placed downstream from the discharge generation region (see Figure 2.2). As the extraction potential was raised from zero to 5 kV, the argon ion beam current increased monotonically with extraction voltage. The hydrogen ion beam current however, seems to saturate beyond 5 kV bias.

The fundamental advantage of this off resonance ion source over other "ECR sources" seems to be that the ion current intensity and ion densities produced in this source are much higher. Due to the high magnetic mirror ratio, the ceramic window is relatively safe from energetic ion bombardment, hence the source has a long lifetime. However, particulate generation off the antenna that is surrounded by the discharge has not been accounted for by analyzing the plasma constituents, which might lead to problems with UHV applications unless specific ion species are mass separated downstream from the discharge generation region.

2.2.3 Compact ECR Source of Ions and Radicals from Russia

A compact ECR ion and free radical source with a very simple design was introduced in 1991 by the then USSR Academy of Sciences, Moscow [Sha-90, Sha-92]. The source, which is shown in Figure 2.3 (not to scale) has a length of 16.0 cm, and a diameter of 11.3 cm. It may be installed on existing chemical beam epitaxy (CBE) machines and other UHV equipment using a standard CF63

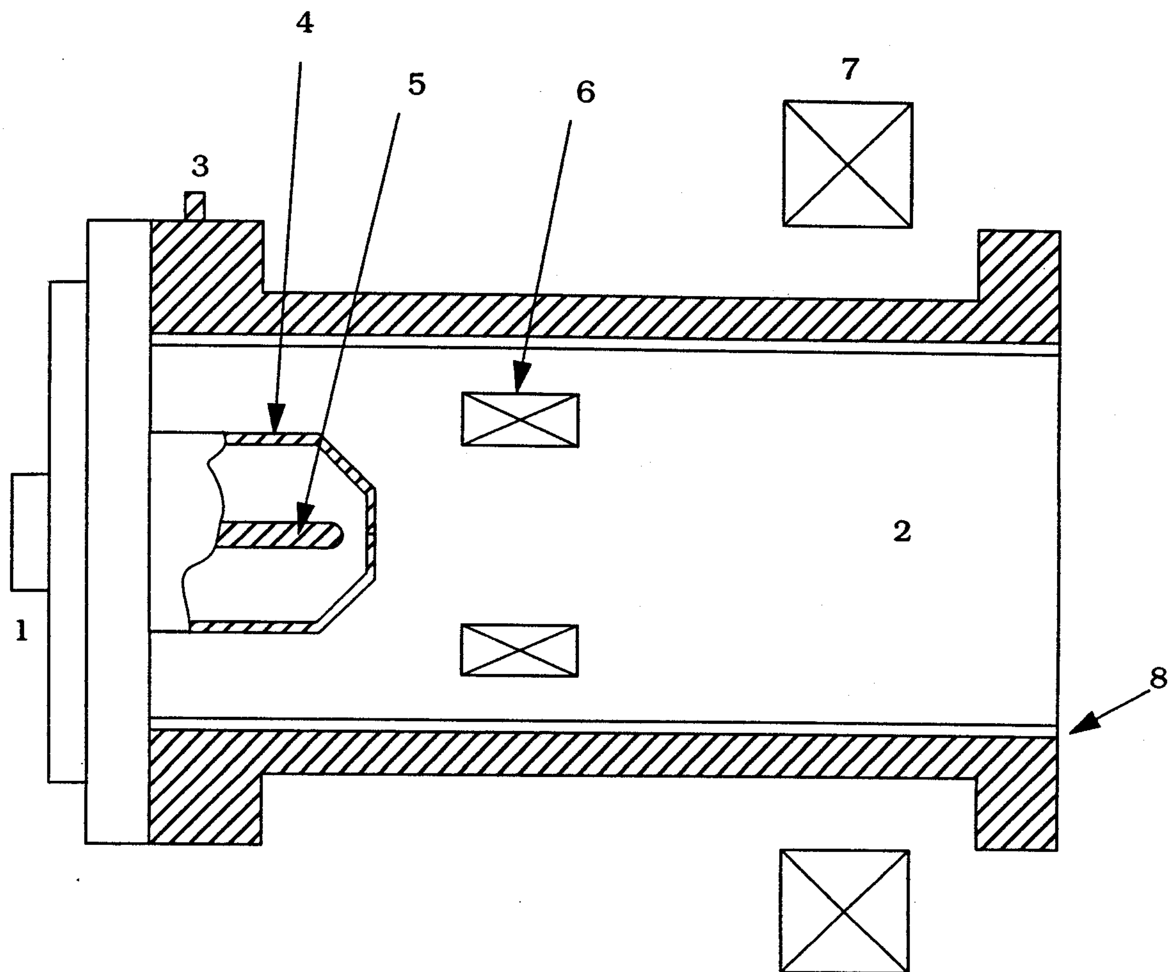

Figure 2.3 Compact ECR source of Ions/Radicals from Russia

1. 50 W Coaxial cable connector
2. Plasma cavity
3. Gas feed
4. Ceramic cup
5. Antenna
6. Ring shaped permanent magnet
7. Electromagnetic coil
8. Quartz tube liner

flange. The source utilizes Sm-Co permanent magnets to create the magnetic fields required for ECR. These ring shaped magnets (6) are placed inside the discharge chamber (2) with special adjusting rods, creating sufficient magnetic field strength for high plasma densities (about 10^{11} cm^{-3}) at a pressure range of 0.1 mTorr to 10 mTorr. An electromagnetic coil (7) is placed outside the source (but in the vacuum chamber) for efficient control of charged particle flux. This variable magnetic field may be used to either extract or deflect the ions away. The stainless steel body of the source is water cooled.

A standard 50 Ohm coaxial cable terminates into an antenna (5), coupling microwaves at 2.45 GHz into the plasma chamber. The antenna is isolated from vacuum via a ceramic cup (4). The diameter of the antenna, and its position with respect to the magnets are critical for stable operation of the ion source; both conditions were determined empirically, and the reported antenna diameter was 4 mm. The variable position of the antenna is the tuning mechanism for matching the load impedance. A quartz tube liner (8) is inserted into the source to reduce losses of radicals and ions to the stainless steel walls. It may also prevent particulate generation (and therefore contamination of the discharge) from the metallic walls, while at the same time providing secondary electrons to the discharge - quartz has a high secondary electron emission coefficient.

Performance characteristics were measured using cylindrical and disc shaped Langmuir probes. These probes were located about 10 cm downstream and were DC biased with a negative potential of 35 volts. Measured saturation ion current density for a 100 W input power hydrogen plasma showed a typical pressure dependence - initially increasing to about 2 $mA\text{-}cm^{-2}$ at 1 mTorr, and

then gradually decreasing to about 1 mA-cm^{-2} as pressure was further raised to 4 mTorr. When experiments were conducted over various power and pressure ranges, it was found that the optimal operating pressure range was 0.1 mTorr to 5 mTorr for moderate power levels of 500 W or less. High ion current densities could be obtained at these low powers, and so there was no need for extensive cooling of the source as required for other sources that rely on higher input power levels to generate the high ion densities. At a constant pressure, the saturation current density increased monotonically with increasing power, ranging from 0.5 mA-cm^{-2} at 10 W, to over 3 mA-cm^{-2} at 200 W input power. The electron temperature of a hydrogen discharge, calculated using Langmuir probe I-V characteristics, was estimated to be about 4.7 eV for 50 W, and 4.3 eV for 25 W net input power.

The source has been successfully used for in situ cleaning of GaAs substrate using arsine (AsH_3) and triethylgallium (TEG) in a chemical beam epitaxy (CBE) reactor made by EPIQUIP™ of Sweden. For this process, a hydrogen plasma at 0.2 mTorr was used to bombard the substrate placed about 40 cm away for 10 - 15 minutes. In situ RHEED, XPS and QMS studies confirmed a complete removal of the GaAs native oxide from the substrate surface, and also confirmed the absence of any carbon and oxygen peaks on the surface. Further, film growth experiments demonstrated a significant increase in growth rates of GaAs, and good surface morphology after the substrate was exposed to a hydrogen plasma from this compact ECR ion source. Future applications for this source are foreseen in CBE growth of III-V semiconductors, and as an ion beam source with extraction grids.

2.2.4 The Japanese ECR Radical Gun

The Institute of Physical and Chemical Research (RIKEN), the Toyo University, and the Irie Koken Co. Ltd., all of Saitama, Japan reported in 1991 the development of a compact ECR source [Oke-91a], and also reported on some of its applications [Oke-91b]. The source is sketched in Figure 2.4 (not to scale). Essentially a free radical source, the radical gun has a low ion current density but a high atomic flux, and is therefore most suitable for applications that require high radical species concentration. The simple design of the source consists of a resonant cavity structure made of stainless steel 2.5 cm long, with a 1.0 cm diameter. Note that, as mentioned in the introduction, the "resonant cavity" in this source means only that the source is based on ECR, and not that the dimensions of the cavity change to generate resonant standing electromagnetic waves (as in the case of the MPDR sources). The overall diameter of the plasma source is about 35 mm, and the overall length of the source is variable, depending on the application. It is mounted on a standard 70 mm conflat flange (7).

Microwave power at 2.45 GHz is fed via a flexible coaxial cable (1), the center conductor of which continues into the vacuum creating a variable length, in-vacuum coaxial cavity structure. The center conductor then terminates into an antenna (4) that protrudes into the plasma creation region. The antenna is encased inside a quartz tube (6), and a BN centering ring (3). There are two ring shaped water cooled permanent magnets (5) that provide the static magnetic field for ECR. A beam may be extracted through an orifice of variable diameter - from 1 mm to 10 mm.

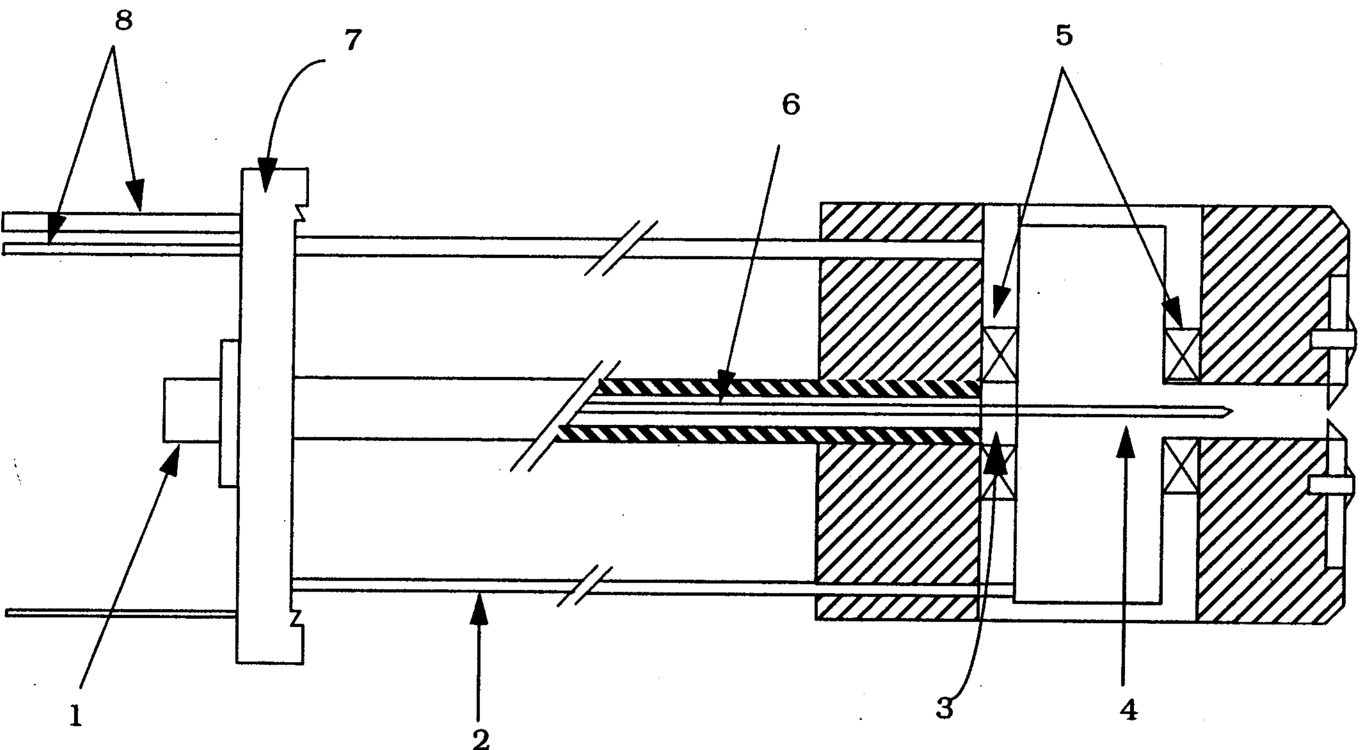

Figure 2.4 Japanese Radical Gun

1. Microwave Cable Connector
2. Gas Feedthrough
3. BN Centering Ring
4. Antenna
5. Ring Shaped Permanent Magnets
6. Quartz Tube
7. 70 mm Conflat Flange
8. Coolant Feedthrough

The performance characteristics of the source were measured using a quartz crystal microbalance (QCM), optical emission spectroscopy (OES), a multi-grid Faraday cup, and Langmuir probes for a variety of gases and under many discharge pressure and input power conditions. For a 0.1 mTorr argon plasma, OES indicated a predominance of the Ar^{1+} ion and Ar^* radicals. The dominant peak in an oxygen discharge at 10 mTorr is the oxygen radical O^*, although there are some minor O^{1+} and O_2^{1+} peaks as well. A nitrogen plasma at 1 mTorr has predominantly N_2^{1+} peaks, but N^* and N_2^* radical peaks are also visible. The three Balmer lines of hydrogen are in evidence for a 20 mTorr hydrogen plasma.

A Faraday cup with a negative 80 V electron suppressor grid and an effective area of 12 cm^2 was placed 4 cm downstream from the radical gun to measure the current density produced by the source. For a 0.1 mTorr hydrogen discharge, the ion current increased with increasing power; the maximum current density was 12 μAmps-cm^{-2} with 160 W input power, (corresponding to a flux of about 8 X 10^{12} cm^{-2}-s^{-1}). Similar ion current density behavior was seen with an oxygen discharge at 10 mTorr - as the input power was increased from 50 W to 150 W the oxygen ion current density increased almost linearly with a maximum of approximately 160 μamps-cm^{-2} (and an equivalent ion flux of 10^{15} cm^{-2}-s^{-1}). For the same range of input power (increased from 50 W to 150 W), Langmuir probe data in a 10 mTorr oxygen discharge indicated that the electron temperature dropped from about 3 eV to about 1.5 to 2 eV, and the oxygen ion density was about 10^{10} cm^{-3}.

QCM analysis was used to obtain quantitative values of radical oxygen flux. When the plasma pressure was decreased from 10^{-2} Torr to 10^{-3} Torr, the

ion flux decreased from 10^{15} cm^{-2}-s^{-1} to about 10^{14} cm^{-2}-s^{-1}, but the radical flux remained almost unchanged at about 10^{15} cm^{-2}-s^{-1}. So decreasing the pressure increased the radical content of the beam with respect to the ionic concentration. This may be due to the drop in ion density (O_2^+ and O^+) as the pressure is reduced. As an example, for an oxygen discharge pressure of 10 mTorr, the O_2^{1+}/O^* percentage was 34%, whereas for a 1 mTorr discharge, this ratio had decreased to approximately 8%.

The radical gun was used in two potential applications: for the in situ oxidation of a superconducting thin film during deposition, and low temperature GaAs substrate cleaning (confirmed by RHEED) using a hydrogen plasma [Oke-91b]. High quality superconducting thin films were produced with the use of this oxygen radical gun. By magnetically deflecting the charged species away and reducing the ion current by as much as 40%, an oxygen radical (O^*) rich beam was created. When the superconducting film was exposed to this oxygen radical beam during deposition, the characteristic temperature of the film increased, and the corresponding properties like the phase transition from normal, to superconducting phase also got better. The improvement in the film properties may be a result of the decrease in the damaging ion bombardment from the beam, once the ions have been magnetically deflected away from the beam that impinges on the film. For the other application, the rate of low temperature (about 100 °C) GaAs substrate cleaning was increased by using higher power. Further applications for this radical gun are expected to include digital integrated circuits etching, surface passivation and semiconductor substrate doping.

2.2.5 The Compact ECR Ion Source from RIKEN, Japan

Collaboration between RIKEN, the University of Tokyo, the Tokyo Institute of Technology and the TOYO University, all of Japan produced another compact high current ECR-type ion source that was reported in 1989 [Tam-89]. The source was designed with a specific application in mind: producing thin oxide layers of composite material. The source is shown in Figure 2.5 (not to scale). The unique and simple design of this non-resonant ECR plasma source consists of a cylindrical pyrex vacuum vessel (8) intersecting a rectangular waveguide (5) that is used to transport the 2.45 GHz microwaves from the magnetron (1) that is placed close to the source. The waveguide terminates into a plunger type tuner whose position is adjusted for optimal power transfer into the ion source. The microwaves are localized in the plasma creation region by a cone shaped structure (2). The outer diameter of the vessel is 7.0 cm, and its height is 5.0 cm.

A modified cusp shaped magnetic field structure is created by two permanent magnets. The first is a water cooled Sm-Co cylindrical magnet (4) with a diameter of 1.0 cm, and length of 3.0 cm. It is placed inside a pipe within the discharge chamber that acts like an antenna (3). The other magnet is a ring shaped structure (6) made of ferritic steel (ID of 6.0 cm, OD of 10.0 cm, and thickness of 1.5 cm), and is placed outside the chamber with its north pole facing the north pole of the cylindrical magnet. This magnet is also water cooled. The magnets are 2.0 cm away from each other and the magnetic field strength inside the source is strong enough to satisfy the ECR condition (875 Gauss at 2.45 GHz operation). The magnetic field structure is such that the field lines also

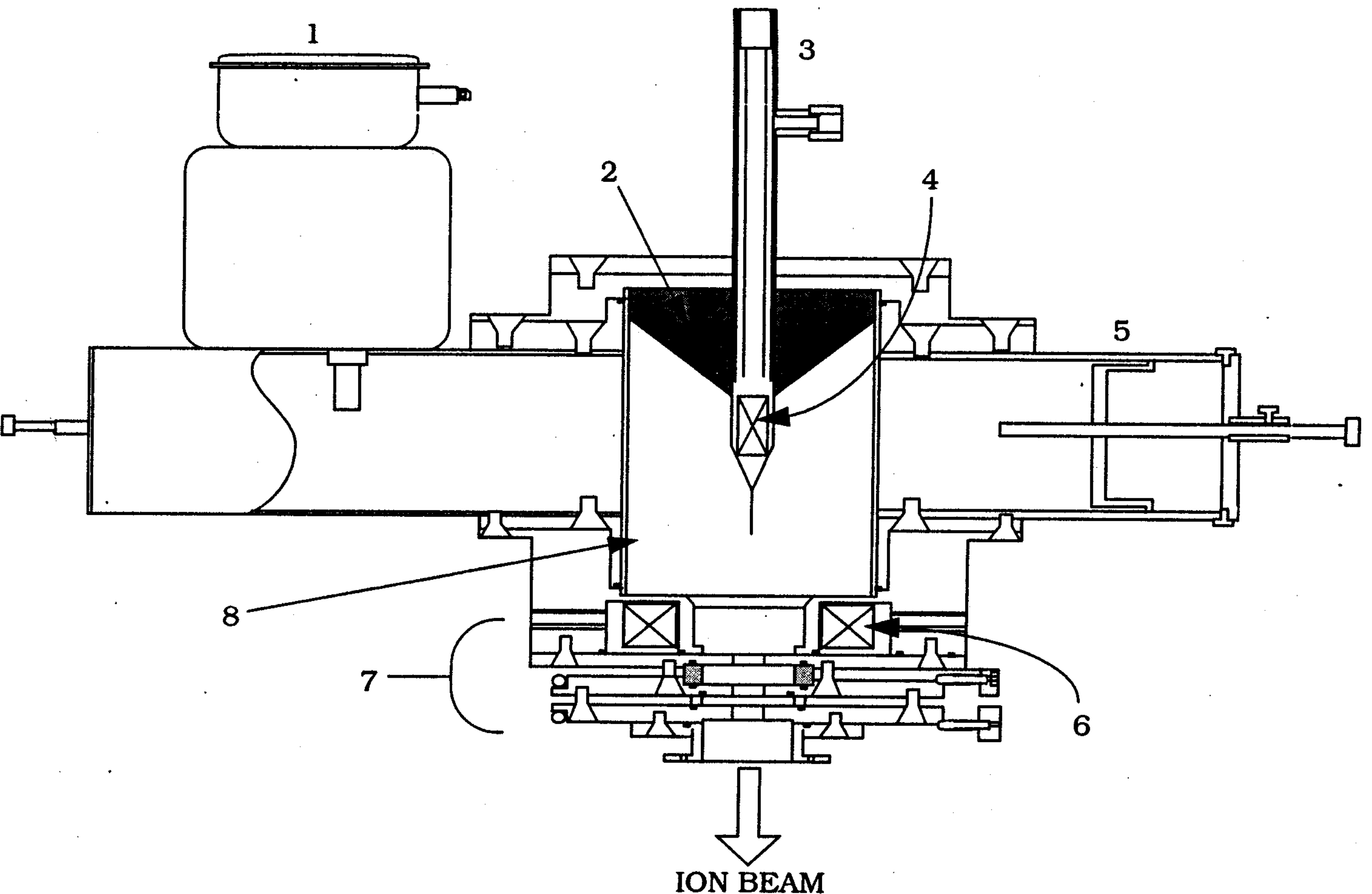

Figure 2.5 Compact Ion source from RIKEN

1. Magnetron
2. Cone
3. Antenna
4. Cylindrical Permanent magnet
5. Rectangular Waveguide
6. Ring Shaped Permanent magnet
7. Extraction apparatus
8. Cylindrical vacuum vessel

efficiently transport the ions to the bottom of the source where they are extracted by a three electrode accel-decel extraction system (7).

Plasma characteristics were measured using a Langmuir probe, and an ion collector electrode - a single plate placed about 16 cm below the extraction electrodes. The probe was located in the extraction aperture of the first electrode. For a 280 W hydrogen plasma, as the discharge pressure increased from 0.02 mTorr to about 1 mTorr, the ion density increased from 2×10^{10} cm^{-3} to about 2×10^{11} cm^{-3}. Hence an over dense discharge is achievable in this source. (The critical density at 2.45 GHz is about 7×10^{10} cm^{-3}.) At the same time, electron temperatures fell from about 12 eV to about 3.5 eV. For a 280 W, 0.01 mTorr hydrogen discharge, a beam current of about 4.5 mA was extracted with an accel-decel voltage of 2 kV and negative 200 V respectively. The current density at the output of the discharge chamber could then be calculated to be about 5.7 mA-cm^{-2} since the area of the extraction hole is 0.785 cm^2. For a 3×10^{-5} Torr hydrogen discharge, the electron temperature and ion density were calculated to be about 11 eV, and about 3×10^{10} cm^{-3} respectively. A QMS analysis indicated that the proton yield of the source was about 20% from a 3×10^{-5} Torr hydrogen discharge. This source was used to efficiently produce H^- ions. From a 0.4 mTorr hydrogen discharge at 280 W input power, the H^-beam had a current of about 0.5 mA-cm^{-2} [Tam-90].

Emittance data was taken for the beam characterization. The measurement system consisted of two plates 75 mm apart, with a 0.5 mm wide slit. The emittance area was estimated to be about 260π mm-mrad with an ion beam divergence half angle of about 8°. This divergence angle is relatively high primarily because of the large ion extraction aperture.

It has been shown that this ECR ion source is very compact, economical and stable, characterized by high electron density and high current intensities for both positive and negative hydrogen ions. The electron temperatures are slightly higher than those obtained with other sources for similar input power levels, probably because the operating pressures are much lower for this source. (As pressure decreases, the electron temperature must increase to sustain the discharge.) The beam characteristics may be improved by using a redesigned extraction apparatus.

2.2.6 The North Carolina State/ ASTeX Inc. Compact ECR Plasma Source

In 1990, ASTeX Inc. of Massachusetts and an engineering team from North Carolina State University reported a distributed, or multicusp ECR ion source [Sit-90a, Dav-90a]. This compact UHV compatible plasma source, shown in Figure 2.6 (not to scale), may be inserted into an existing 2.25 inch diameter MBE effusion cell. The basic structure is similar to that of the Japanese radical gun (Section 2.2.4) - an ECR resonant coaxial microwave applicator, and also to that of the MPDR 610 - detailed later in the dissertation. Note once again, that the "resonant" cavity for this source refers to it being an ECR base source, and not the tunable cavity structure of the MPDR sources (as was mentioned for the Japanese radical gun in Section 2.2.4).

Three small water cooled electromagnets (8) produce the ECR, mirroring and extraction magnetic fields within the source. The magnetic field strength is greater than the 875 Gauss required for ECR at 2.45 GHz throughout the

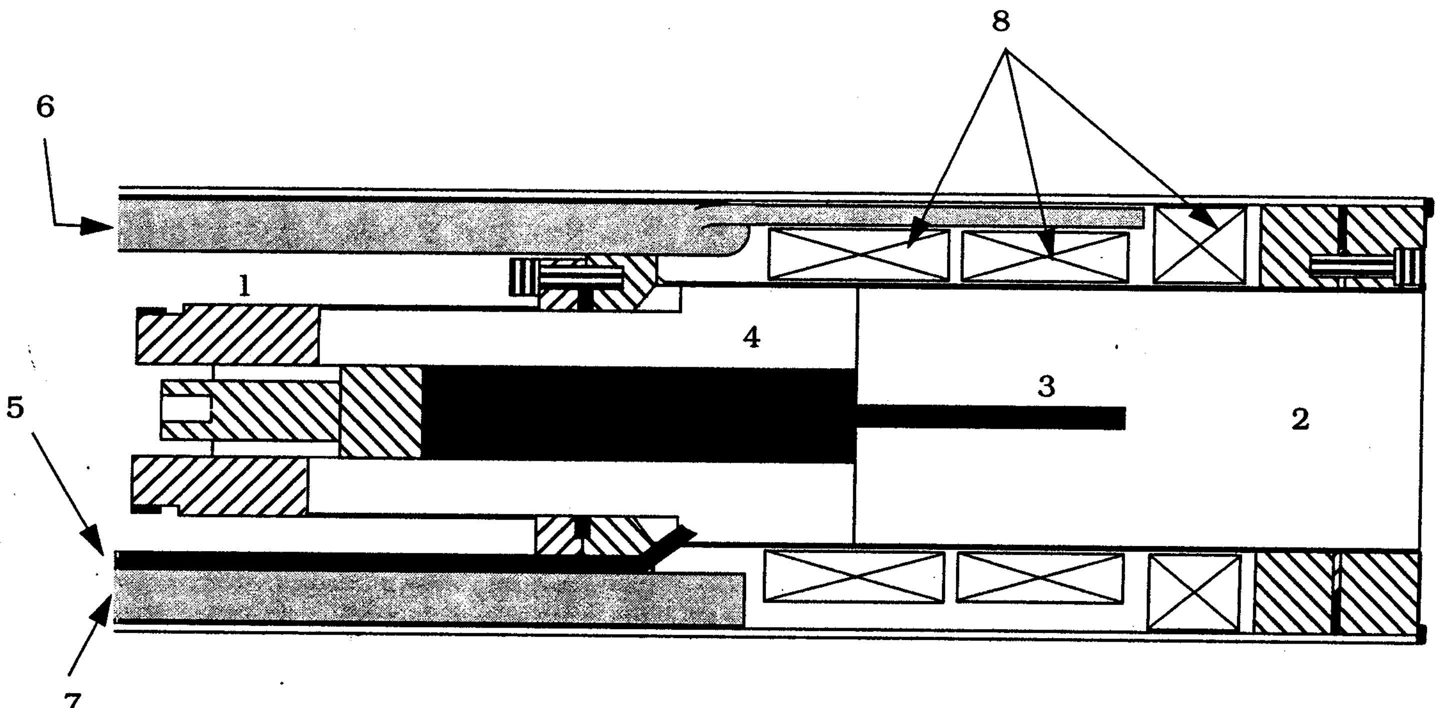

Figure 2.6 N. C. State/ASTeX Compact ECR Plasma Source

1. N-type 50 Ω coaxial feedthrough
2. Plasma cavity
3. Microwave Antenna
4. Boron Nitride insulator
5. Gas input
6. Water inlet
7. Water outlet
8. Electromagnets

plasma generation region, as measured on the axis of the source. Separate position and current controls for each magnet provide flexibility with specific magnetic field configurations, proving specifically useful during the initial design testing and optimization of the source. Due to low input power requirements for plasma ignition (maximum of about 120 W), and an external tuning mechanism for impedance matching, no circulator or dummy load is needed, making the microwave circuitry simple. The body of the source is made of a 13 inch (33.0 cm) long stainless steel tube and has an inner diameter of 2.3 cm, and an outer diameter of about 5.7 cm. Since the discharge generation region is fixed in dimensions, the overall length of the source may be varied, as required by the application, similar to the MPDR 610 - the plasma source that is the main subject of this dissertation.

Like the Japanese radical gun and the MPDR 610, a standard 50 Ohm coaxial cable feeds microwave power through a type N microwave connector (1) into the source, continuing into vacuum as the center conductor of a coaxial cavity structure, and terminating into an antenna (3) that protrudes inside the discharge chamber (2). A sliding slug tuner placed between the source and the microwave power supply is used to match the plasma impedance, and reduce reflected power. A BN plug (4) acts as an insulation window at the top of the source, and also prevents a discharge from being generated there. The diameter and length of the antenna is critical for the characteristics of the discharge, with best results being obtained when the antenna length is between one-quarter and one-half wavelength of the exciting microwave energy (this wavelength is 12.2 cm for 2.45 GHz microwaves). The effects of antenna diameter on plasma characteristics were studied: a large diameter (~ 5 mm diameter) gives a

somewhat "hollow" discharge with a local minimum in the center, while a thin antenna (~ 1 mm diameter) gives a more typical radial profile - maximum current density at the center, falling rapidly across the radial direction.

At MBE conditions, for which this source was tested, no cooling of the antenna was required. The housing tube of the source may be mounted on the test stand, or an existing port of an MBE machine using a standard 4.5 inch conflat flange. Gas breakdown begins at about 0.1 mTorr of pressure and for less than 10 W of power, without any need for pre-ionization of the gas. A stable discharge can be maintained over four decades of pressure ranging from 10^{-5} Torr to 10 mTorr.

Plasma parameters were measured using a cylindrical single Langmuir probe placed 15.0 cm downstream from the source, with an area of 0.1 cm^2. A Faraday cup with a collecting area of about 1 cm^2, and a QMS were also used to evaluate the performance of the plasma source. The source was characterized for 2.45 GHz input microwave power of 50 W in a nitrogen discharge at a pressure of 0.1 mTorr. It was observed that the floating potential and current density decreased exponentially with distance downstream, indicating typical ambipolar diffusion in the vacuum processing chamber. At a constant pressure of 0.1 mTorr, the ion current density was about 0.04 $mA\text{-}cm^{-2}$ for 10 W input power, and about 0.3 $mA\text{-}cm^{-2}$ at 120 W - the ion current therefore increased with increasing input power. For a constant input power of 50 W, the ion current density was 0.2 $mA\text{-}cm^{-2}$ at 0.1 mTorr, and about 0.4 $mA\text{-}cm^{-2}$ at 1 mTorr - the ion current increased as pressure was raised. At 0.1 mTorr and 50 W absorbed power, electron temperatures of above 100,000 K and ion densities of about 10^{10} cm^{-3} were measured outside the plasma cavity.

When the discharge gas was switched from nitrogen to hydrogen, no further tuning of the source was required to optimize power transfer to the plasma load. Ion current densities for a hydrogen plasma were about 5-6 times higher than those for nitrogen at similar gas flow rates and power conditions. Also, the electron temperature of a hydrogen discharge was lower (about 70,000 K) than that of a nitrogen plasma for the same operating conditions. The floating potential for hydrogen was found to be positive (+5 V), while it was negative for nitrogen (-15 V). QMS studies indicated the presence of N_2^{1+} and N^{1+} ions in a nitrogen discharge, with the N^{1+} concentration constituting about 15% - 20% of the total ionized species. This ratio was seen to be somewhat independent of discharge pressure and input power.

The source has been successfully used in an MBE machine for low temperature (400°-600° C) and low pressure (5×10^{-5} to 1×10^{-4} Torr) epitaxial growth of III-V nitride thin films (like GaN, and AlN) [Sit-90b, Pai-90, Mou-93]. Other potential applications include high T_c superconducting thin film deposition using oxygen radicals, for cracking various molecular gases (like organometallics), and also for in situ substrate cleaning prior to deposition using reactive atomic hydrogen. A commercial version of the source is available from ASTeX Inc. of Woburn, Massachusetts.

2.2.7 The NTT LSI Laboratories Compact ECR Ion Source

The parent design of this high current ion source was developed in 1987 [Tor-87] for mass production of SIMOX substrates in oxygen ion implanters. Since then, very active research and development has led to several variations

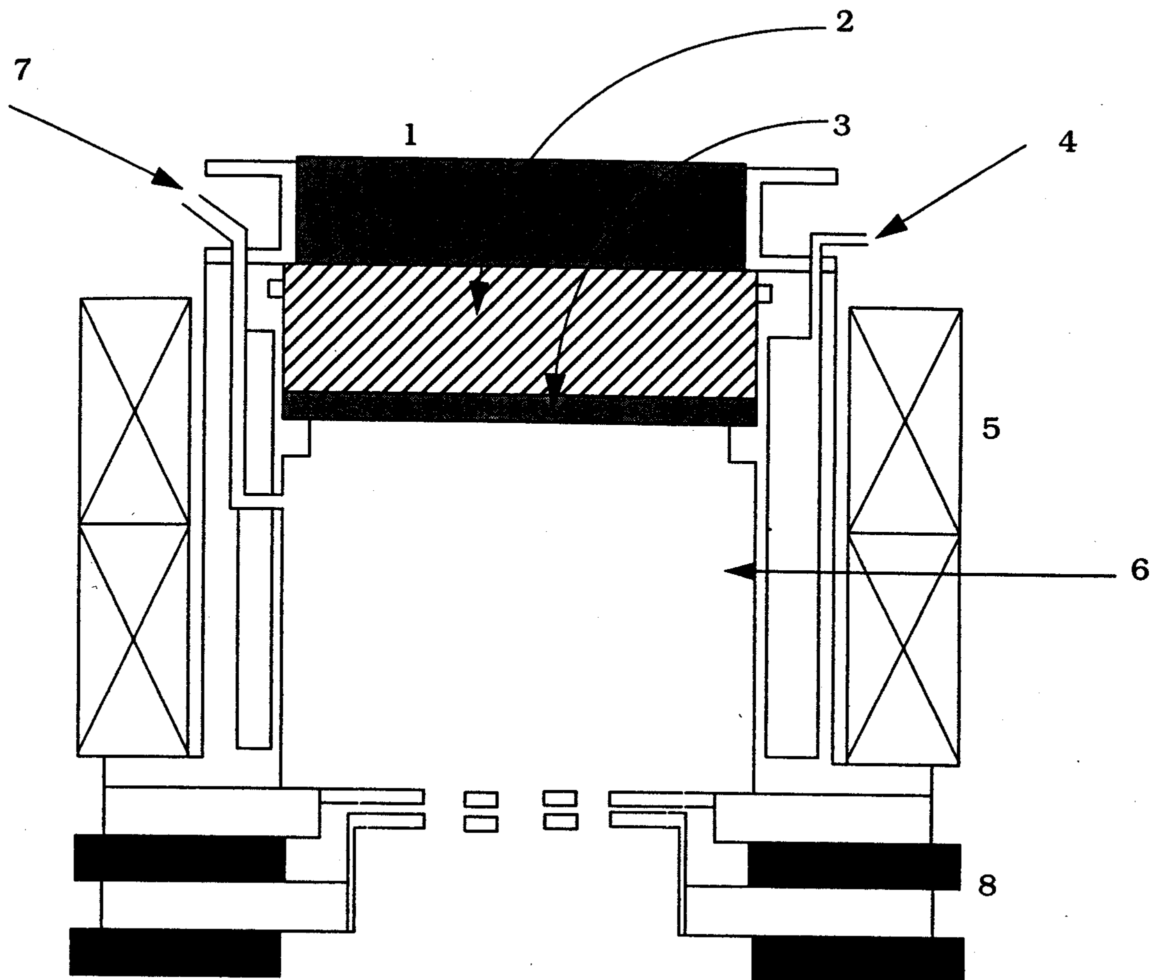

Figure 2.7 NTT LSI Laboratories Compact ECR Ion Source

1. Waveguide Filled with Alumina
2. Quartz
3. Boron Nitride/Alumina
4. Water Cooling
5. Magnetic Coils
6. Plasma Chamber
7. Gas Inlet
8. Extraction Electrodes

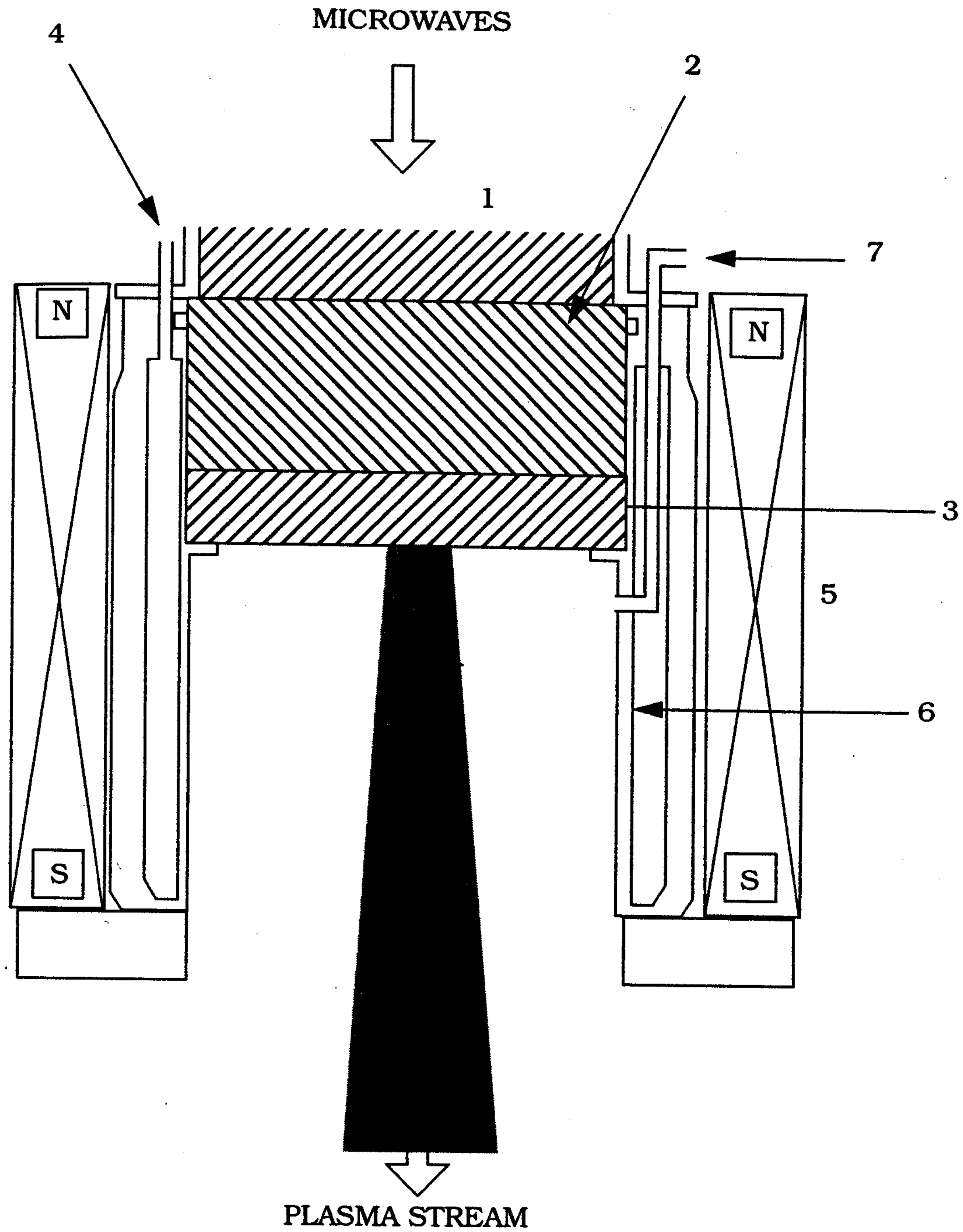

Figure 2.8 NTT LSI Laboratories Compact ECR Ion Source with permanent magnets

1. Waveguide Filled with Alumina
2. Quartz
3. Alumina
4. Water Cooling
5. Permanent Magnets
6. Plasma Chamber
7. Gas Inlet

being reported in at least three journals, each with minor modifications to the preceding design along with the operational results of these modifications [Shi-89, Tor-90, Shi-91, Tor-92, Shi-93]. Since this section discusses several versions of essentially the same source, a brief introduction to the original source is first presented. Broader coverage of the compact versions is provided later in this section.

Two of the compact versions are shown in Figures 2.7 and 2.8 (not to scale). The basic design of all the variations of this source consists of essentially four components, as shown in Figure 2.7: a cylindrical plasma chamber (6); a multi-layered dielectric window for microwave transport, vacuum seal and prevention of damage from back-streaming energetic electrons (1, 2, 3); an extraction system (8) when beams are to be extracted; and either some coils, or permanent magnets (5).

In the original report [Tor-87], the plasma chamber had a diameter of 11.0 cm, with a height of 9 cm. Microwaves were transmitted into the source through a rectangular waveguide. A double layered microwave window was used for the electromagnetic wave transmission and vacuum seal, and several combinations of quartz, boron nitride (BN) and alumina were tested. It was found that the highest ion current density was achieved with a quartz and alumina combination, the alumina layer facing the plasma. Three solenoid coils were used to create the magnetic fields required for ECR and ion transport out of the source. A three grid accel-decel extraction structure with seven holes (5 mm diameter) arranged over an area of 2.0 cm diameter was used to extract an ion beam. The beam characteristics were measured with a water cooled copper plate biased positively to suppress secondary electron emission The plate was placed

about 40 cm downstream of the extraction system. At an extraction voltage of 30 kV, a very high oxygen ion current of about 160 mA, or an equivalent current density of about 120 mA-cm^{-2} was obtained. Mass spectrum studies indicated that the ratio of O^{1+} ions is more than 80%, with an equivalent O^{1+} ion current of more than 125 mA. A disadvantage of this source was that the alumina window facing the discharge was heavily bombarded by back streaming energetic particles, leading to degradation of the window, and a decreased lifetime of the source.

An improvement in the source design was reported in 1989 [Shi-89] when a triple layered window was used. Quartz formed the vacuum seal, alumina helped in microwave transmission and impedance matching of the source, and a BN layer - due to its hardness and better thermal conductivity - was used to prevent damage from energetic back streaming particles. The optimal thickness of the BN layer was determined by studying the reflection coefficient of the source as this coefficient varied for different BN layer thicknesses, the choice being made for a thickness that minimized the reflection coefficient. The window, and hence the source lifetime was increased to over 200 hours, with little damage to the BN layer. An improved extraction system allowed for stable operation over extended periods, with the same high current density as its predecessor was achieved (i.e. 80% O^{1+} ions with over 180 mA total current at 30 kV extraction potential). It was also observed that as the microwave power increased from 100 W to over 600 W, the O^{1+} concentration increased, while the O_2^{1+} density decreased.

The next modification to this source design was reported in 1990 [Tor-90] when the triple layered window was further modified to couple microwaves more

efficiently into a narrow high density plasma mode. The chamber length was optimized relative to magnetic field configuration, which was itself optimized to produce a high density plasma in the center of the source. This allowed highly efficient ion beam extraction, where the extraction region coincided with the highest density plasma confined to the center of the source. The optimized magnetic field configuration also leads to lower impurities concentration in the plasma since wall bombardment by high energy particles is reduced. The O^{1+} ion beam was transported through a commercial NV-200 implanter beam transport system with an efficiency of about 60% indicating low beam divergence, and an efficient use of the extracted current. Just like in its predecessor, the source too can provide over 200 hours of a stable oxygen plasma. Damage to the BN layer is minimized by the centralized location of the plasma generation region, and also by the efficient extraction of ions.

A compact version of the source was introduced at the American Vacuum Society (AVS) symposium, 1990 [Shi-91] with another report soon thereafter [Tor-92]. Shown in Figure 2.7 (not to scale), the compact source has a cylindrical plasma chamber with a diameter of 5 cm, surrounded by two magnetic coils (outer diameter 11 cm). These magnets provide the static magnetic field necessary for ECR, containment of hot electrons, and also ion divergence out of the source. As before, microwave power at 2.45 GHz is fed from the top of the source through a waveguide. However since the plasma chamber diameter is too small for the lowest cutoff wave mode - TE_{11} - to be propagated (which requires a minimum of 7.2 cm diameter for propagation through air/vacuum at 2.45 GHz), the miniaturized rectangular waveguide feeding the microwaves is filled with alumina. Since alumina has a dielectric constant of 9, and the cutoff diameter is

proportional to one over the square root of the dielectric constant, filling the waveguide with alumina effectively decreases the cutoff diameter by about a third of that required for a vacuum, or air filled waveguide. This alumina filled waveguide is now able to propagate microwaves at 2.45 GHz.

The ceramic window used in this modification was the original double layered design - quartz for vacuum seal, and a hard BN layer for protection from hot electrons. The thickness of the two layers was calculated such that for an assumed plasma density of 10^{12} cm^{-3}, the transmission coefficient of the microwave fields is one. A 2 cm diameter double grid extraction system (37 holes, each with a 2 mm diameter) with a 1 mm grid separation was used to extract low energy ion beams.

Plasma parameters were measured using a plane Langmuir probe (6 mm diameter) mounted at the center of the extraction electrode. Also, an ion collector placed 5 cm downstream from the extraction region measured the beam characteristics. The pressure dependence of a 200 W oxygen plasma was studied. As the pressure increased from 9 X 10^{-5} Torr to about 4 X 10^{-4} Torr (corresponding to a change in oxygen flow rate from 1 sccm to about 4.5 sccm), the ion density decreased slightly from 4 X 10^{11} cm^{-3} to about 2.5 X 10^{11} cm^{-3}. For the same increase in flow/pressure, the electron temperature decreased from 12 eV to about 7 eV. When the BN layer was replaced by alumina, there was a twenty fold increase in the oxygen ion density, the maximum being about 10^{13} cm^{-3} (200 W absorbed power, 0.24 mTorr pressure). However, the source lifetime suffers with this replacement since alumina is not as resistant to sputtering as BN. An anomalous behavior was observed in the electron temperature dependence on input power for the two types of microwave

windows: T_e increased with increasing power for a quartz-BN window, but T_e decreased when power was raised for a quartz-alumina window. This abnormal temperature dependence on window type has not been explained yet.

Preliminary ion extraction experiments at 1 kV extraction voltage (100 W oxygen plasma, 1 sccm flow), indicated that the source was able to provide a maximum ion current density of about 1.3 mA-cm^{-2}. Beyond 100 W, the ion current density (measured with a collector placed 5 cm downstream) decreased, although the total current density increased. This may be because as the power was raised, the plasma density increased, and hence, the plasma boundary (the meniscus) began to extend beyond the extraction holes, thereby increasing the species' divergence. The total ion current increased due to the higher ion density, however the current density measured by the collector decreased due to the larger divergence of the beam at higher powers. The radial profile of ion saturation current at 20 cm downstream (6 sccm, 200 W oxygen plasma) shows a relatively flat distribution, with a maximum of about 1.5 mA-cm^{-2}. Potential applications for this compact version of the source are expected to be in etching, oxidation and plasma assisted deposition.

Yet another version of the original ion source was introduced at the 1992 AVS symposium [Shi-93]. This design is shown in Figure 2.8 (not to scale). This too is a compact source, with most design parameters the same as above, but with one major change - the electromagnetic coils of the previous versions are replaced by permanent magnets (5). This simplifies the source design, although the diameter of the plasma chamber had to be further reduced to 40 mm to accommodate the bulky axially directed Sm-Co magnets (outer diameter 10 cm, inner diameter 6.2 cm, 10 cm high). The magnets successfully produce a

magnetic cusp mirror field, with a mirror ratio of about 2 at the exit of the source. The peak field strength is about 920 Gauss, and is maintained relatively uniform over the entire plasma excitation region. The maximum current density is observed at 920 gauss, rather than the 875 gauss for ECR 2.45 GHz. The multi-cusp mirror configuration effectively confines excited electrons in a donut shaped region at the output of the source, which is then able to generate high density of multiply charged ions.

The resulting high density mode plasma stream was very collimated and directional with a diameter of about 1.8 cm, and a divergence angle of about 3 degrees. Saturation current density measured with a Langmuir probe (6 mm diameter, placed 12 cm downstream) at a bias of negative 80 V was seen to be about 18 mA-cm^{-2} for a 200 W, 10 sccm (about 1.2 mTorr) argon discharge. This current density was higher than that obtained in the previous plasma source design with the magnetic coils. At 5 cm downstream, the saturation current density peaked at about 80 mA-cm^{-2} for a 200 W, 10 sccm argon discharge, decreasing rapidly with radial distance. As the argon flow rate was reduced further, the peak current decreased also, until at about 2 sccm, there was a local minimum at the center of the distribution - a "hollow" beam. This is claimed by the authors to be due in part, to the smaller number of available energetic electrons at such low pressures in the donut shaped confinement region near the output of the source. At a constant power (200W) and flow (10 sccm), the radial profile of the ion beam became more uniform as the probe was positioned further downstream from the generation region. As expected, the saturation current density increased monotonically as input power was raised (at fixed flow rates of 4, 6 and 10 sccm), and also as flow rate/pressure was increased (at fixed

power levels of 50 - 200 W).

QMS measurements indicate a high level of Ar^{2+} ions in the plasma, the ratio of Ar^{2+} to the total ion current (Ar^{+} + Ar^{2+}) increasing with argon flow, and being as high as 50% for a 6 sccm argon discharge. According to the authors, the increase in the 2+ charge state production is probably due to an elevated ion density at higher pressures. This elevated 2+ production may also be due to the confining cusp shaped field produced near the exit of the source. The applications for the various versions of this source are postulated to be for thin film processing such as MBE, and to provide multiply charged ions (oxygen) for high energy ion implantation.

2.2.8 The Oxford Applied Research Atom/Radical Beam Source

An atom/free radical beam source has been developed by Oxford Applied Research of UK and was introduced at the European Vacuum Conference in 1990 [Dav-90b]. Since then, several studies on this source - mostly applications oriented have been conducted [Cla-88, Hok-91, Par-90, Qiu-91, Wat-91]. The electrodeless source, operating at the radio frequency (rf) of 13.56 MHz excitation frequency is shown in Figure 2.9 (not to scale), and is essentially a free radical source due, as claimed by the authors, to the unique electric potentials generated within the discharge tube (6) that prevent most charged particles from escaping the tube. The ion/electron density in the beam is, therefore claimed to be negligible. Note that this is the only inductively coupled rf source that is reviewed in this chapter. The standard body length is 29.0 cm and the vacuum seal is made through a DN63CF flange (3). Similar to the

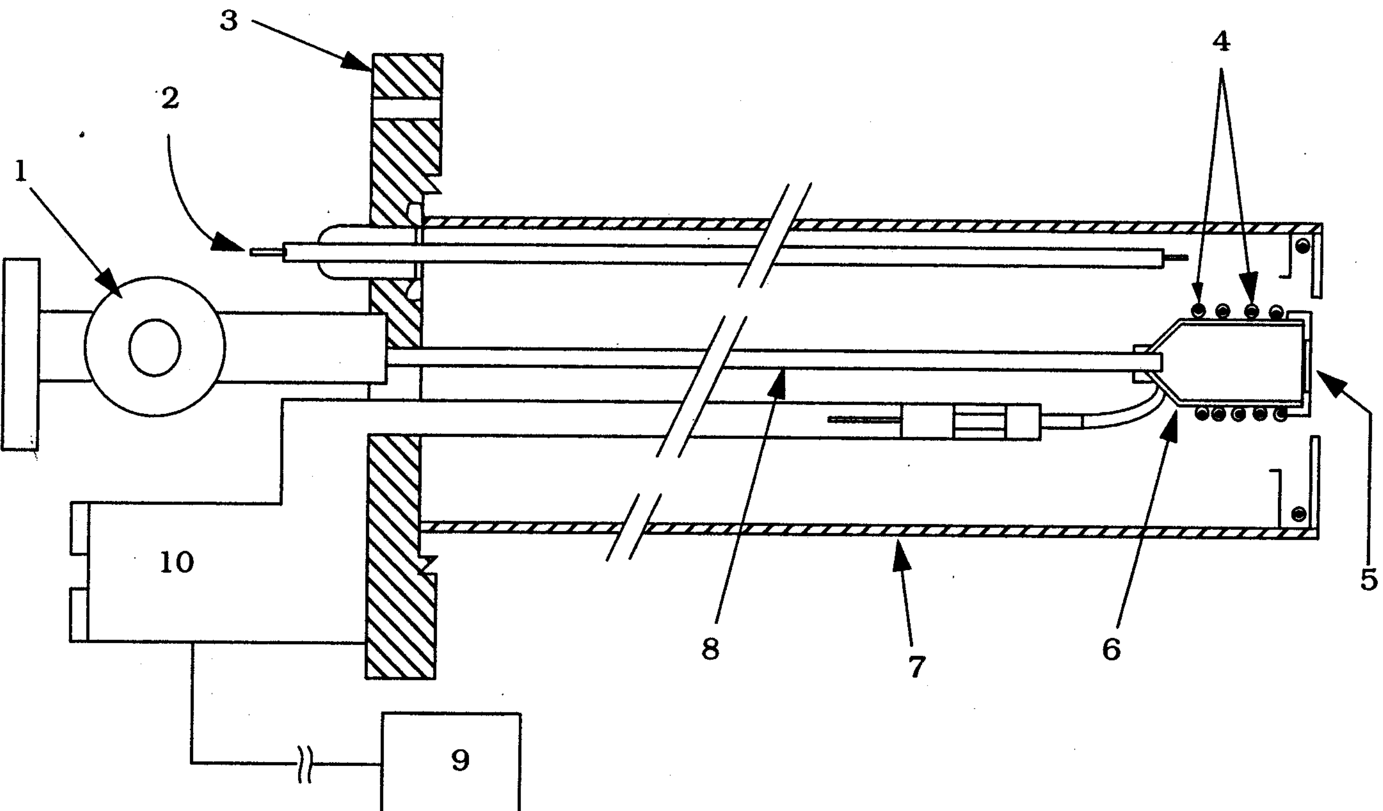

Figure 2.9 Oxford Applied Research Atom/Radical Beam Source

1. Gas Inlets
2. Water Feed
3. DN 63 Conflat Flange
4. Water Cooled RF coil
5. Beam Exit
6. Discharge tube
7. RF Shield
8. Gas Feed
9. RF Generator
10. RF Matching Unit

Japanese radical gun, the over-all length of the source is application specific, since the actual discharge producing region is small and at the end of the source. The rf coils (4) around the discharge tube are water cooled, while the material of the tube is dictated by the application- high purity quartz is used when the source is to be used for producing oxygen radicals since quartz has a very low recombination coefficient for atomic oxygen. Ultra-pure pyrolytic boron nitride is used for UHV applications. The discharge gas is fed through a small alumina tube (8) that extends up to the plasma containment tube. The source produces high densities of atomic radicals which have been found useful in oxide/thin film deposition, low temperature etching, hydrogen radical cleaning of wafers, and low temperature nitriding.

Most studies done with this source have been application oriented, with some evaluation data available. Performance characteristics regarding the atomic flux were measured using the quartz crystal microbalance (QCM) for O^*, H^* and N^* radical species. The oxygen atom flux was estimated to range between 10^{14} cm^{-2}-s^{-1} and 10^{15} cm^{-2}-s^{-1}. For a 500 W discharge, and at a pressure of 2 X 10^{-5} Torr, the radical flux is about 5 X 10^{14} cm^{-2}-s^{-1}, increasing to about 4 X 10^{15} as the pressure is raised to 2 X 10^{-4} Torr [Loc-91, Dav-90b]. In situ reflected high energy electron diffraction (RHEED) analysis confirmed the QCM oxidation data. XPS spectra of copper films after exposure to an oxygen beam were found to be identical to the Cu(II)O spectrum, while exposure of the film to molecular oxygen was found to produce no significant oxidation. It was therefore confirmed that it is the reactive oxygen radicals that oxidize the film, and molecular oxygen has little or no oxidizing effect. RHEED and Auger Depth profile electron spectroscopy for GaAs substrates passivated by nitriding have

also been used to monitor the performance of the radical source. QCM studies were used to test low temperature etching of GaAs by radicals using a CCl_2F_2 discharge.

A comparison of the atomic radical production between this radical beam source, an ECR source (the Michigan State University/Wavemat MPDR 610™, to be detailed later in this dissertation), and a microwave source (the Evanson cavity), seems to indicate that the gas flow rate needed to produce approximately the same amount of atomic oxygen (as measured with a QCM) was much lower for the Oxford rf source [Loc-91] than for the other two sources. The cracking efficiency for oxygen in this source is estimated to be about 30%. The source has also been used in MBE growth of InN and GaN films [Hok-91] with a nitrogen discharge, and as a source to incorporate p-type nitrogen acceptor impurities in ZnSe/GaAs epitaxial layers using a nitrogen atomic beam doping during MBE growth [Par-90, Qiu-91]. A hydrogen radical beam from this source has been used in metal organic MBE (MOMBE) to effectively remove the native GaAs oxide layer [Wat-91]. This atomic radical beam source has therefore been extensively characterized and practical applications have been aggressively explored. A commercial version of the source, called the "Oxford Applied Research, Model MPD21" is available from Oxford Applied Research.

2.2.9 A 2.45 GHz Compact ECR Source from France

Preliminary results of a new compact ECR ion source from Paris XI, France were presented at the International Conference on Ion Sources (ICIS-93) at Beijing, China [Bou-94], and subsequently published in the proceedings. This

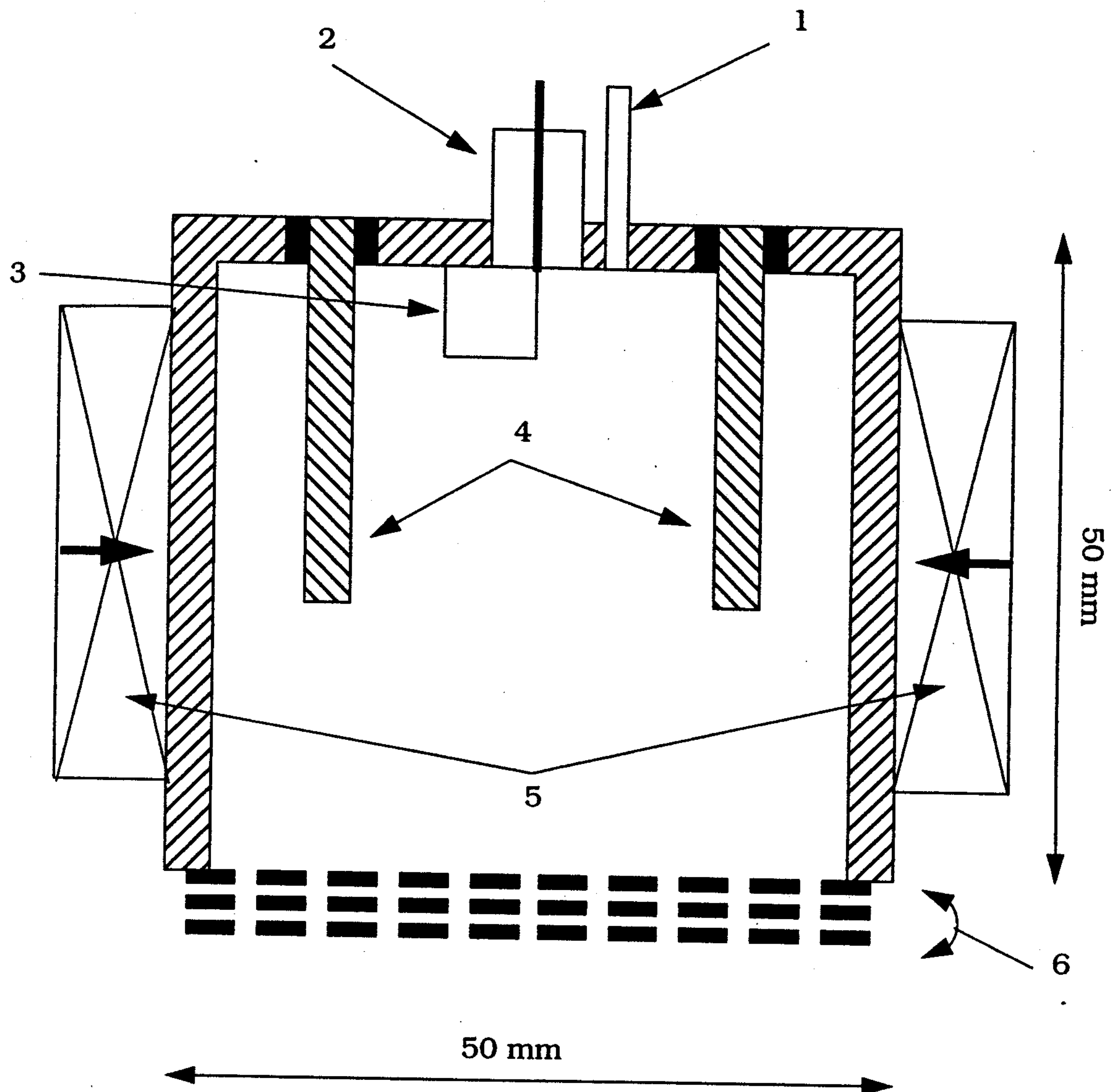

Figure 2.10 Compact ECR ion beam source from France

1. Gas Inlet
2. SMA Connector
3. Excitation loop
4. Lecher lines
5. Permanent Magnets (SmCo)
6. Multi-aperture extraction optics

new source incorporates the unique principle of coupling energy into the discharge through two shielded quarter-wavelength "Lecher line resonators". As can be seen from Figure 2.10 (not to scale), the source is very simple in design and quite compact - only 5.0 cm in diameter (not including the magnets), and 5.0 cm high. The stainless steel discharge chamber is surrounded by four radially magnetized parallelepiped shaped Sm-Co magnets measuring 2.5 X 2.5 X 1.2 cm^3. These magnets create a multi-cusp static magnetic field configuration, generating the 875 Gauss field strength for ECR. Discharge gas is leaked through a feedthrough on the top of the source. The two Lecher lines, or pads, are placed 30 mm apart and are coaxially coupled to an off-axis square loop antenna. The Lecher lines fulfill the orthogonality condition between the static magnetic field and the microwave electric field.

Microwave power at 2.45 GHz is supplied to the antenna through a 50 Ω coaxial SMA connector. Depending on the orientation of the loop with respect to the Lecher lines, there are two separate electromagnetic modes that can be excited in the microwave cavity. In the "odd mode," electrical energy is concentrated between the pads and the chamber wall, and in the "even mode," the energy is confined between the two pads. The loop orientation for these two modes is 90° apart. A hybrid dual mode with characteristics of both electromagnetic modes described above can be excited if the loop antenna is part way between the two extreme orientations - that is, at 45°. Initial experiments with the source were conducted with an external tuning mechanism to optimize the source performance. However, this was apparently soon discarded, and source optimization was conducted essentially through selecting the exact Lecher pad length and maximizing the measured current density. The length of

these resonators was restricted to a range from 2.5 cm to 3.5 cm, since a stable discharge ignition was not possible for pad lengths beyond this range. An ion beam was extracted through the bottom of the source using a multi-aperture triple grid electrode system.

A fixed Lecher pad length of 30 mm was used in all source characterization. The hybrid dual mode produced the most ion current density among the three electromagnetic modes, possibly due to the more distributed electric fields through the plasma generation region. Incident power was kept constant at 75 W, and the source was operated at the dual hybrid mode, with an extraction potential of 100 V. As a function of argon discharge pressure, the current density displayed two local maxima - at about 2.5 10^{-3} mbar (2 mTorr) with a current of 0.5 mA-cm^{-2}, and at about 2 X 10^{-2} mbar (15 mTorr) where the maximum current was 0.7 mA-cm^{-2}. At the lower pressure, the current density maximum is attributed to the resonance of the Lecher lines that produces a maximum ionizing electric field at the end of the line structure. The second maximum at the higher pressure is due to an increase in the collision frequency of the electrons with neutrals in the chamber. This is confirmed by the fact that the maximum at higher pressure is independent of the Lecher pad length, while the maximum at the lower pressure is highly dependent on this length. At 29 mm and 31 mm Lecher line length (optimal length is 30 mm) the low pressure maximum is completely blurred out, while the high pressure maximum is relatively undiminished.

At a constant pressure - 9 X 10^{-3} mbar (about 7 mTorr) the ion current density increases almost linearly as the power is increased. Plasma ignition occurs with a minimum of about 40 W, producing a current density of 0.4 mA-

cm^{-2}, which increases to about 1 $mA\text{-}cm^{-2}$ as power is raised to 110 W. If the input power is now reduced, a stable discharge can be sustained to power levels as low as 20 W.

Although particulate generation due to ion bombardment on the Lecher lines in the discharge has not been tested, this source is capable of sustaining a high intensity discharge from which high beam currents may be extracted. Applications of the source are expected to be for reactive species cleaning or other surface treatment of substrates, MBE, or as a neutralizer for ion assisted deposition techniques.

2.2.10 The Microscience Inc. Ion Beam Source

Microscience, Inc. of Massachusetts has recently introduced a compact ECR ion beam source capable of producing high intensity beams at medium energies (200 - 1700 V) [Pop-94b]. This source is shown in Figure 2.11 (not to scale). It's design is interesting in that it employs a hybrid technology to inject microwave energy into a plasma cavity that has a diameter below cutoff for 2.45 GHz microwave transmission. Sakudo et al. [Sak-77] used an antenna fed microwave cavity with a high magnetic field (Section 2.2.2), while Shimada et al. [Shi-91] utilized microwave transparent windows for their design (Section 2.2.7), and used alumina as a dielectric that essentially reduced the cutoff diameter of the source (or waveguide) for microwave transmission at 2.45 GHz. The new Microscience Inc., source uses an antenna enclosed inside an alumina cup that also acts as the dielectric window of Shimada's design. This is somewhat similar to the antenna being enclosed by an alumina cup in the Russian design [Sha-90]

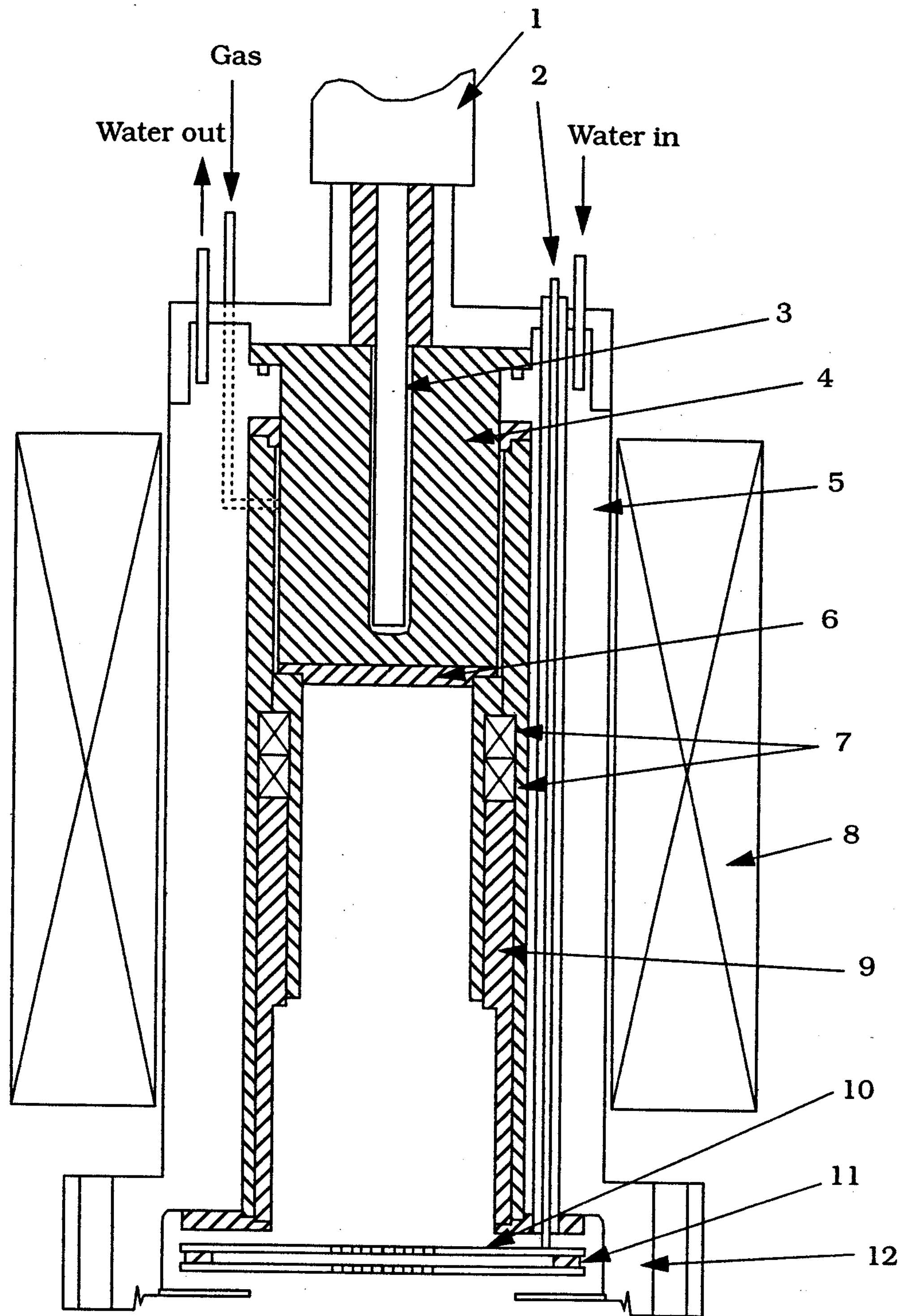

Figure 2.11 Microscience, Inc. Compact ECR Ion Beam Source

1. Type N Coaxial Connector
2. High Voltage Bias Feedthrough
3. Half wavelength Antenna
4. Alumina Cup
5. Plasma Chamber
6. Alumina Spacer
7. Permanent Magnets
8. Electromagnet coil
9. Boron Nitride Encloser
10. Bias Grid for Ion Extraction
11. Alumina Spacer
12. 4.5 Inch Conflat Flange

of a compact ECR ion source (Section 2.2.3) except that here, the alumina fits completely into the quartz chamber. Construction of this source is now described in detail.

The plasma chamber (5) is 5.5 cm in diameter, and 12 cm in length, and is attached to a 4.5 inch Conflat flange (12) on the bottom. Low power microwaves (less than 200 W) at 2.45 GHz are fed into the plasma chamber through an antenna attached to a type N connector (1). The antenna (3) diameter is substantially larger than that of the inner conductor of the cable to retain the continuity of the 50 Ω microwave circuitry. This antenna is enclosed by an alumina cup (4) that fills part of the source body, and also makes the vacuum seal with a Viton O-ring. The antenna is therefore, on the atmospheric pressure side of the alumina cup. This antenna enclosing cup is shielded from the high intensity plasma with an alumina spacer (6).

Two Sm-Co ring shaped magnets (7) with 2.5 cm inner diameter below this alumina spacer are placed a few mm downstream from the alumina cup, with a BN cylinder (9) protecting the magnets from the plasma. These magnets provided the static magnetic flux density for ECR. There is also a large current coil (8) around the outside of the source whose magnetic field strength and relative position can be adjusted. This coil aids in sustaining the plasma and efficiently extracting an ion beam by controlling the divergence of the ions out of the source. The body of the plasma chamber is water cooled. For the low power levels at which this source was used there was no need to cool the antenna, although it is provided with air or water cooling fixtures. Discharge gas is leaked through a feedthrough on the top, and injected into the plasma chamber through tiny holes made in the BN cylinder.

An ion beam may be extracted through two multi-aperture grids (10) about 8 cm downstream from the alumina spacer. Both grids are 1 mm thick pyrolytic graphite, separated from each other by a 1.5 mm thick alumina spacer. Each grid has 65 holes (each hole 2 mm in diameter) leading to a hexagonal beam extraction area of about 2 cm^2. The body of the ion source is always grounded, while the plasma is placed at a higher potential. Hence the need for the BN cylinder that electrically isolates the grounded cavity from the high potential plasma discharge. The plasma grid (closest to the discharge) is biased positively (DC) at 150 - 2000 V, while the second grid (called the suppressor) is biased at a negative potential of about -50 to -1000 V. Due to this high negative voltage, secondary electrons are repelled from the grid and do not contribute to the total grid (and beam) current.

Different BN liners and other ceramic enclosures are used in this plasma source to prevent shorting or arcing across biased surfaces, and plasma ignition in regions other than the discharge chamber. As mentioned before, these dielectric liners also allow the body of the plasma source to be at ground potential, while the plasma inside the source is raised to the high extraction potentials.

The source normally operates at low power levels (30 - 200 W incident power, with about 10% reflected back from the source), and generates ion beam currents of 0.5 - 3.0 $mA\text{-}cm^{-2}$ with ion beam energies of 200 - 1700 V. Despite the alumina cup that fills the top part of the plasma chamber that should allow microwave transmission, the authors claim that it is the evanescent microwave fields that sustain the plasma. Hence the magnetic field configuration is designed such that the ECR zones are only a few milli-meters away from the

alumina spacer where the attenuating electric fields are strong enough for ECR breakdown. While characterizing the source, the operating pressure ranged from 2×10^{-5} Torr in the beam line, to about 2-3 $\times 10^{-4}$ Torr. This pressure is limited on the low end by the 1 sccm minimum flow rate of the discharge gas, and on the high end by the minimum necessary ratio of ion acceleration grid current to the ion suppression grid current. (If pressure is raised beyond this, no beam can be extracted because the current exceeds the maximum current rating of the power supply. This "problem" will re-surface when the MPDR 610 is used as an ion beam source later in this dissertation.)

It was noticed that the power required to breakdown the gas into a discharge remained almost unchanged as the discharge pressure decreased, up to the minimal pressure of about 2×10^{-5} Torr. The breakdown power (P_{br}) for igniting a discharge was measured to be about 5 - 20 W in this pressure range. If the pressure was reduced further, P_{br} increased dramatically, in part due to the rapidly decreasing collision frequency between electrons and neutrals that sustains the discharge. For example, at a pressure less than 1×10^{-5} Torr, P_{br} is greater than 250 W. A similar dependence of P_{br} was observed with a variation of the magnetic coil current. At 5 - 6 Amps of coil current, the power required to ignite a discharge was several hundred Watts, but as the coil current increased (and the magnetic flux density increased), the break down power requirement dropped dramatically, and ignition occurred at less than 20 W. Note that it is the axial component of the coil magnetic field that is primarily responsible for ECR break down in the plasma chamber near the alumina spacer.

Beam characteristics of the source were measured primarily by studying the current being extracted through the acceleration grid. Although not quite the

same, the ion beam current was taken to be equal to this acceleration grid current. Ion beam current increased as input power was raised. About 8 mA of total current was extracted at a voltage of 1000 V (with a suppression voltage of -220 V) from a 250 W argon discharge (7 X 10^{-5} Torr). Further increase in the forward power led to a saturation of the extracted current, due in part to a growth in the reflected power. For 100 W incident power, 25 W were reflected for a 7 X 10^{-5} Torr argon discharge. However, if the power was raised to 250 W for the same discharge, the reflected power rose to about 50 W. Another reason for this saturation may be the de-focussing effects of the beam optics once the ion density begins to increase as the power is raised. The Child's law "3/2" power variance of extracted current with extraction voltage was not observed, which may be because the extracted current is limited by the plasma density, and not the acceleration voltage. For an argon plasma with an estimated electron temperature of about 3 - 5 eV, the ion beam current corresponded to an argon ion density of about 6 - 9 X 10^{10} cm^{-3} (assuming that the beam has an extraction cross section of about 3 cm^2).

Once ignited, a plasma discharge of this source could be easily sustained even without magnets. The two ring shaped permanent magnets were pulled from the source, and this did not impede the process of plasma ignition. Once a stable plasma was generated, the current in the external coil too could be reduced to zero. The plasma was still very stable, though at a lower density, switching off once the ion density went below the critical density (about 7 X 10^{10} cm^{-3} at 2.45 GHz). As expected, the quenching of the plasma was accompanied by a sharp increase in the reflected power.

The source was used for sputter deposition of various metals (Al, Mo,

SiO_2, Si, etc.). Based on the beam characterization, the following optimal conditions are recommended for these applications: Microwave power of about 100 W, argon pressure of 7 X 10^{-5} Torr, coil current about 22 A, acceleration voltage 1000 V and suppression voltage about -220 V. Under these conditions, the ion beam current is about 4 mA, and the suppression grid current about 0.05 mA. When a conducting target is placed 17 cm downstream at a 45° angle, the beam divergence angle could be determined from the impact marks of the beam. The minimum half angle of divergence for the beam was measured to be about 4° at 2 X 10^{-5} Torr discharge pressure and with 1000 - 1500 V extraction voltage. This rose to about 6° at 2 X 10^{-4} Torr and 200 - 400 V extraction voltage. The divergence angle increased if the target was a dielectric, and also increased when the coil current was raised. Other characterization results, and practical applications of this source are being considered.

2.3 Discussion - Ion/Ion Beam/Plasma Sources

Table 2.1 summarizes all the information pertaining to the design of the ion/plasma/ion beam sources discussed in Section 2.2. For each source, the first column indicates the reported, or most probable application - as an ion beam, free radical, or a plasma source. The next two columns indicate whether the source is ECR based, and if it has a resonant cavity structure. Note that "resonant" cavity does not necessarily mean that the dimensions of the microwave (or plasma) cavity can be changed to tune the source for specific electromagnetic modes - only the MPDR family of sources have "tunable resonant cavities" in which dynamic modification of the cavity height may be

Compact Source	Type			ECR	Resonant Cavity	Dimensions (cm)			Magnets		Energy Transfer			Tuning				Beam Extraction	
	Ion Beam	Plasma	Radical			ID	OD	Height	Permanent	Coils	Window	Ant.	RF	none	stub	Ant.	Cavity (dimensions)	2 Grid	3 Grid
1. Kyoto University	X			X			5	6.5	X			X		X				X	
2. Hitachi	X						6			X		X			X				X
3. Russia/Epiquip		X		X	X	11.4		16	X	X		X				X			
4. Radical Gun from Japan		X	X	X	X	3.5	1		X			X				X	X		
5. RIKEN	X			X		7		5	X			X			X				X
6. ASTeX		X		X	X	5.7	2.3	33		X		X				X	X		
7. NTT LSI (a)	X			X			10.8	7-9		X	X			X					X
(b)	X			X		11	5			X	X			X					X
(c)		X		X		10	4	10	X		X			X					
8. Oxford Radical Source			X					29					X	X					
9. Paris XI	X			X		5		5	X			X				X			X
10. Microscience Inc.	X			X	X		5.5	12	X	X	X	X		X				X	

Table 2.1 A comparison of compact ion/plasma/ion beam sources

used to match the plasma impedance and decrease the reflected power, thereby increasing power coupling to the plasma load. (This tuning may also be done using external stub, or EH tuners as in the case of the ASTeX compact source.) In several cases, the authors report that their source has a resonant cavity - this may mean just that the source is ECR based, and not the EM resonance which, as mentioned earlier, is a different issue altogether. The source dimensions are provided (where reported) to give an indication of the size, and are followed by the type of magnets employed by the source.

Note that only the Oxford rf source has no magnets, since it is a free radical source, and free radicals do not require ECR, focussing, or diverging magnetic fields. The next column shows the method of energy transfer - via antenna, or microwave transparent ceramic windows, or rf coils, and is followed by information on external tuning mechanisms. For the sources where the antenna is used to inject microwaves into the plasma, and minimize the reflected power (the Russian compact source, or the ASTeX compact source, for example), the dimensions of the antenna, and its relative location to the discharge are important. Some sources, like the Russian compact source have a "static, or discrete antenna tuning," where the antenna dimensions and location are fixed a priori, and once the experiment is under way, the antenna remains fixed. The MPDR sources, on the other hand have "dynamic" tuning where antenna locations may be adjusted during the course of the experiments to match the changing impedance of the plasma load. Finally, for ion beam sources, the type of extraction system is indicated in the last column - whether the beam is extracted from a two grid, or a more typical three grid system.

As the different columns in the table are compared, several interesting

points come to light. Most of these sources have been designed for a specific purpose - to generate an ion beam, or a reactive radical beam, or to create a free flowing quasi-neutral plasma that impinges on the substrate. However, for some sources, like the MPDR 610, the addition of extraction grids can easily convert a plasma source into an ion beam source, as will be seen in Chapter Nine. Also, external magnets, like those for the radical gun from Japan, can bend the ions away from the substrate, generating a reactive radical rich beam. Hence there is flexibility in the applications of some sources.

Almost all the sources employ electron cyclotron resonance for generating the plasma, the significant omissions being the rf coil based Oxford radical source and the Hitachi "non-ECR" ion beam source (the latter falling under the broader, and more recent terminology of "wave heated discharges" [Lie-94]). Hence, for the ECR and ion transport requirements, all sources, other than the aforementioned radical source from Oxford Applied Research, have permanent magnets, or current coils (or a combination of both). Many sources have specifically designed magnetic field configurations that provide the ECR fields, while at the same time helping in efficient ion extraction from the discharge generation region as the ions follow the magnetic lines of force out of the plasma source. In general, current coils (usually solenoids) provide flexibility to modify the magnetic field configuration around the plasma but they are normally bulky, and also lend a degree of complexity to the source design. Power costs, current carrying leads, and heat dissipation are also some other factors that make permanent magnets more appealing to some plasma source designers who want to reduce the complexity of operation and overall size of the source.

As mentioned earlier, of all the sources, only the MPDRs have tunable

resonant cavities, through which microwave power is efficiently coupled to the plasma load. This is usually done by matching the impedance of the load to that of the microwave transport device (either a waveguide, or a coaxial cable). Other plasma sources (like the ASTeX compact source) also match the load impedance by employing stub, or EH tuners. Due to efficient power coupling, tuning allows a source to be operated with less input power, while protecting the cables, waveguides and other microwave apparatus from excessive heating due to large reflected power. Tuning structures also allow the flexibility of dynamically modifying the cavity to match the power as plasma load impedance varies with pressure, power, gas type, or other transient changes without having to switch off the plasma source. Note that some source designs (like the Chinese version of the Ishikawa small source) have no external tuning mechanisms, and have to operate at times with up to 60% reflected power.

Power transfer to the plasma load is an important factor in designing a plasma source. The Oxford rf source of course, employs rf inductive coils to launch the microwaves at 13.56 MHz, but most other sources use some sort of antenna to launch the 2.45 GHz microwave energy. In some sources the antenna is outside of vacuum (like the MPDR 610 - as will be seen in Chapter Four), while sources like the Kyoto University small source immerse the "T" shaped antenna into the plasma. Another method of power transfer is via direct feed from the waveguide through ceramic windows that are transparent to microwaves at 2.45 GHz - this technique is used in all the NTT/LSI sources, where Shimada et al. have designed several versions of their source with multi-layered ceramic windows with specific thickness - allowing a transmission coefficient of 1 for an assumed ion density of 10^{12} cm^{-3}. Indeed, for the compact version of their

source, Shimada et al. filled part of the plasma chamber with alumina (that effectively reduces the minimum diameter required for 2.45 GHz microwave transmission in a cylindrical waveguide - or the plasma chamber - due to the higher dielectric constant of alumina). A significant development was the Microscience Inc. source design which employs a hybrid method of power transfer - a standard antenna launches microwaves into a plasma chamber, the upper part of which is fully filled with alumina (as for the compact Shimada et al. type source) that allows the chamber diameter to be below the empty waveguide cutoff for propagation of microwave fields at 2.45 GHz.

Ion beam sources use either a two grid, or three grid (accel - decel) extraction system. Some ion beams are extracted by simple multiple aperture plates biased at the appropriate potentials, while the design of other extraction systems (like that for the MPDR 610) is based on specialized spherical quasi-Pierce type accel - decel geometry. This will be seen in Chapter Nine, where beam characterization of the 610 is discussed. The main advantage of using the three grid system is that it provides more control over the beam focussing, and also the directed energy of the beam. Most ion beam sources employ grids that have multiple apertures producing a broad beam made by the summation of many small beamlets. These broad beams are important for uniform processing of large diameter substrates. An exception is the MPDR 610 that was tested with a large, centralized single aperture in the three grids.

As mentioned in the introduction of this chapter, many of the sources discussed above have been extensively used in industrial research laboratories. These applications range from nitriding GaN or AlN films (using reactive nitrogen species), high T_c superconducting film growth (using oxygen radicals), reactive

hydrogen pre-cleaning of III-V substrates prior to further operations, to providing ion beams for ion implantation, or injection of plasma species from a compact source (the MPDR 610) into the main stage of a larger ECR ion source for multiply charged species - the SCECR (see Chapter Eight for details). Indeed, the design of several ion/plasma sources discussed here has been predicated by their eventual application. For example, sources like the ASTeX, Inc. compact source, and the MPDR 610 were specifically designed to fit inside existing MBE effusion cell ports, and to create a discharge close to the substrate. Since its inception, the MPDR 610 source has found applications outside of MBE, including possible direct injection of He^{2+} (alpha particles) into cyclotron beam lines [May-95] at the Texas A&M cyclotron facility, and is evidence of the developing requirements and innovations of industrial and academic research.

2.4 Discussion - Figures of Merit

A comment needs to be made about the method of reporting the evaluation results of any ion/plasma/ion beam source. As may be discernible from the details of Section 2.2, different researchers utilize different techniques to measure the same plasma parameter - like using disc shaped, or cylindrical Langmuir probes for ion current density measurements. Often these results are also reported in different ways. This makes a comparative study of the source characteristics very difficult, since the basis for comparing the results is not the same for all sources. A common set of criteria - or figures of merit need to be developed so that the performance of any ion source may be compared to that of others in its class.

As a counter example to this problem, consider the reporting of ion beam currents obtained by multiply charged ion sources: data are presented as the total ion current of a particular charge state extracted from the source, as measured by a Faraday cup placed somewhere downstream (for example, 100 μA of O^{7+}). Since the beam is mass separated and focussed into this collector, the entire beam contributes to the total current. This allows for the performance of a multiply charged state ion source to be compared to that of another such ion source, simply based on the total current produced by that source for that particular charge state. The frequency of operation, the incident and reflected power levels, discharge pressure, type of gas or gases used, extraction apparatus design and the accel - decel potentials, and the very design of the ion source - all of these factors are important. However, ultimately it is the net current output of the ion source for any particular charge state that matters, and a better source is that which can produce the most current.

In industrial plasma sources like the ones reviewed in Section 2.2, the power levels, discharge pressure, etc. are criteria that are more important because they determine the ultimate cost of purchasing the peripheral electronics or microwave apparatus, and of operating the ion/plasma source A cost-benefit analysis would have to be conducted before a particular plasma source can be chosen over other competing technologies. Indeed this analysis may result in the choice of an ion/plasma source with a slightly lower performance, but a more simplified and cost effective turn key system of operation. Hence the importance of a comparative study.

When reporting the power dissipation in the plasma source, it must be clearly mentioned whether this is the total incident power, or the incident minus

the reflected power (called the net input power throughout this dissertation). Discharge pressure is normally stated, but usually not in conjunction with the flow rate of the operating gas. Sometimes there is a variable conductance valve in the vacuum system that allows more than one pressure in the processing chamber for any one gas flow rate. Also, a particular gas flow rate may produce a significantly different pressure in the chamber for different vacuum stations depending on the pumping capacity of each station. Hence pressure and flow rates for each experiment need to be reported simultaneously.

Perhaps the simplest measurement to characterize the output species of a plasma source, and one that is most often mis-reported is the ion saturation current (or saturation current density). Normally, this data is taken with a Langmuir probe (cylindrical, or disc shaped) biased at a certain "saturation potential". (A shielded Faraday cup may also be used to collect the ion current.) In an ideal plasma, where several assumptions like a Maxwellian electron energy distribution function are presumed true, there is a specific probe bias potential at which the collected current does indeed saturate, with no further increase in the ion (or electron) current as the voltage is raised. However, in a real discharge, many of the assumptions are not valid. Specifically, direct measurements on the MPDRs prove that the electron energy distribution function (EEDF) follows the Druyvesteyn distribution function more closely than the Maxwellian distribution (see for example, data on EEDFs presented in Chapters Four through Six). This departure from theory is reflected in the measurement of the probe current, which still increases beyond the "knee" of the I-V characteristics as the bias potential is further raised, although with a significantly lower slope.

So the question arises, about how to determine this "saturation

potential." To simply state that the saturation current density is *x* mA-cm^{-2} (total probe current divided by the probe area), is ambiguous. The probe potential at which the current data were taken (for example -50 V), and the specific coordinates of the probe relative to the discharge generation region (like distance downstream), or its radial position from the center axis also need to be reported. Along with information on discharge pressure, gas flow rate and input power, this would present a complete picture of the plasma source, and allow for a more thorough and relevant comparative study, specially in an industrial environment where companies tend to present their products vis-a-vis other competing technologies.

Similar arguments may also be made for reporting ion densities, radical flux densities and electron temperatures. These numbers (in cm^{-3}, atoms-cm^{-2}-s^{-1}, and eV or degrees K respectively) mean very little unless they are complemented with information regarding method of collection, the location of the collecting instruments, and the exact plasma parameters (like power, pressure, gas flow etc.) while data were taken. Perhaps other figures of merit like Watts per beam amp (or the equivalent eV/ion) that factor out the discrepancies in plasma source designs and measurement techniques need to be considered as important data for reporting on the performance characteristics.

2.5 Concluding Remarks

There are many other "compact" plasma sources that have not been studied here. However, all the sources reviewed in this chapter are excellent examples of the variety of engineering techniques used in designing plasma

sources, and provide a flavor of the intuitive thinking of the "sourcerers" - ion source designers. Many companies like Wavemat Inc., Oxford Applied Research, Applied Science and Technology Inc. (ASTeX), Kimball Physics, etc. offer compact plasma sources as turn key systems, indicating the confidence that these companies have in the maturity of understanding their products and the ability of their products to deliver the required plasma species for specific applications. Success of such companies over the past few years has also demonstrated the high interest of industry and research laboratories in these small plasma sources.

Experimental research is generally used to confirm theoretical predictions. Laboratory measurements can either supplement and support theory, or conflicting results may bring focus to some of the oversights that have been used to derive the currently reigning theory. Some interesting disparities become apparent when the experimentally measured plasma properties are compared to theoretical predictions. For example, at 2.45 GHz, the theoretical "critical density" limit that can be obtained in a plasma is 7×10^{10} cm^{-3} [Nic-83]. However, state of the art plasma sources that are currently used in the industrial environment routinely exceed this limit, as has been reported in almost all of the ion, or ion beam sources reviewed in this chapter. This so called critical density limit is reached by over simplifying the theoretical analyses.

Without these simplifications, the complex theoretical models of plasma fluid dynamics do not achieve closed form solutions. For example, in order to obtain such solutions the plasma is defined as being a high pass filter, and as being an infinite, homogeneous, cold, and non magnetic. While some of these conditions may hold true for small volumes inside a very large plasma source, or

for the huge tokamak reactors for fusion research, *almost none of the simplifications hold true for the smaller plasma sources*. That the ion density obtained in ECR sources is routinely reported to be higher than the critical density for the frequency of operation is proof of the over simplification that has to date preceded theoretical development. It is therefore obvious that analytical theories derived to date do not adequately explain plasma phenomena, and it is imperative that a next generation of theoretical analysis be developed, based on numerical simulations, if necessary to further explain the secrets of gas discharges.

Chapter 3

Characterization Principles

3.1 Introduction

3.2 Theory of Langmuir Probes

3.2.1 Assumptions of a Simplified Probe Theory

3.2.2 Single Langmuir Probes

3.2.3 Double Langmuir Probes

3.24 Limitations of Probe Analysis

3.2.5 Data Acquisition using Langmuir Probes

3.3 Multi-grid Ion Energy Analyzer

3.3.1 Theory of the Ion Energy Analyzer

3.3.2 Design of the Ion Energy Analyzer

3.3.3 Limitations of the Ion Energy Analyzer

3.3.4 Data Acquisition using the Ion Energy Analyzer

3.4 Energy Distributions - Proposal for a New Method

3.5 Micro-coaxial Probes

3.5.1 Theory and Design of the Micro-coaxial Probes

3.5.2 Sources of Error with the Micro-coaxial Probes

3.6 Ion Beam Characterization

3.6.1 Charge State Distribution of the Ion Beam

3.6.2 Emittance of the Ion Beam

3.6.3 Emittance Measurement Techniques

3.7 Concluding Remarks

Chapter 3

Characterization Principles

3.1 Introduction

In this chapter, some general techniques of characterizing a plasma/ion/ ion beam source are discussed, with a purpose to centralize this discussion in this dissertation. Since several plasma/ion beam sources will be evaluated in the forthcoming chapters, this discussion of the actual methodologies of evaluation will provide a foundation for measuring, and studying the characteristics of these sources. This chapter is not meant to provide an exhaustive theoretical analysis of each technique mentioned in the forthcoming sections, but to provide all relevant information (including equations, circuit diagrams, and the appropriate references, etc.) in one location. As was seen in the previous chapter, there are a large variety of compact plasma/ion beam sources. A large number of diagnostics also exist that may be conducted on these sources to evaluate the performance, and to standardize the comparison of these ion sources. Knowledge of the salient features of the plasma or ion beam constituents - like the electron and ion density, their respective energies, the

charge states of an ion beam, etc. - represents an understanding of the fundamental properties of plasma/ion/ion beam sources.

Characterization techniques that are in frequent use today range from the invasive, yet simple Langmuir probes inserted into the plasma, to the non-invasive but more complex optical emission spectroscopy (OES) and laser induced fluorescence (LIF). For a plasma/ion beam source designer it is absolutely imperative to understand these fundamental properties (ion density, electron temperature, etc.), and how they are influenced by varying controlled external parameters like gas flow, pressure, gas type and input power, etc. Such knowledge renders a judgement on the plasma source itself, its design and assembly, its efficiency of transferring power, its resource utilization (like the power and gas feed requirements), and its ability to generate the stipulated plasma species in the required abundance. This in turn, allows for further optimization in the design process, which is inherently facilitated by comparison with previous design versions. On the other hand, under circumstances where plasma sources are used as turn-key systems, the knowledge of plasma properties is necessary since design of peripheral systems (for processing, manufacturing or research) relies on accurately predictable properties of the plasma/ion beam source.

Diagnostic methods exist for characterizing almost any and all species generated in the plasma and a number of these techniques were used to evaluate the four principle plasma sources that were studied during the research for this dissertation. In this chapter, these ion source characterization principles and data acquisition techniques will be discussed in detail. A brief introduction into the theory of each technique, including assumptions and

possible sources of error, is given along with the requisite equations that lead to the measurement methodology. Relevant references are provided to supplement the descriptions given here if further detailed study of any technique is required. The closure of each section is devoted to explaining the exact data acquisition methods as performed in the laboratory for each characterization technique. Also, in Section 3.4 a new method for acquiring data for ion and electron energy distribution functions is proposed. While this method was never used to report the results presented in this dissertation, it may be the next generation of state-of-the-art data acquisition techniques that are a testimony to the continuous evolution of the characterization procedures. This new method needs to be mentioned here so that its applicability (with subsequent acceptance in the battery of characterization techniques in use today) may be tested in the near future as an alternative, and simpler way of acquiring the electron and ion energy distribution functions.

3.2 Theory of Langmuir Probes

One of the most widely used instruments to characterize the plasma discharge are Langmuir probes [Her-89, Sch-68, Dru-30, Lan-23, Joh-49, Coh-1, Swi-69, Pod-71, among many other references]. Simple in design and easy to construct and use, Langmuir probes provide a wealth of information on ion or electron densities (n_i or n_e, typically measured in cm^{-3}), average electron temperatures (T_e, in eV or degrees Kelvin), ion saturation current densities (I_s, in $mA\text{-}cm^{-2}$), plasma potentials (in eV, or Volts) and electron energy distribution functions (EEDFs). While the complete theory of Langmuir probes is well beyond

the scope of this study, and may be found in several of the references mentioned above, the salient features of two of the most universally used probe techniques - the single Langmuir probe (SLP), and the double Langmuir probe (DLP) are now presented.

In plasma diagnostics, the word "probe" automatically brings to mind some sort of a wire like appendage inserted into the discharge. Although not all probes fit that general description, a majority of probe analysis is done with a thin wire like protrusion into the plasma. As will be seen below, the simplicity of such probes, and also the vast variety of data provided by them, far outweigh the limitations caused by this very simplicity, and the rather complex theoretical developments necessary to attain analytical solutions. It will also be noted below that these analytical solutions rely heavily on assumptions (often inaccurate) to simplify the derivations, which lead to several sources of error inherent to probe analysis.

While the initial work done by Langmuir was confined to low pressure discharges, where collisions in the plasma may be neglected, later work has managed to modify his theory to fit more practical applications of today (like a high pressure plasma, or a discharge under the influence of strong magnetic fields) where Langmuir's original, and relatively simple theoretical developments had failed. Today, Langmuir probes may be successfully operated under a tremendous range of plasma parameters: ion (or electron) densities ranging from 10^0 to 10^{13} cm^{-3}, with electron temperatures ranging from 0.1 eV to hundreds of eV, at plasma potentials of 0.1 V to many kV, and for neutral pressures of less than 10^{-6} Torr, to greater than 1 Torr [Her-89].

3.2.1 Assumptions for a Simplified Probe Theory

Analytical solutions that have led to closed form solutions require many simplifying assumptions to be used. Before going into the details of probe theory, it is desirable that some of these assumptions (and related terminology for probe diagnostics) be understood, with their consequences, and limitations being brought up at appropriate moments in this discussion. A major assumption made while working with gas discharges - upon which a large part of plasma theory is based - is that the electron energy distribution functions are non-drifting Maxwellian in nature. As early as the 1940's it was known that the velocity distributions of electrons, specially in low pressure plasma are not only far from being Maxwellian, but are rarely isotropic, and may also have a drift velocity. A more agreeable analysis may be done with the Druyvesteyn distribution function for electron energies proposed in the early 1930s [Dru-30, Dru-35]. Indeed, it will be seen in the following chapters that the EEDFs in the plasma/ion beam sources like the microwave plasma disk reactors - MPDR 610, and the MPDR 5 are closer to being Druyvesteyn, than Maxwellian.

When a probe is immersed in a discharge, the very presence of a surface creates an electron, or ion rich layer (depending on the probe bias) on the surface called a “sheath”. The concept of quasineutrality ($n_e = n_i$) is not valid in this sheath, and the large concentration of positive, or negative, charge can maintain high electric fields near the probe itself, thereby repelling (and attracting) charged species and leading to somewhat erroneous data collection. While the sheath effects are dependent on the very parameters whose calculations they retard - like ion density for example, certain generalized

parametric values may be used to negate some of the error, the real values determined, the sheath effect correction done again, and the process iterated till the margin of error is reasonably reduced. Complete rectification for errors induced by the sheath requires a complex development of the concepts of the plasma sheath the pre-sheath regions, and the establishment of the Bohm criterion [Man-89], and is generally not necessary. The concept of sheath thickness itself remains somewhat vague and undefined (the sheath is supposed to be "several Debye lengths - λ_D" in thickness), and really has no quantitative value that can be exactly estimated. This makes it difficult to correct the probe theory for the sheath effect, although efforts may be made based on estimation of the sheath thickness. Most of the potential drop inside the sheath occurs within five λ_D of the probe surface. However field gradients associated with the pre-sheath may extend out as far as 100 λ_D [Man-89].

A "weakly ionized plasma" (less than 10% ionization) can easily be perturbed by the presence of a foreign body in the form of a probe and its holder, specially in the plasma generation region where the probe may interfere with the impressed electric field and the static magnetic field. For this reason, in this dissertation research, probe measurements were not taken within the plasma generation region. All probe data were taken downstream from the plasma generation region, although this data may be extrapolated to obtain order of magnitude parametric values within the discharge confinement chamber. Throughout the theoretical development of probe theory, it is assumed that the probes do not "significantly" perturb the downstream plasma, and that all such disturbance is heavily localized.

The ions and electrons created in a plasma are highly energetic, specially

as they are accelerated by the sheath potential on their way to being collected by the probes. Upon striking the probe, these energetic particles might be able to transfer significant energy to the valence electrons of the metal atoms. If this energy is greater than the binding energy of the valence electrons to the atoms, these atoms can get ionized, as the valence electron is expelled from the probe. This is known as secondary electron emission, and may lead to large discrepancies in actual current striking the probe, as compared to the current that has been tempered with secondary electron emission. Although this effect is very difficult to rectify in a probe setup without biased grids, it may be lessened by using a less emissive material for the probe, like platinum. Also, metallic sputtering off the probe tip may locally increase impurity levels to the extent that collisions occur between electrons and the impurity atoms, thereby cooling the electron gas, leading to underestimation of the actual electron gas temperatures, while at the same time interfering with the ionization and excitation processes within that micro-volume of the plasma. Finally, such metallic sputtering may lead to coating of the plasma vessel which might require expensive down time for cleaning the vessel.

3.2.2 Single Langmuir Probes

Although electrostatic probes were used for the investigation of gas discharges as early as the turn of the century, the ground breaking work was done by Irwin Langmuir in the early 1920s and 1930s [Lan-23, Lan-31]. He used a thin cylindrical electrode immersed into the discharge - what is now known as the single Langmuir probe (SLP)- for localized measurement of electron density

and temperature, and developed his technique into one of the most powerful tools of plasma diagnostics. His method involved biasing the immersed probe with respect to some other readily available electrode in contact with the plasma, like the metallic containment vessel. The probe current is then collected as a function of the applied bias and the I-V characteristics analyzed for a wealth of information on the plasma. The exact equations and methodology are now described [Man-89].

A typical SLP I-V characteristic is shown in Figure 3.1. This curve may be divided into three distinct regions, depending on the probe bias. Consider a negative bias on the probe. As this negative voltage is increased, the probe repels electrons and attracts ions, creating a positive sheath around it, till an equilibrium is reached, and any further increase in probe voltage incurs a much smaller increase in the ion current. Region C corresponds to "ion saturation," reached when the probe is biased sufficiently negative and driven into saturation. Also, the ions thus collected are actually accelerated in the sheath, but since the sheath itself is only weakly dependent on voltage, the ion saturation current does not vary much with increasingly negative probe bias.

As the voltage is reversed and made positive beyond region C, the ion current to the probe reduces further, till a voltage is reached at which no current flows through the probe. This bias voltage at which there is zero probe current is called the floating potential V_f of the plasma, and may be positive, or negative depending on the plasma/ion beam source, or the plasma conditions. When the applied voltage is further increased beyond V_f, the positive potential rapidly attracts the fastest electrons from the tail of the electron distribution function. Further increase in the potential leads to more and more of the bulk distribution

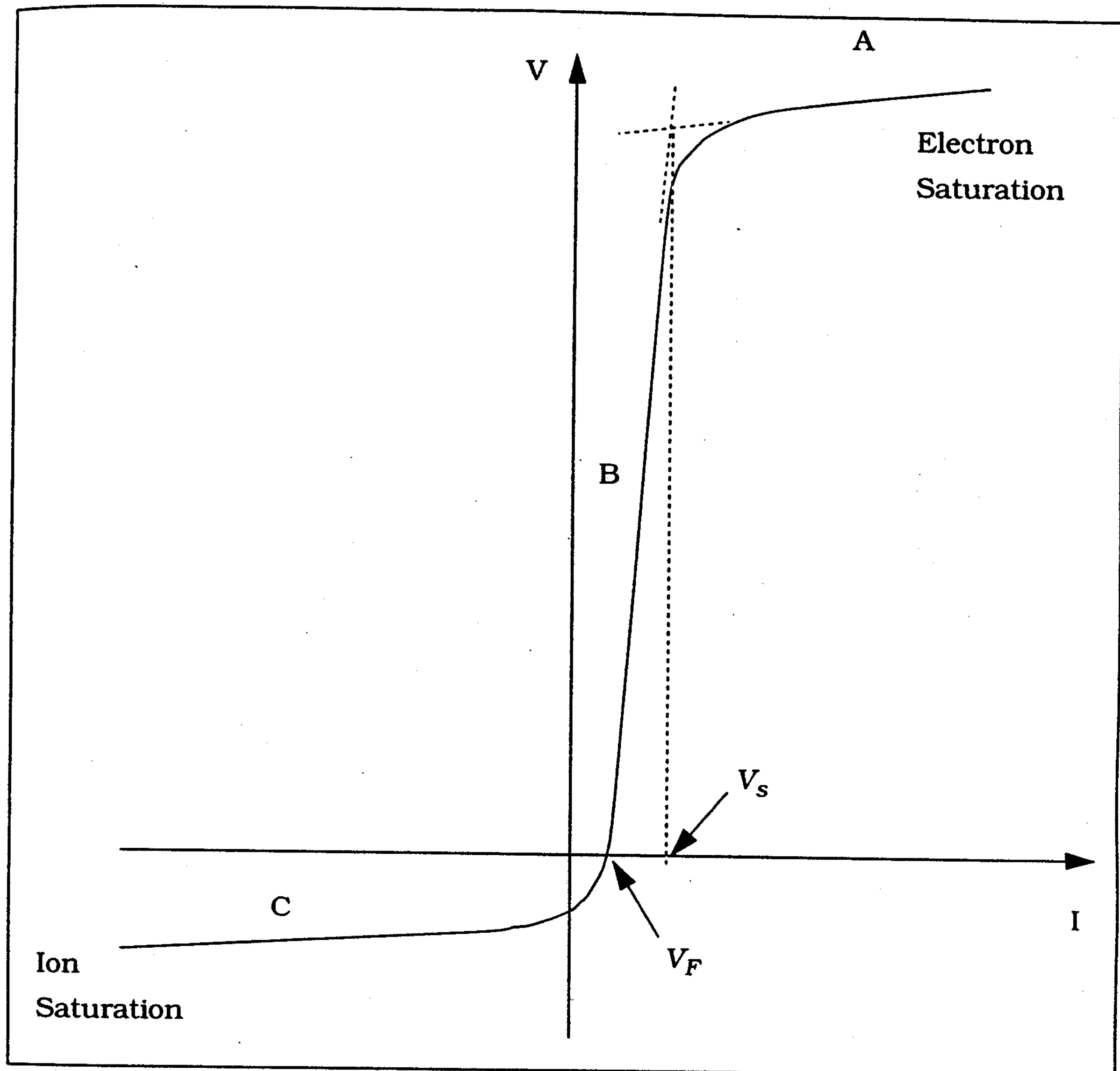

Figure 3.1 An I-V characteristics of a Single Langmuir Probe.
Here, V_F is the floating potential, V_S is the plasma potential. Region C corresponds to ion saturation, while Region A is the Electron Saturation. Note that the electron saturation current is much higher than the ion saturation current.

to be attracted to the probe, and therefore a larger electron current in the probe. This increase in electron current is described by a Boltzman-type equation, somewhat similar to the I-V equations of a diode. There is an almost linear increase of the current versus the applied voltage.

A limit however is reached, when the electron current levels off, and further increase in bias does not affect an equivalent increase in the current, although the current still increases with a smaller slope. This is shown in region A, beyond the "knee" of the curve, and the probe is said to reach "electron saturation". If the electron energy distribution function in the plasma is exactly Maxwellian, theory predicts that there would be no further increase in current in the saturation region. That the current still increases beyond the "knee" of the curve, albeit with a much smaller slope than in the linear region, is one indication of an off-Maxwellian electron energy distribution.

Whereas the SLP I-V characteristics may be used to provide information on the electron and ion density of the plasma [Man-89], this is more readily available through another technique - the double Langmuir probe method discussed in the next section. Instead, more valuable information is buried in the SLP I-V characteristics. This data may be reduced to get a direct, and more accurate measurement of the average electron temperature, the plasma potential, and the electron energy distribution function (EEDF) [Hop-91]. It was shown by Druyvesteyn [Dru-30, Dru-35] and others [Swi-69] that the second derivative of the probe current with respect to the applied probe potential is directly proportional to the energy distribution function *f(E)*:

$$\frac{d^2 I}{dV^2} = \frac{1}{4}Aqn\left(2\frac{q}{mV}\right)^{1/2} f(E) \tag{3.1}$$

where A is the total collection area of the probe,

n is the neutral gas density, with an ion mass m

V_s is the plasma potential, the potential at which the second derivative of the I-V characteristics is maximum [Run-79, Coh-89],

V is the applied bias, and $E = V_s - V$

While Druyvesteyn himself graphically took the second derivative of the I-V plot, a Princeton Applied Research (PAR-128) lock-in amplifier and other peripheral circuitry may be used to differentially measure the signal proportional to the second derivative in this age of computers. Following Hopwood [Hop-91], Figure 3.2 shows a typical SLP circuit to measure the EEDF. All data acquisition was done using computer controlled apparatus, and the exact methodology will be discussed in a later section of this chapter. A low frequency (1KHz) small AC signal (with an amplitude typically less than 0.5 V_{rms}) is superimposed on the DC probe voltage. Under certain conditions, the output of the PAR-LIA is proportional to $\frac{d^2 I}{dV^2}$, as shown by the Taylor series expansion of the modulated electron current equation on the next page [Sch-68, Run-79]:

$$I(V + \sin\omega t) = \left[I + \frac{a^2 I''}{4} + \frac{a^4}{64} I'''' + \dots\right] + \left[aI' + \frac{a^3 I'''}{8} + \dots\right]\sin\omega t$$

$$-\left[\frac{a^2 I''}{4} + \frac{a^4}{48} I'''' + \dots\right]\cos 2\omega t \quad + \text{higher order harmonics} \qquad (3.2)$$

where primes denote differentiation with respect to V, while a and w are the amplitude and frequency of the AC signal respectively. Note that the first square

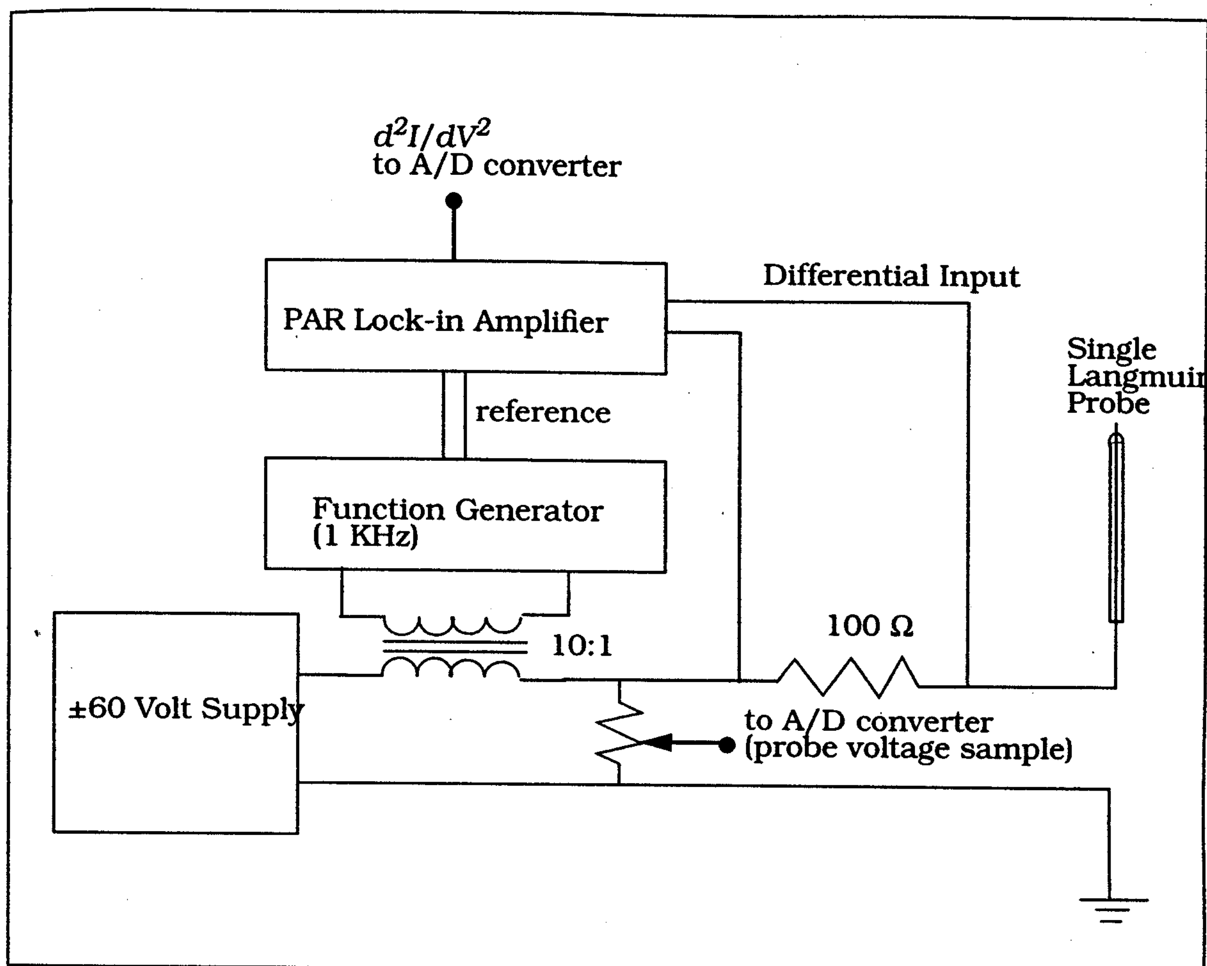

Figure 3.2 The Single Langmuir Probe circuit.
Adapted from Reference Hop-91, this circuit shows the "semi-automated" method of measuring EEDFs, Plasma potential and average electron energies.

bracket contains the DC component of the signal, the second square bracket contains the undistorted AC component, and the third square bracket contains the second harmonic of the signal. Then for sufficiently low values of $a << V$, the increase in current can be approximated by [Sch-68]:

$$\Delta i \approx \frac{i}{4} a^2 I''(V) \tag{3.3}$$

From Eqn. 3.2, it is seen that the second harmonic of the probe current is proportional to the second derivative if the AC signal is small relative to the DC voltage. This information is utilized to measure the second derivative, and hence to directly obtain the EEDF. A small oscillation in the plasma is initiated by the AC signal which is superimposed on the probe voltage, and effects of this oscillation on the plasma are measured by the probe and external circuitry. This is known as the Druyvesteyn method and is valid for all probe types if the plasma may be considered isotropic. However, an anisotropic plasma requires a spherical probe surface for the validity of the result [Sch-68]. It is therefore seen that even with the many simplifying assumptions made, or perhaps due to them, the method yields qualitative results at best and exact plasma parameter values may vary significantly from theory. This is shown clearly on Figure 3.3 which depicts a typical EEDF of the MPDR 5 (that is characterized in Chapter Seven). The experimental curve seems to deviate from the Maxwellian distribution, and is seen to be closer to the Druyvesteyn distribution, as mentioned above. Similar, near-Maxwellian EEDFs have also been reported for non-ECR microwave discharges [Hei-88].

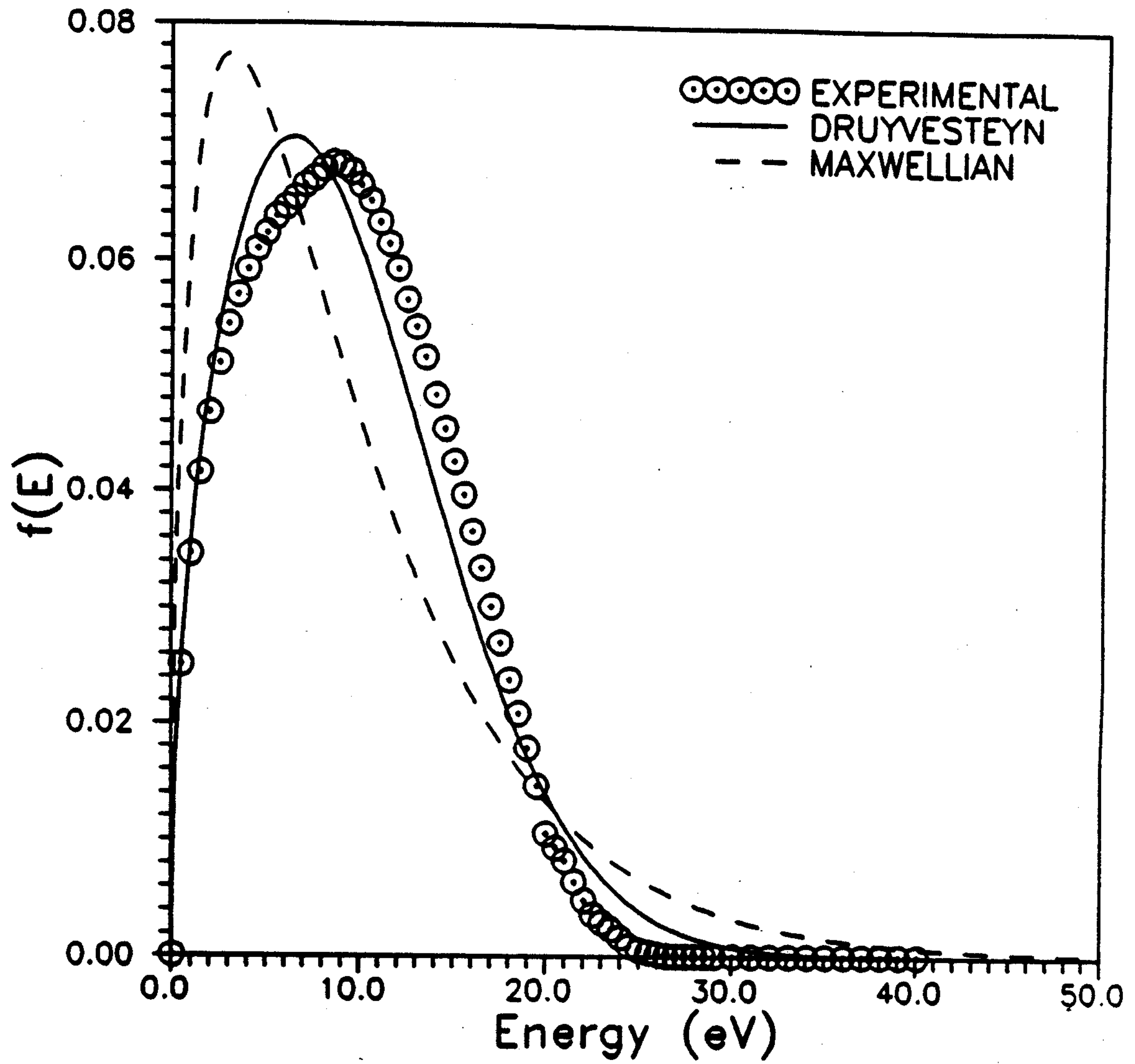

Figure 3.3 A typical EEDF of the MPDR 5
Data taken for an argon discharge at 1.0 mTorr at 100 W input power with the SLP 5 cm downstream (Refer to Chapter Seven).

3.2.3 Double Langmuir Probes

The concept of using two probes was born out of the fact that very often a reference electrode for the SLP is absent, or difficult to define. An example may be measurements in the ionosphere, or a toroidal rf discharge in a glass tube. First proposed by Johnson and Malter [Joh-49, Joh-50], this method employs two similar, single probes with a dc bias applied through an otherwise electrically floating circuit. The double Langmuir probe (DLP) method has been extensively studied [Joh-49, Joh-50, Che-65, Swi-69]. The circuit itself, shown in Figure 3.4(a) is extremely simple and does not require any specialized equipment to operate. Due to this simplicity, and also the very important information it imparts about the plasma, the DLP is widely utilized for plasma diagnostics.

Other than the self contained floating circuit within the plasma, another advantage of the DLP over the SLP system is that the former is limited by the ion saturation current, while the SLP must measure the electron saturation current. As is seen in Figure 3.1, the electron saturation current is much greater than the ion saturation current. Due to these high electron currents specially in intense discharges, the SLP may suffer from over heating, warping or even melting - a problem that does not exist for the DLP.

Figure 3.4(a) shows that the DLP has two small conducting probes immersed in the discharge close to each other. Note the DC isolation of the DLP using transformers. As mentioned earlier (Section 3.2.1), care must be taken in designing the probes so that they are sufficiently far away (several tens of λ_D) and do not reside within the other's sheath, while at the same time are close

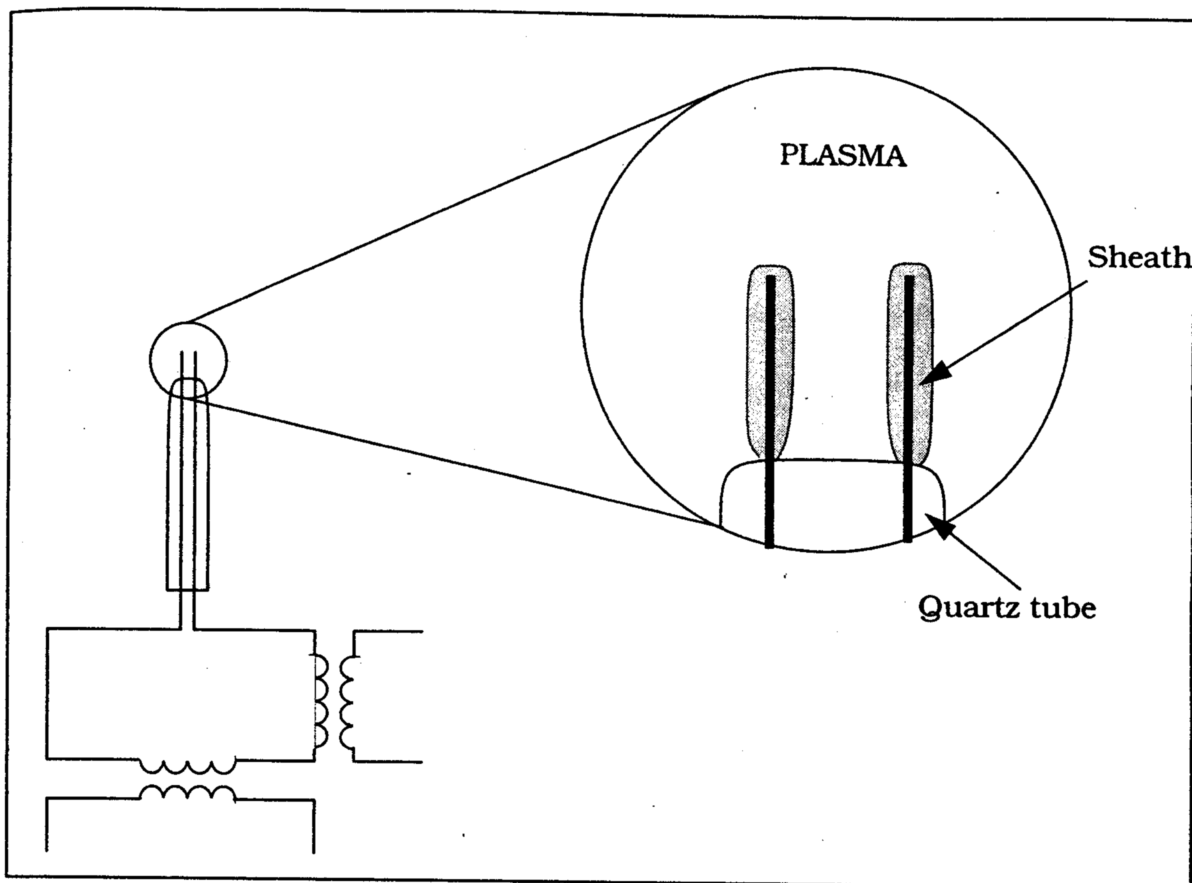

Figure 3.4(a) A DC isolated Double Langmuir Probe circuit.
Inset shows the sheath development around the tungsten wires. Shaded region is the sheath. Note that the quasi-neutral plasma surrounds both probes.

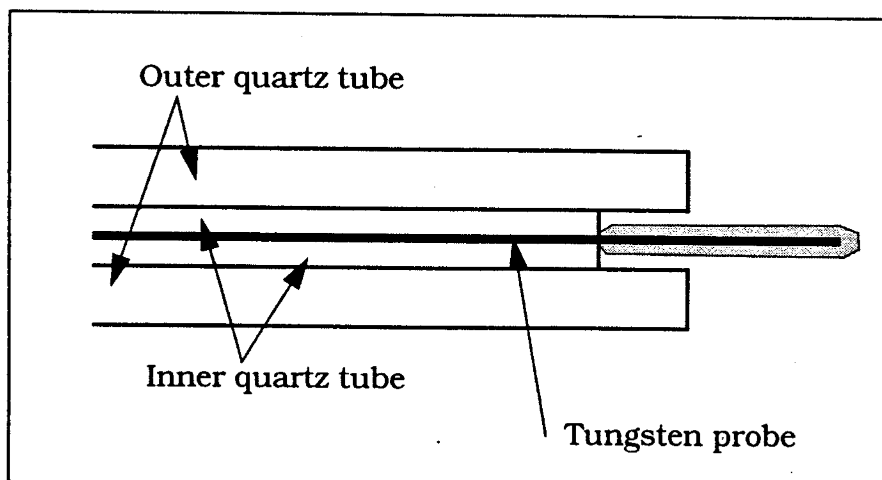

Figure 3.4(b) Recessed Langmuir Probe.
Two such probes glued together with UHV compatible adhesive constitute the Double Langmuir Probe.Note the step like topology that prevents the probes from shorting out. Shaded region is the sheath around the probe tip.

enough such that the plasma potential on both probes is the same. There must exist a quasi-neutral plasma with little or no change in the plasma potential between the sheaths of the two probes. This is shown in the inset of Figure 3.4(a), where the sheath of each probe is comfortably far removed from the other probe, and the plasma encloses each probe completely. Figure 3.5(a) shows the potential drop between the two probes indicating clearly the sheath around the probes. A good explanation of the variation of the plasma sheath and potential drop across the probes as the bias voltage is changed may be found in reference Swi-69 (see, for example Figure 2.3, page 19 of this reference). The probes are floating with respect to ground, and the current circulating between the two probes is measured as a function of applied voltage. A typical DLP I-V characteristics is shown in Figure 3.5(b), and this can be reduced to provide the T_e and n_e. The derivation for extracting the appropriate quantities from the I-V characteristics follows (from Reference Lie-94):

Assuming that the circuit of Figure 3.4(a) is electrically floating with respect to the common ground, the current going into one probe must equal current flowing out of the other, i.e.

$$i_1 = - i_2 \tag{3.4}$$

In terms of the electron and ion components, each probe current may be decomposed into:

$$i_{i1} - i_{e1} = i_{e2} - i_{i2} \tag{3.5}$$

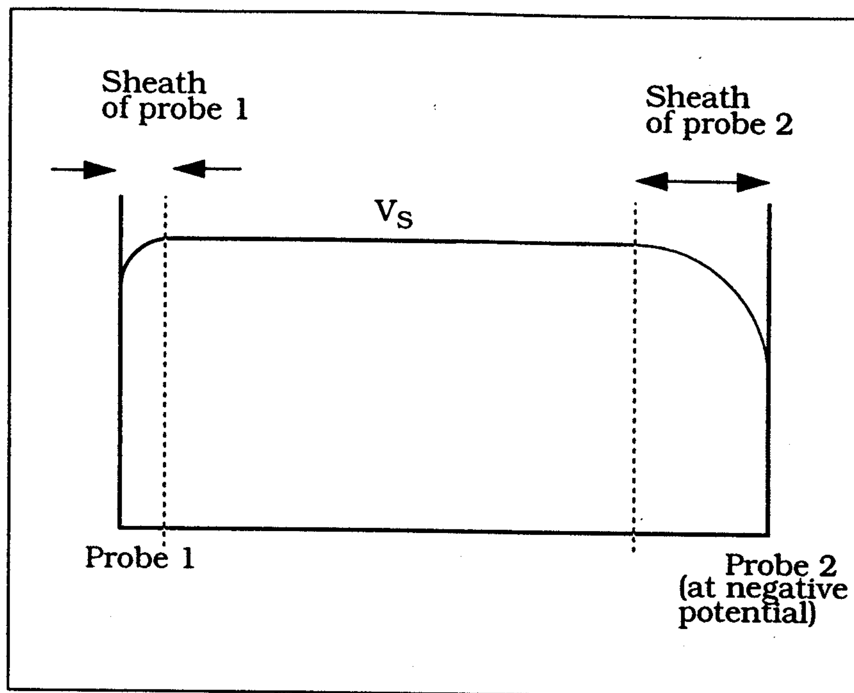

Figure 3.5(a) Potential drops across the Double Langmuir Probes.
Here, V_S is the plasma potential. Note that the potential variation occurs only in the sheath.

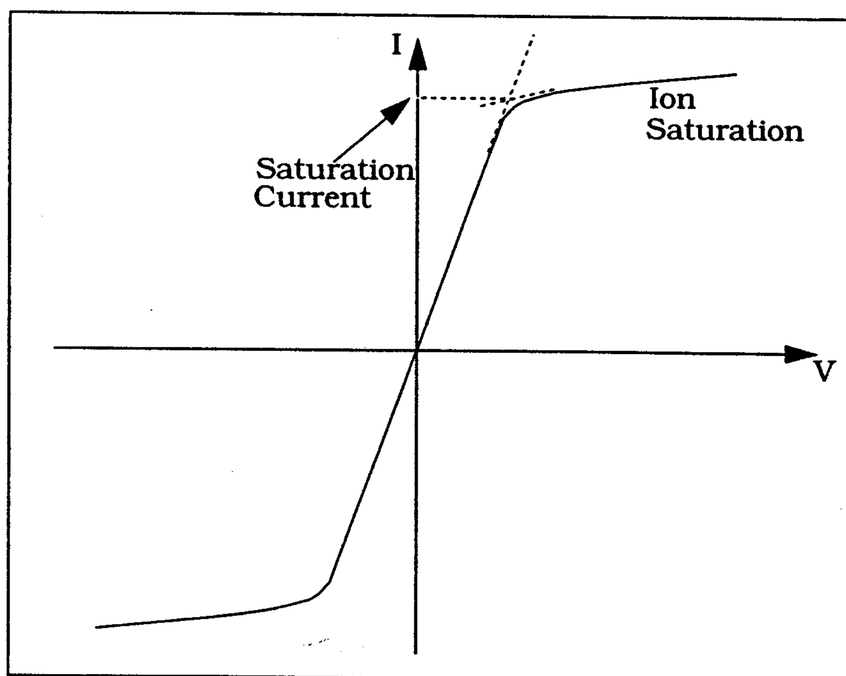

Figure 3.5(b) An I-V characteristics of a Double Langmuir Probe.
The "knee" of the curve indicates where the saturation current value is taken, despite the fact that current still increases with increasing potential beyond this knee.

And a total current expression may be written as:

$$I = i_{i1} - i_{e1} = i_{i2} - i_{e2} \tag{3.6}$$

Now, making use of the Maxwellian electron energy distribution assumption (note, from Figure 3.3 that this assumption may not be exactly valid), the currents can be expressed with Boltzmann like variation with applied potential:

$$i_{e1} = I \cdot \exp\left(V_1/T_e\right) \text{ and} \tag{3.7}$$

$$i_{e2} = I \cdot \exp\left(V_2/T_e\right) \tag{3.8}$$

Here, V_1 and V_2 are the probe potentials with respect to the plasma potential, I is some random electron saturation current, and T_e is the electron temperature. With the assumption that the plasma potential does not vary significantly on the two probes, the relative applied bias is then the sum of the two probe voltages:

$$V = V_1 - V_2 \tag{3.9}$$

Then, using Eqns. 3.6, 3.7 and 3.8, a ratio of currents may be written as:

$$\frac{I + I_{i1}}{I_{i2} - I} = \exp\left(V/T_e\right) \tag{3.10}$$

If $I_{i1} = I_{i2} = I_i$ the above equation may be reduced to:

$$I = I_i(\tanh(V/T_e)), \tag{3.11}$$

To calculate the electron temperature, an easy method is to obtain the derivative of the above equation at zero potential. Note that the derivative of the hyperbolic tangent function is equal to the square of the hyperbolic secant:

$$\frac{d}{dV}\tanh\left(\frac{V}{T_e}\right) = \left(\operatorname{sech}\frac{V}{T_e}\right)^2\left(\frac{1}{T_e}\right) \tag{3.12}$$

At the origin ($V = 0$) all terms cancel out and,

$$\left.\frac{dI}{dV}\right|_{V=0} = \frac{I_i}{T_e} \tag{3.13}$$

The above equation may be used to calculate the electron temperature by plotting the DLP I-V characteristics, and equating the derivative of the curve at the origin to the ratio of the saturation current (known) and the unknown electron temperature. Note that the saturation current may be obtained from the I-V characteristics by extrapolation, as shown in Figure 3.5(b). The ion density may then be calculated from the electron temperature and the ion saturation current, using the approximate relation, as shown by Chen [Che-65]:

$$I_i \sim 0.6 n_i e A \sqrt{\left(\frac{kT_e}{m_i}\right)} \tag{3.14}$$

where n_i is the ion density, m_i is the ion mass, and A is the probe collection area. Note that since the sheath surrounds the probes, the area A has to be corrected

for the sheath effect that makes the effective collection area more than the actual surface area of the probe.

3.2.4 Limitations of Probe Analysis

As mentioned earlier, probe theory (specially Double Langmuir probe theory) has some sources of errors. At best, it offers good order of magnitude results that may be used for a comparative study. Exact quantitative data must be obtained from more precise methods, like spectroscopy or laser induced fluorescence. Effects of non-Maxwellian distribution, sheath effect, plasma perturbation etc. have already been considered earlier in Section 3.2.1, and now some other possible sources of error are described.

Other than secondary electron emission, probe surfaces are prone to another problem due to bombardment of high energy particles from the discharge. These high energy particles may also cause sputtering of ions from available metallic surfaces, like the containment vessel (specially if it is made of metallic parts with low sputter thresholds), that may contaminate the probe, leading to inaccurate current values that are measured running through the probe. If such deposition occurs on the insulated part of the probe close to the exposed region, it may actually increase the effective collection area, creating large discrepancies. In the MPDR-610 excited at 915 MHz (see Chapter Five) for example, the plasma at 200 W input power was very intense, and the sputtering off the metallic end of the 610 actually shorted out the probes due to metallic deposition between them. Also, in intense discharges, there may be arcing between the cathodic probe, and the anodic sheath edge. This is called a

"unipolar arc", and can destroy a probe [Coh-89], or at the very least result in erroneous data. Using metals that are less subject to such arcing, like platinum, or tungsten reduces this problem.

All the above dialogue about probes is limited to collisionless plasma with no magnetic fields acting upon the particles. Some applications of ion sources today not only have strong magnetic fields, but also are sufficiently high in pressure to repudiate the predictions of the rather simplistic analysis done above. It is imperative that corrections be made to incorporate the effects of the magnetic field and pressure variance on the simplified theory presented here (see for example, Reference Her-89 page 142). It may be safely assumed that the ion sources characterized with Langmuir probes during the research for this dissertation have no stray magnetic fields or pressure gradients that may require complex corrections to the simple probe theory discussed here. This will become clear when the designs for the ion source are described in detail in the forthcoming chapters.

From the above discussion it is clear that at best, probe theory is able to present data to plus or minus three to five times the exact values, and to "order of magnitude" calculations at worst. It is nonetheless a most valuable tool in characterizing a plasma. Apart from being almost trivially simple in operation (specially the DLP), electrostatic probes maintain many advantages over other more refined and complex techniques like LIF. The humble electrostatic probe is "distinguished by the possibility of direct local measurement of plasma parameters," while other techniques often rely on averages over a volume. And so, even though the resolution of the results from probe theory may be no better than order of magnitude (in the worst case), it aptly retains its position as being

a premier plasma characterizing technique.

3.2.5 Data Acquisition using Langmuir Probes

In this section, the actual methodology for Langmuir probes as they were used in the laboratory is explained. All data were taken using computer controlled apparatus, and the relevant peripheral circuitry needs to be explained in detail. For sake of simplicity, DLPs for measuring n_e and T_e are covered before the more complicated SLPs for T_e, V_s and EEDFs.

Care must be taken in constructing the probes. As explained earlier, the probe tips are somewhat invasive. To reduce the plasma perturbation, the probes need to be made as small as possible. However, as explained in Reference Hop-91, if the probe area is made too small, the relative sheath effect around it increases, and to minimize this, the probe's actual area must be increased, which is in direct contradiction with the efforts to minimize perturbation mentioned above. So a compromise must be reached for the probe length and diameter. Also, small non-planar probes may read saturation currents that are orbital motion limited (OML) - a theory covered in References Mor-85 and Sch-68. This may occur if the probe radius is less than one plasma λ_D, and in such a situation, the OML probe current given by Eqn. 3.14 is not valid, and the ion density thus measured is erroneous.

To construct a double probe, therefore, the first order of business must be to determine the length of Debye shielding. This is given by the following equation [Lie-94]:

$$\lambda_D = 743\sqrt{T_e/n_e} \text{ cm,} \tag{3.15}$$

where, T_e is in eV, or V and n_e is in cm^{-3}. Assuming a typical ion density of 1 X 10^{11} cm^{-3} and an electron temperature of about 70,000 K in an ECR MPDR, the Debye length is calculated to be about 60 μm. To avoid OML effects, the radius of the probe needs to be made much greater than a Debye length. The dimensions of each recessed probe is - radius = 0.762 mm, length 0.795 cm, with a total area or about 0.399 cm^2.

A problem with the DLP that was mentioned in Section 3.2.4 had to do with the sputter deposition on the probe tips from the metallic part of the ion source when the DLP was immersed in a high intensity 915 MHz discharge. The two probes were shorted in a matter of minutes. This problem was rectified using a recessed probe. The design of this probe is shown in Figure 3.4(b). As may be seen, instead of two tungsten wire tips protruding from a closed quartz tube (as seen in Figure 3.4(a)) the recessed probe design used two separate probes, each enclosed in a small quartz tube, into which the tungsten wire was a snug fit. This tube was then enclosed in a larger quartz tube. Both tubes were open at the top. The two probes were then stuck together using a UHV compatible adhesive. This created a staggered quartz structure near the two probes instead of a smooth finish. The probe could then be inserted into intense discharges. While there was some sputtering, the recessed nature of the probes prevented their shorting out, and also kept the probe area from increasing due to deposition of metallic ions onto the quartz. This was confirmed when current values read with this probe were consistent before, and after being immersed in an intense discharge for a period of time.

The first experiments that were performed using DLPs actually involved manual data acquisition, where about 50 - 60 current values were written as the voltage was varied from -60 V to +60 V (a data point every one or two Volts). These data points were then manually entered into the computer, and the appropriate reduction programs (generic) were then used to calculate the electron temperatures and ion densities. Very soon, the monotony of manual data acquisition was replaced by a computer controlled system. The circuit used in this work follows several other researchers' work [Hop-91, Sze-93a, Hop-90a] and is sketched in Figure 3.6, following Hopwood. The explanation presented here for this technique, therefore, borrows heavily from the three references mentioned above.

As mentioned in Section 3.2.3, it is imperative that the two probes of the DLP be electrically isolated from ground. To maintain this isolation, a Metrabyte DAS-8 analog to digital (a/d) converter was isolated from the Langmuir probe using a Metrabyte ISO-4 optical isolation amplifier card in the computer. The ISO-4 allows voltages to be differentially amplified with up to +/- 500 Volt electrical isolation. As shown in Figure 3.6, the bias voltage supplied to the probe is calibrated using a multi-turn potentiometer, channeled through an ISO-4 with no gain, and sent to the DAS-8 a/d converter to be read by the computer. The probe current is sampled as a calibrated voltage signal across some current sampling resistors of a voltage divider circuit. The ammeter and voltmeter shown in Figure 3.6 are used for the initial calibration of the current and voltage readings of the data acquisition system.

The DC voltage is then swept from 0 to +60 V, the I-V data being taken automatically every Volt or so at specific time intervals. A lower sweep rate

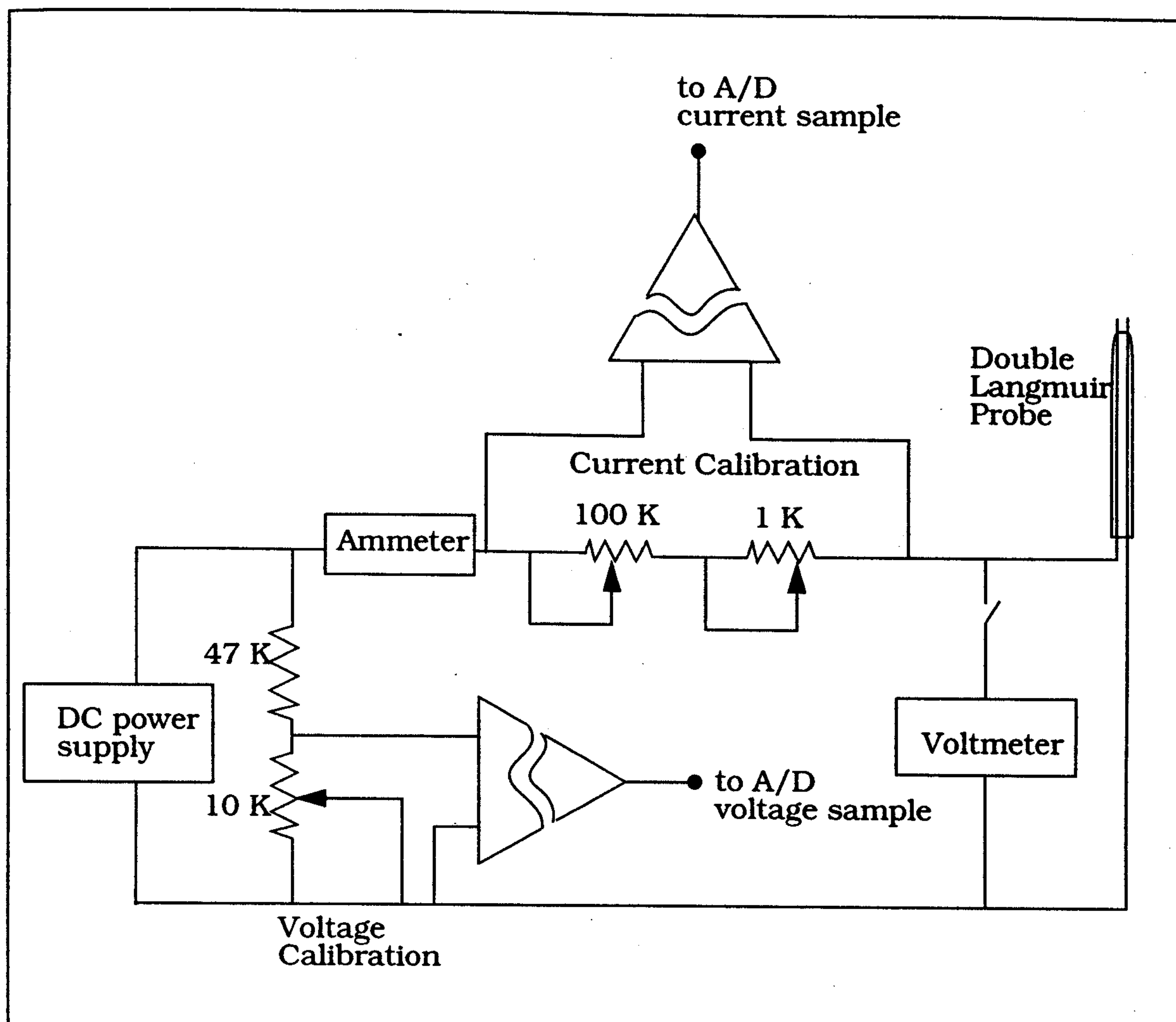

Figure 3.6 Double Langmuir Probe data acquisition circuitry.
The two triangles signify the optical isolators of the ISO card. Adapted from Hopwood [Hop-91].

allows for a higher density of data points to be taken. This is essential near the knees of the I-V characteristics for precise saturation current estimation, as will be detailed below. A double pole double throw switch then exchanges the polarity of the two probes and the subsequent voltage sweep from 0 to 60 Volts is actually converted to be 0 to -60 V. If the two probes are of identical areas, and they are both close enough to sample a volume of the plasma with "similar" plasma potential, the I-V characteristics thus obtained should be mirror images in the 1st and 3rd quadrants, passing through the origin. To minimize random noise, about 60 to 100 samples were taken for each data point, and then averaged by the computer before saving, to provide a smooth I-V characteristics. Control of all data acquisition cards and frequency of current sampling is done through a simple Q-BASIC program.

Data reduction is then carried out by importing the DLP I-V data into another generic program. The electron temperature is found by using Eqn. 3.13, as was discussed earlier. To find the ion density, ion saturation currents need to be determined from the I-V curve. In certain cases, as in low density plasmas, the "knee" of the I-V curve - where the probes are driven into saturation, may be vague and undefined, since real saturation (beyond which the collected current does not change with applied voltage) is never really reached. In such cases, it is necessary to estimate the knees as the intersection of a tangent to the curve passing through the origin, and another tangent to the curve through the "saturation region." This is seen in Figure 3.5(b).

A better method employing a manual selection of the two saturation currents was coded into the generic reduction program. A plot of the data using Eqn. 3.11 is generated. If the plot is linear, then the initial guess of the

saturation points was valid. Two points a little farther may then be tried, till the linear plot shows a discontinuous jump into non linearity near the edges. If the plot is non-linear near the edges, the saturation current values are too large, and must be reduced. The method is iterated till appropriate (maximum) linearity is reached. The current value at this point is picked to be the saturation value. The ion density may then be calculated using Eqn. 3.14. Sheath effects on the probe area, and any other corrections may be incorporated in this equation. Note that Eqn. 3.14 is valid for Maxwellian electron energy distributions only, and for an EEDF that is non-Maxwellian, Eqn. 3.11 will never produce a completely linear plot. Indeed, slightly non-linear plots of Eqn. 3.11 are another indication of the off-Maxwellian EEDFs. In such a case, the validity of Langmuir probe techniques is itself called into question, however the "order of magnitude" results of DLPs re still valid.

As mentioned earlier, the SLP method is more desirable to make average electron temperature measurements than the DLP. This is because of the problems faced while estimating the saturation current values of the DLP I-V characteristics. It has already been stated that the EEDF is not fully Maxwellian, and hence Eqn. 3.11 will only plot a semi-linear curve. Hence the electron temperature data gathered using DLP is suspect. Also, DLPs only measure the high energy tail of the EEDF, and the average electron temperature is calculated from an extrapolated distribution function from this high energy sample. No estimation need be done for the SLP system that directly measures EEDFs, and data on plasma potential, average electron energy (or temperature) are generally more accurate. Hence this direct measurement of the EEDF with no initial assumption of its outcome, and the T_e calculation from this directly acquired

EEDF leads to the accuracy of this so called Druyvesteyn method. Dimensions of the SLP used in for data acquisition are - length = 0.8 cm, radius = 0.5 mm, with an area of about 0.26 cm^2.

Actual data acquisition was done using two different methods. A semi-automatic system, following Hopwood and Sze [Hop-91, Sze-93a] used the circuit of Figure 3.2. After a low amplitude 1 kHz signal is modulated on the DC carrier bias, the Princeton Lock-In-Amplifier (PAR LIA 128) was used to pick out the second harmonic of the signal, which is proportional to the second derivative of the SLP current (see Eqns. 3.2 and 3.3). The SLP was manually biased at a DC voltage that ranged from 0 to about 40 V, assuming the maximum electron energy in the plasma is about 40 eV. The signal form the LIA then took anywhere from three to 10 seconds to stabilize. Once a stable signal was attained, the key to sample the second harmonic was pressed on the computer, and that data point $(d^2I/dV^2, V)$ was stored. The DC bias was then increased by about a Volt and the process repeated. The same Metrabyte hardware was used to isolate the SLP from ground as for the DLP system. This was a labor intensive process since the sampling was done by manually pressing the correct key. Also, the amplitude of the small AC signal is dependent on the DC bias. It was therefore necessary to make the appropriate adjustments in the AC signal amplitude after each sampling such that it was the same throughout the experiment. This too meant that the method required constant attention, and increased the total time for the acquisition of an EEDF.

A fully automatic system was developed during the course of these experiments to measure the EEDF, and the ion energy distribution functions (IEDFs). Figure 3.7 shows the block diagram view of this setup. The AC wave

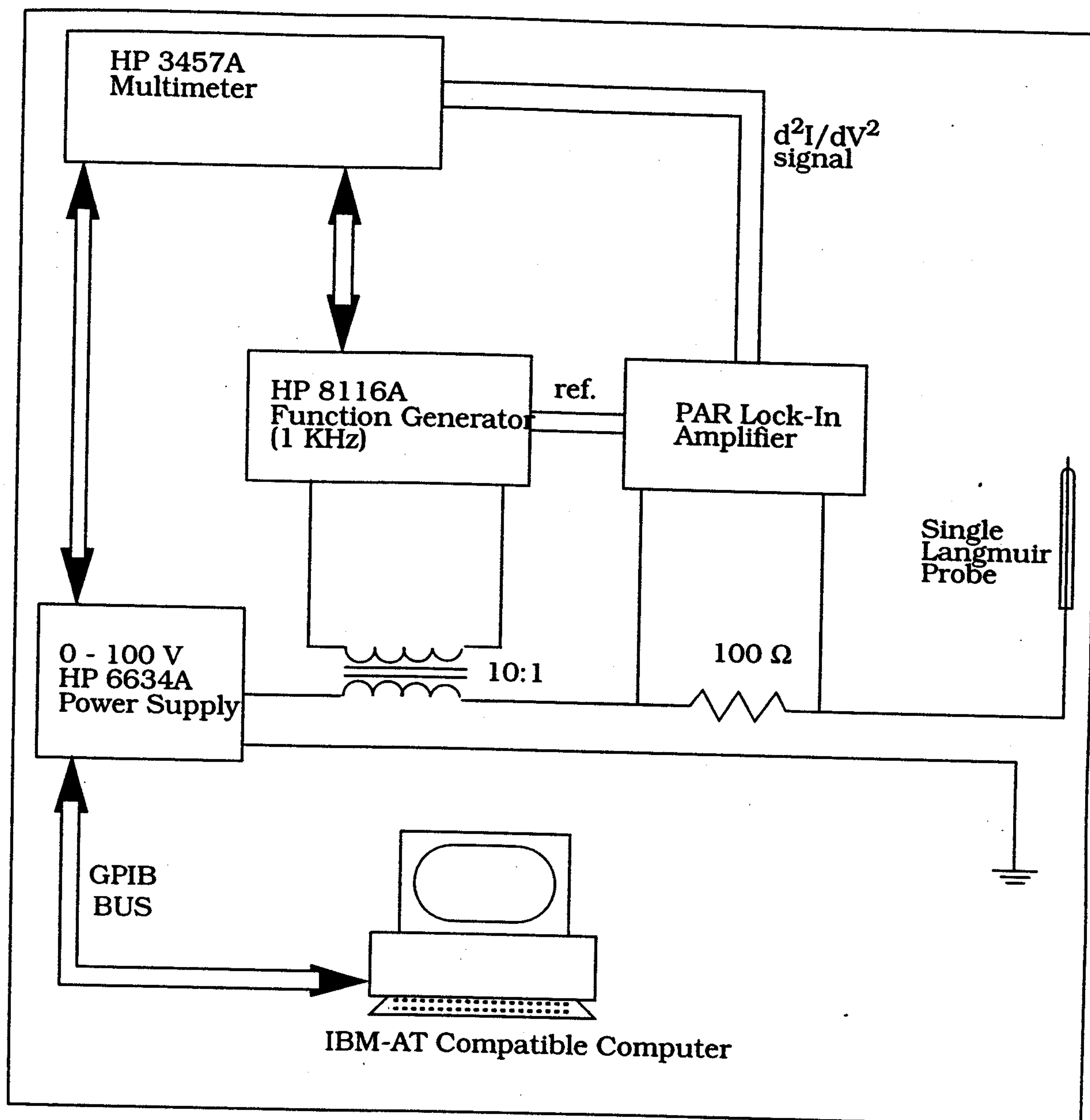

Figure 3.7 A fully automated GPIB controlled single Langmuir probe circuit.

Note that the computer controlled apparatus may be daisy-chained in any order (here, it is shown to be from the computer, to the power supply, to the multimeter and then to the function generator).

generator was replaced by a GPIB controlled Hewlett-Pacard 8116A function generator. The generic DC power supply was also replaced by a HP 6634A, 0-100 V, 0-1 Amp digitally controlled DC power supply. A GPIB controlled HP 3457A multimeter with dual ports was used to measure the AC voltage amplitude, and the second harmonic from the LIA. Finally, a computer program was written in GW-BASIC that would control all the electronics, leading to a sort of turn-key EEDF/IEDF measurement system.

Once the parameters of the experiment (like the AC signal amplitude, the DC voltage sweep range, ΔV which is the incremental increase in voltage after each sample, etc.) are input into the computer, the program sets the digital wave generator and the power supply to the appropriate amplitudes and frequency. Port 1 of the multimeter then reads the AC amplitude and ensures that it is within the required x% of the input strength (x is also an input into the computer), increasing or decreasing the signal amplitude to conform to the maximum allowed variation. Port 2 then waits from 10 to 30 seconds for the signal from the LIA to stabilize, at which time the second harmonic data is sampled. Once the signal is stabilized, several such samples (up to 50, if necessary) are taken to accurately reduce random noise from the data. The DC bias voltage data is fed to the computer directly from the digital DC power supply. The DC voltage is then incremented by ΔV, typically being 0.5 V, or 1.0 V, as requested by the experimenter, and the process repeated till the user input maximum DC voltage is reached, providing a smooth (d^2I/dV^2, V) curve.

This system removes all errors relating to manual control of the apparatus, specially the sampling of the second harmonic data, and also all errors related to the initial software calibration that was necessary for the semi-

automatic method of Hopwood and Sze. It was also noticed that while the AC signal amplitude still fluctuated on varying the DC voltage, digital control of the apparatus allowed for much cleaner, faster and easier correction of the AC signal amplitude, and thereby quicker data acquisition. Note that it is no longer necessary to use the optical isolator card, or the A/D converters, since the digital controls automatically isolated and digitized the data. Due to the automation, it is also not necessary to tend to the data acquisition station while the computer is taking the data.

All EEDFs were normalized to one for standardized comparison according to the following equation:

$$\int_0^\infty f(E)\,dE = 1 \tag{3.16}$$

Finally, the average electron energy were calculated using the following equation:

$$\langle E_e \rangle = \int_0^\infty (E \cdot f(E))\,dE \tag{3.17}$$

The results from this method were seen to be within experimental error of the results original semi-automatic method. Most EEDF and IEDF data reported in this study were acquired using this system. Each EEDF and average energy calculation was carried out a number of times to ensure repeatability, and consistency of the results. The raw data collected using either method (each EEDF normally took 20 - 30 minutes) was fed into another generic program that calculated the plasma potential and the average electron energy. The post

acquisition program (1) determined the plasma potential, (2) plotted the final EEDF, and (3) calculated the average electron energy using Eqn. 3.15, and finally, (4) using the calculated average electron energy, this program plotted the appropriate Maxwellian and Druyvesteyn distributions for comparison with the measured electron energy distribution. All EEDFs presented in this dissertation will therefore have all the three curves.

Another set of Langmuir probes was used in this study to measure the radial profile of ion saturation currents and ion density at a fixed z location, but at various r values (z is taken as the axial direction). While this is best accomplished with a Langmuir probe attached to a computer controlled UHV compatible translation stage, the lack of such a stage necessitated the design of a probe array. Seven recessed single Langmuir probes (0.76 mm radius, 0.8 cm length) were attached 0.5 cm apart using UHV sealant to a pyrex plate. This plate was then attached to two other plates such that the probe array is at the required height, and level with the output of the MPDR 610 (see Figures 4.3 and 4.4 for the 610 mounting position on the vacuum station).

Once the plasma is ignited, the saturation currents, and I-V characteristics across the radius of the ion source may be measured (by alternately switching from probe 1 and 2, to probe 2 and 3, etc.) without having to open the vacuum system to reposition the probes that would invariably involve switching off the plasma source, venting the system, waiting for the system to pump down once again after the probes have been re-positioned, and reigniting the plasma. There is no guarantee that the plasma conditions (pressure, power, etc.) are faithfully reproduced during this prolonged change over. Using the probe array prevents this time consuming and potentially error

filled exercise, and provides accurate measurements of the plasma source output parameters (ion density, saturation current, etc.) at different radial positions across the ion source for any given z location.

3.3 Multi-grid Ion Energy Analyzer

As in the case of electrons, the energy of ions in a plasma also exhibit a distribution function. For a variety of applications, it is extremely important to know this ion energy distribution function (IEDF), and the average ion energy. High ion energies may be detrimental to some substrate processing - energetic ion bombardment on a substrate, for example, may cause damage to the surface. Low energy ions may, on the other hand, catalyze chemical reactions on the surface - it is now believed that while actual anisotropic etching of substrates immersed in a CCl_2F_2 plasma is caused by the atomic chlorine radicals, bombardment of low energy ions on the surface enhances this etch process by providing sufficient energy to the reaction products that are adsorbed on the surface.

While physical effects of high energy ion may be undesirable in most substrate processing experiments, a moderately high energy ion beam is used for implanting ions deep within a substrate. Another application of high energy ion beams is for injection into particle accelerators, where the ions are further accelerated for atomic and nuclear physics fragmentation experiments. A wide range of ion energies, therefore, are in use for various applications, and it is imperative that the energy distributions generated by the plasma/ion beam sources be understood. This section describes the multi-grid ion energy analyzer

(IEA) that was used to measure the IEDFs and average ion energies of the discharge generated in the MPDR plasma sources. The section delves lightly into the theory behind the experimental setup, and also some of the sources of error. It then concludes with the description of the actual experimental technique used with the IEA.

3.3.1 Theory of the Ion Energy Analyzer

Following Hopwood [Hop-91], it may be shown that the IEDF, given by *N(E)*, is proportional to the first derivative of the collector current in the IEA:

$$N(E) = -\left(\frac{d}{dV_{ir}} I_c\right)\left(V_{ir} - V_{ic}\right)^{-1/2} \tag{3.18}$$

where V_{ir} is the ion retardation potential,

V_{ic} is the ion collector plate potential,

I_c is collected current.

The first derivative of the collected current with respect to the ion retardation potential can, therefore, provide information about the IEDF. As for the SLP experimental system, the PAR 128 lock-in amplifier may be used to differentially sample the magnitude of the fundamental frequency, which is proportional to the first derivative of the collected current, after a 40 Hz small amplitude sinusoidal wave is superimposed on the DC ion retardation grid bias. The theoretical development is now explained.

The current collected in the shielded Faraday cup is given by $I_c = F\left(\tilde{V}_{ir}\right)$ where F is some energy function, and the ion retardation voltage is the sum of

the DC and AC signals. This may be written as:

$$\tilde{V}_{ir} = V_{ir} + \varepsilon \sin \omega t \tag{3.19}$$

where, V_{ir} is the DC ion retardation bias, and

ε is the small AC signal amplitude superimposed on the DC bias.

The current expression may be expanded in a Taylor series as was shown for the SLP development in Section 3.2.2:

$$I_c = F\left(V_{ir}\right) + \frac{d}{dV_{ir}}F\left(V_{ir}\right)\varepsilon \sin \omega t + \frac{d^2}{dV_{ir}^{\ 2}}F\left(V_{ir}\right)\frac{1}{2}\varepsilon^2 (\sin \omega t)^2 + \quad H.O.T. \tag{3.20}$$

Substituting the trigonometric identity $\sin^2\omega t = (1 - \cos 2\omega t)/2$, the above equation reduces to:

$$I_c = F\left(V_{ir}\right) + \frac{d}{dV_{ir}}F\left(V_{ir}\right)\varepsilon \sin \omega t + \frac{d^2}{dV_{ir}^{\ 2}}F\left(V_{ir}\right)\frac{1}{2}\varepsilon^2\left(\frac{1}{2} - \frac{1}{2}\cos 2\omega t\right) + \quad H.O.T. \tag{3.21}$$

It is seen that there is only one term that is dependent on the fundamental frequency ω, and is also proportional to the ε term of the order of 3 or less. If ε is much less than V_{ir}, all terms ε^3 and above may be ignored. Hence the magnitude of the fundamental frequency may be approximated as being proportional to the $dF(V_{ir})/dV_{ir}$. Once this magnitude is differentially sampled by the lock-in amplifier, the IEDF, written as *N(E)*, as a function of the applied DC bias may be qualitatively obtained. As in the case of EEDFs, all IEDFs are recorded in arbitrary units, and therefore must be normalized to one.

$$\int_{0}^{\infty} N(E)\,dE = 1 \tag{3.22}$$

and the average ion energy may then be calculated as the first energy moment:

$$\langle E_i \rangle = \int_{0}^{\infty} (E \cdot N(E))\,dE \tag{3.23}$$

3.3.2 Design of the Ion Energy Analyzer

Initial experimental setup of the IEA followed the work of previous research [Hop-91, Sze-93a, Hop-90a]. Design of the IEA is based on a shielded Faraday cup that collects only the ion current. It has a top membrane with an aperture that severely limits the current flowing into the Faraday cup and into a collector plate. Various grids biased at different potentials between the top membrane and the collector plate allow for accurate collection of the ion current. Design of each part of the IEA is critical to the success of the experiment, and these parts are now discussed. Figure 3.8 shows the IEA, while Figure 3.9(a) shows the potential drops across the grids.

The top membrane, about 50 μm thick, is made of conducting stainless steel chosen to simulate a moderately doped silicon wafer. A tiny aperture in the center of the membrane allows a small percentage of the ions from the quasi-neutral plasma to flow into the Faraday cup. Now, as was the case with Langmuir probes, when the grounded IEA is immersed in the plasma, a sheath forms on top of the membrane - the IEA therefore is a very invasive device. If the

aperture in the top membrane through which the ions fall into the IEA is too large, the sheath will deform around the edges of the aperture, making a teardrop like dip into the aperture. This will allow the neutral plasma meniscus to enter the IEA, thereby emit ions directly inside the Faraday cup and cause large scale errors in the final results. It is absolutely imperative for the success of this experiments that this sheath remain as undisturbed and as parallel to the top surface as possible - otherwise the results of the IEA will be erroneous. Hence the aperture diameter is a critical design parameter - it must be large enough to permit a legitimate signal strength to enter the Faraday cup, however small enough to not disturb the sheath too much.

As calculated in Section 3.2.5 (Eqn. 3.13), the approximate Debye length in a moderately ionized plasma is about 60 μm. The aperture diameter should not exceed 10 λ_D. For this study, an IEA with an aperture diameter of 250 μm was used. This aperture was drilled into the membrane using an electron beam drill. Hopwood and Sze have used an IEA with a smaller aperture (50 μm) in their experiments [Hop-90a], however the ion sources they characterized were typically more intense than the ones used in this study. Hence the signal to noise ratio for their ion sources was higher to begin with, and a smaller aperture was adequate. For the MPDR 610, it was deemed necessary to use the IEA with a larger aperture so as to retain a high signal to noise ratio.

As may be seen from Figure 3.8, inside the IEA there are two grids and a collector plate, following the work of Matsuoka and Ono [Mat-87]. This IEA was designed and built by co-workers before the research for this dissertation was started, and so it is their design that is described here. Each grid is made of a nickel mesh (100 lines per inch) welded on an aluminum frame, and each grid

has independent and electrically isolated bias leads. The grids and the collector plate are also electrically isolated from each other using Teflon, or Mycor rings. The first grid, nearest to the top membrane is called the electron repulsion grid and is biased at a negative potential high enough to repel the most energetic electrons from the plasma that might enter the Faraday cup. SLP measurements on the MPDR 610 (see Chapter Four) indicated that the EEDF tail may contain electrons of up to 30 eV. Hence a -30 Volt bias may be used on the electron repulsion grid.

The second grid is known as the ion retardation grid, and is positive biased at a variable 0 to +60 Volts to selectively allow ions to fall through. At a low bias potential, most ions are able to get through the retardation grid. As the bias is increased, the ions must travel uphill to overcome the potential, and the rising bias allows only the energetic ions to fall through the ion retardation grid. This decrease in the ion current as the retardation potential is increased determines the energy spectrum of the ions. The third grid, or plate is called the collector plate and is biased at a constant negative potential to attract the ions falling through the ion retardation grid. Note that the double arrow on the ion retardation grid implies a variable potential on that grid.

3.3.3 Limitations of the Ion Energy Analyzer

There are some sources of error that have to be kept in mind when the IEA is used. By far the biggest limitation is that the theoretical development of Section 3.3.2 assumes that all ions entering the Faraday cup have no divergence, i.e. they are all impinging perpendicular to the IEA. For most plasma

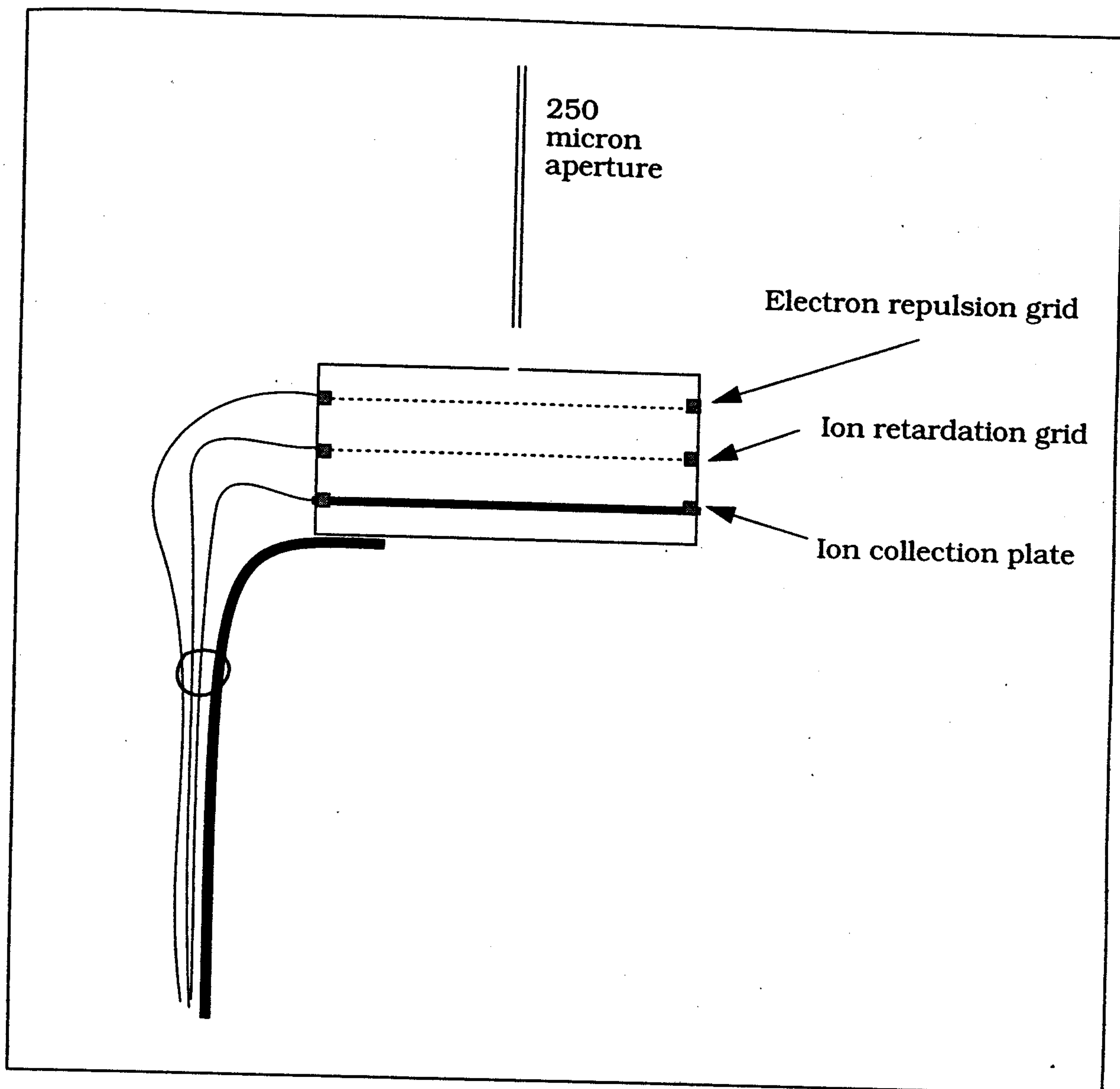

Figure 3.8 The Ion energy analyzer with three grids.
Note that all three grids, and their wiring are electrically isolated from each other, and from the grounded IEA body.

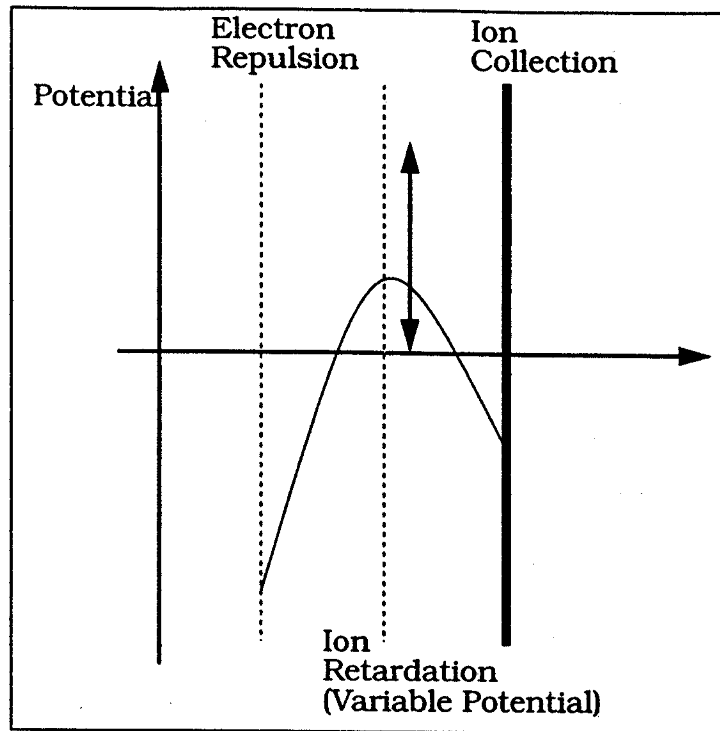

Figure 3.9(a) The potential drops for a three grid IEA.
Note that the potential on the ion retardation is variable (from 0 to about 50 V in most experiments here).

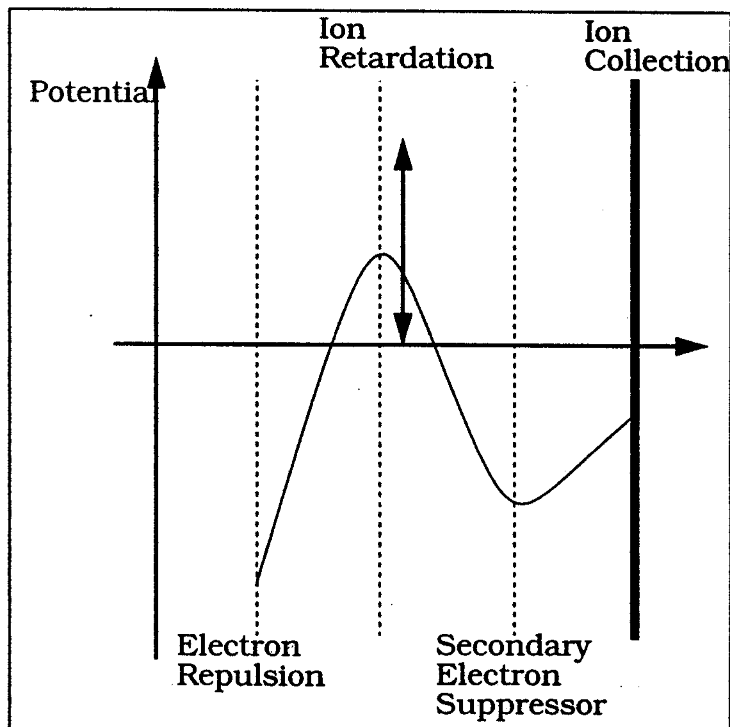

Figure 3.9(b) The potential drops for the IEA with a fourth grid.
Again, the retardation grid has a variable potential.

sources with free diffusion, this is an inaccurate assumption, specially if the IEA is placed in the plasma away from the center axis (*r = 0*) of the plasma source. The radial component of the ion velocity may also be attained if the aperture in the top membrane is larger than the requisite number of Debye lengths. As explained before, the sheath then deforms, dipping the ion emitting plasma meniscus into the IEA and accelerating ions into the analyzer at various angles. The radially directed velocity of the ions is indicated by a broadening of the IEDF, and hence the IEA results must be taken as the upper bound for ion energy measurements.

Another problem that may exist in intense discharges with relatively high ion energies is that of secondary electron emission from the ion retardation grid and the collector plate due to the bombardment of high energy ions. As for Langmuir probes, secondary electrons cause quantitative errors in the actual amount of current that is collected. This may be corrected for to some extent by an additional grid to between the ion retardation grid and the collector plate. Biased negative to ward off electrons, this is known as the secondary electron suppressor grid. The subsequent potential drops across the grids with this new IEA are shown in Figure 3.9(b). As before, the ion retardation grid has a double arrow, implying a varying potential.

3.3.4 Data acquisition using the Ion Energy Analyzer

As with the SLP, two methods were used while collecting IEDFs and average ion energies also. Initial experiments were conducted with the Metrabyte boards and manual sampling of the lock-in amplifier's first harmonic signal once

this signal had stabilized. Following Hopwood, this circuit is shown in Figure 3.10. It must be noted that while the external circuit for using the IEA is more complicated than that of the SLP, there is no dependence of the AC signal amplitude on the variable DC bias. Hence data collection is relatively simpler, and less time consuming.

However, the GPIB control apparatus was again put to good use and a modified SLP program made the IEA system completely automated. Figure 3.11 shows the fully automated IEA measurement circuit, and as may be seen it is similar to the fully automatic EEDF measurement support circuitry of Figure 3.7. With no correction needed for the AC signal (as was needed for the EEDF measurements), the GW-BASIC control program was considerably less complicated, and as for the semi-automatic method mentioned above, the data acquisition for IEDFs was relatively faster. The data obtained with the fully automated GPIB controlled circuitry were consistent with the semi-automated manually sampled data. As in the case of EEDFs, several IEDFs were collected for any given set of experimental conditions to ensure repeatability. The average ion energies reported in this dissertation are therefore the average of the several values measured in the various runs. Figure 3.12 shows a typical set of IEDFs for the MPDR 5 (refer to Chapter Seven).

As in the case of the EEDF measurements, raw data collected using either the automated, or semi-automated method was then imported into another program (different for EEDFs from that for the IEDFs) that reduced the (dI/dV, V) characteristics to generate the ion energy distribution function, normalized it to one, and calculated the average ion energy.

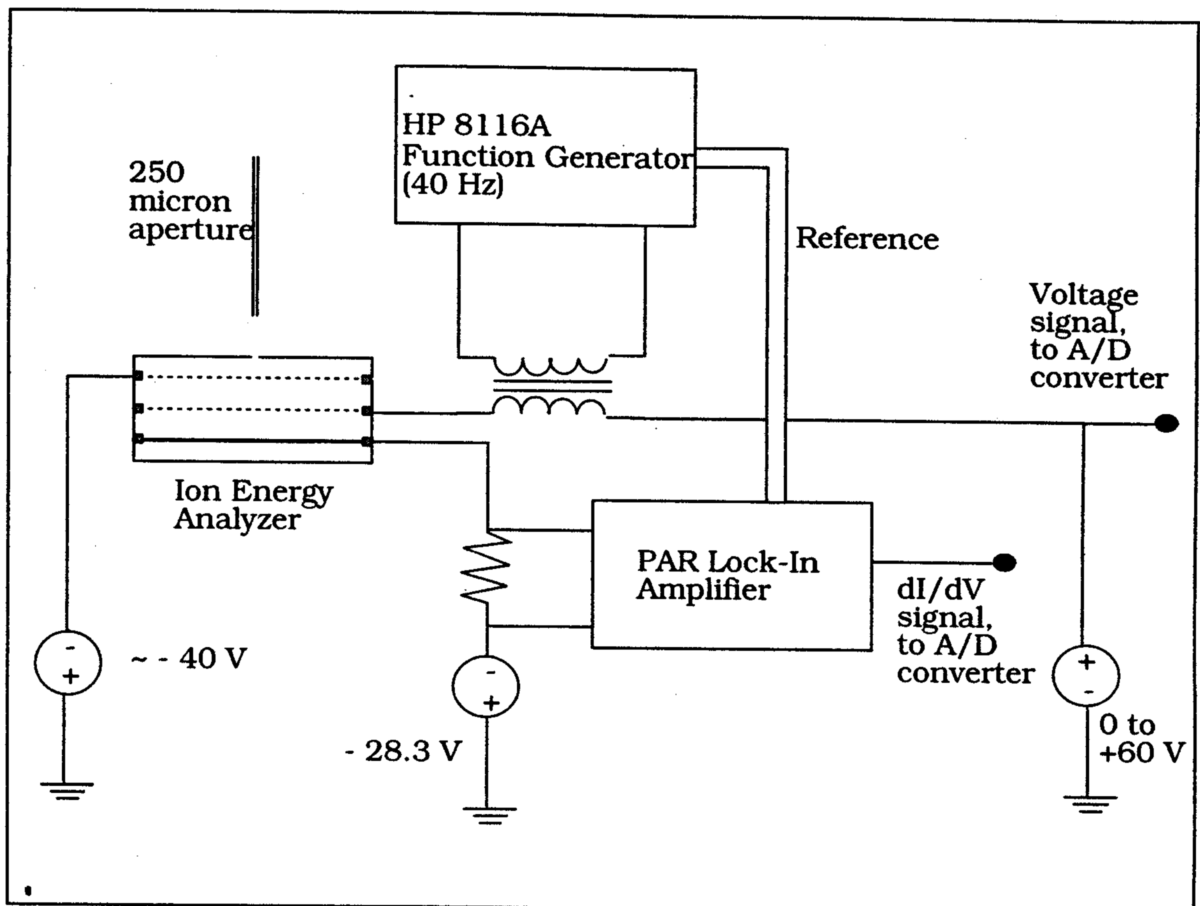

Figure 3.10 Ion Energy Analyzer measurement circuitry.
This is the "semi-automated" method of IEDF measurements, adapted from Hopwood [Hop-91, Hop-90a]

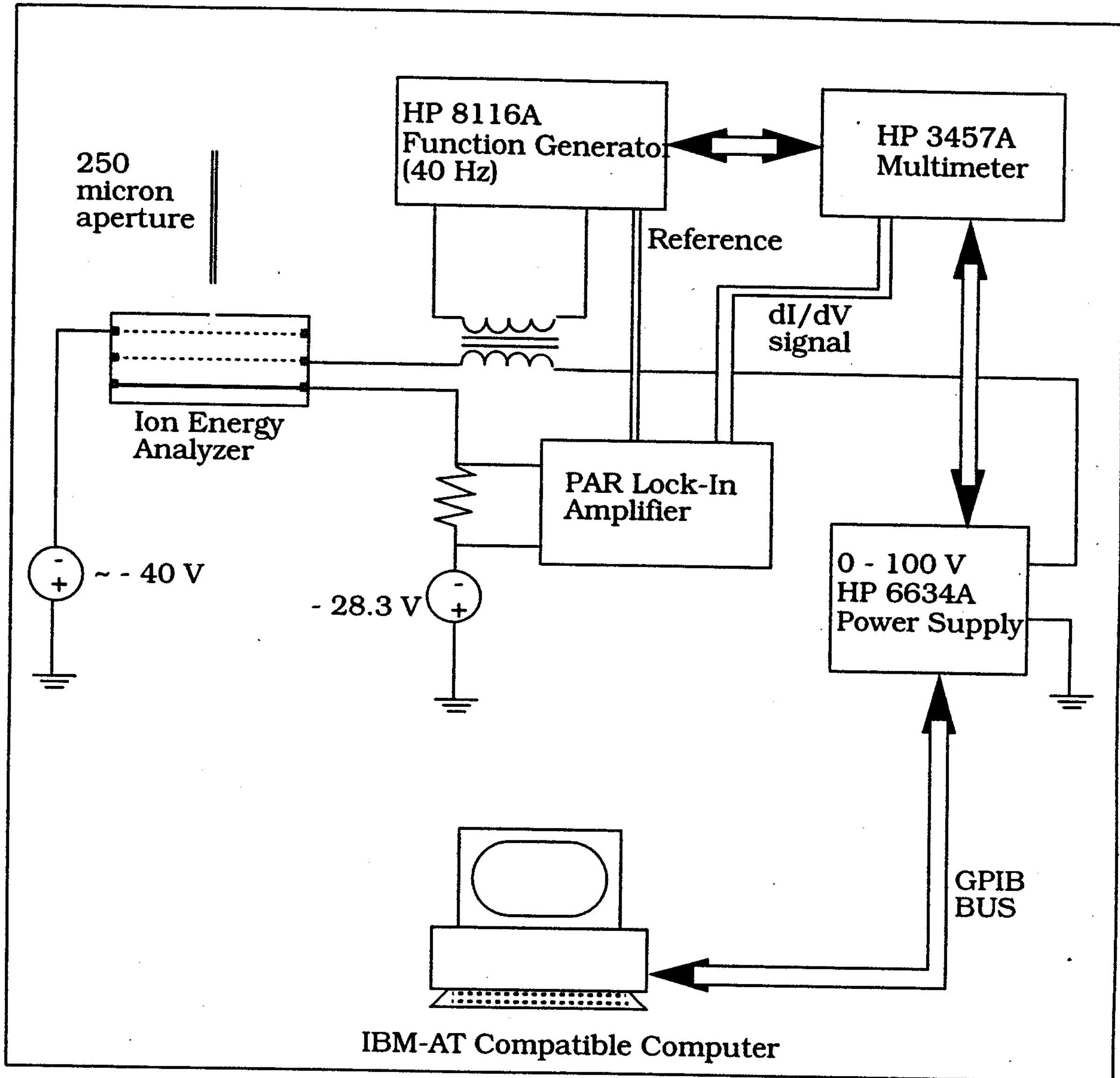

Figure 3.11 Fully automated GPIB controlled IEDF measurement technique. Note the resemblance to the EEDF measurement circuitry of Figure 3.7.

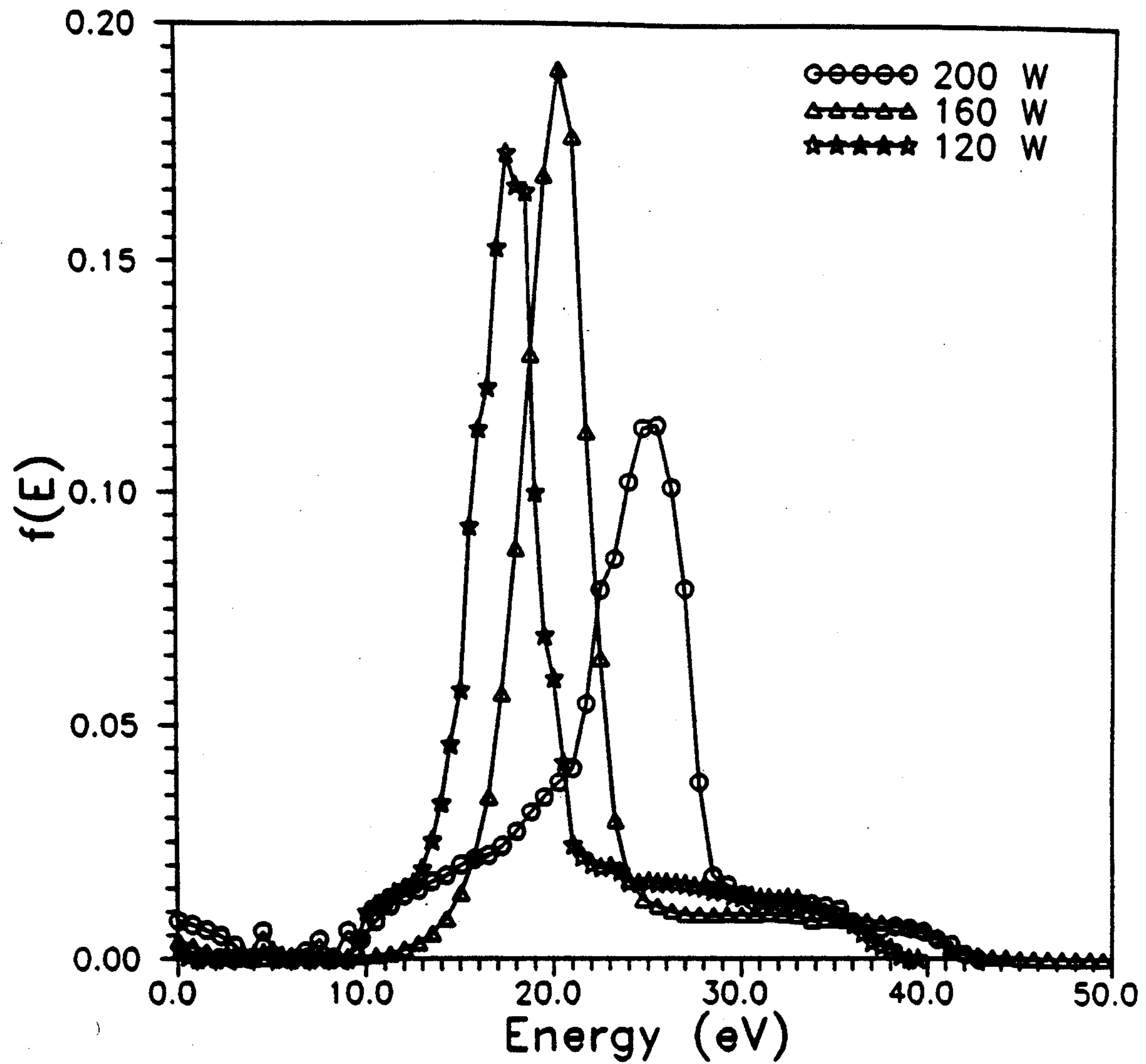

Figure 3.12 Typical IEDFs for the MPDR 5.
Data taken for an argon discharge at 1.2 mTorr, with the IEA positioned 5 cm downstream for various input powers. (Refer to Chapter Seven)

3.4 Energy Distributions - Proposal for a New Method

When Druyvesteyn measured the first electron energy distribution function, he graphically calculated the second derivative of a smooth I-V characteristics of the single Langmuir probe. This "Druyvesteyn" method to measure energy distribution functions that has been described in the sections above, and used throughout this dissertation, is based on indirectly measuring a voltage signal proportional to the second derivative (or the first derivative in the case of ion energy distribution functions) once a small AC signal is modulated over the DC probe (or IEA) bias. While the process is somewhat simplified by using the fully automated system described above (with the GPIB controlled apparatus), there is still some degree of chance involved, specially in sampling the lock-in amplifier signal - when has this signal stabilized enough to be considered a data point?

All this uncertainty, and the very need for the LIA may be done away with by reverting back to directly differentiating the I-V characteristics, but using numerical means rather than graphical. This unique method was tested as an auxiliary acquisition technique but due to time constraints, it was not completely analyzed under varied operating conditions and therefore never incorporated into the battery of characterization principles used during the research detailed in this dissertation. This method is proposed here with the hope that in the near future its applicability may be completely tested.

When an I-V characteristics of the SLP is measured, it becomes obvious why direct differentiation, even if done numerically, would produce erroneous EEDFs. Despite each probe current value being an average of 60 to 100 data

points taken by the computer at every bias voltage, there is some random error, and upon differentiation ($\Delta I/\Delta V$), this error is amplified further, becoming even larger for the second derivative in the case of electron energy distribution functions. It is therefore a practical impossibility to measure an I-V characteristics smooth enough for direct differentiation - this method suffers from successive error propagation.

The new method proposed here incorporates three requirements. First, a computer controlled power supply (like the one used in the GPIB controlled method described earlier) takes as smooth an I-V curve as possible. The frequency at which data are collected determines the ultimate resolution of the results, and a data point every 0.5 Volts is recommended. This I-V characteristics may either be that of the single Langmuir probe, or that of the ion energy analyzer. This I-V characteristics is then fed into a curve fitting program that statistically fits a smooth curve to the data - this fit does not have to pass through every data point. Such curve fitting programs exist in commercially available libraries like NAG, and it is recommended that a routine that fits an nth degree polynomial to the I-V characteristics be used. Note that it is this intermediate curve fitting step that is most crucial to this method of data acquisition, and prevents the errors from propagating. It was noticed during the test runs that the higher the degree (n), the better the computer was able to fit the curve to the data. Finally, when the nth degree polynomial to smoothly fit the measured I-V characteristics is realized, this polynomial may be differentiated any number of times with ease - hence the initial choice of a polynomial fit. It was observed that $n = 9$, or $n = 11$ provided the best fits - lower degrees of polynomials may also work for some cases.

This numerical method completely removes the necessity of the AC function generator (AC small signal), the lock-in amplifier, and most other peripheral circuitry required for energy distribution function measurements. Also there is no error incurred due to the sampling time discrepancy for the lock-in amplifier signal. A fully automated system that incorporates the raw data acquisition, curve fitting and differentiation routines may be set up with the aid of the appropriate computing and electronic support. However, before induction into the characterization techniques, a comprehensive evaluation of this method is required, at various plasma pressure/power/gas type conditions. Also, a comparison of the results obtained from this method, with the "semi-automated" or the fully automated GPIB controlled methods that have been used to date needs to be performed. However, there is no doubt that this new method heralds the next generation of energy measurement methodology, and will soon be incorporated as an alternate way to measure energy distributions.

3.5 Micro-coaxial Probe

Several types of MPDRs have been designed, and they all have one thing in common - they are, or may be operated as single mode microwave cavities. Power is coupled from the waveguide, or coaxial cable and into the plasma through this microwave cavity applicator. Inside the cavity, a single electromagnetic mode is excited, with the plasma acting as the major loss mechanism (small amounts of energy may also be lost to the non-perfectly conducting cavity walls, and also to the coupling apparatus - loop, probe, etc.). The design of these reactors aims at choosing the appropriate transverse

magnetic (TM), transverse electric (TE) or transverse electromagnetic (TEM) mode for the requisite application.

While the EM modes of a perfectly conducting, empty, and lossless cavity are well known and may be found in several references [Har-65, Ram-65], the presence of a plasma, or the brass walls that are not perfectly conducting may significantly alter these modes. Knowledge of the actual EM mode that is excited inside the cavity is therefore essential for understanding the complex dynamics of the cavity. This knowledge aids in further reactor modifications, or design of other reactors that have to satisfy the conditions of ECR that require that the impressed electric fields compliment the static magnetic fields for the power to couple to the electron gas. If the exact electric field structure inside the cavity is known, experimentation with the magnetic field design may lead to a B-field topology that maximizes the ECR "zones" for optimal power transfer. Also, valuable information on the power loss to the cavity walls and the reactor's coupling efficiency may be obtained through this electromagnetic mode data (see, for example Chapter Six). The relative electric field pattern, and the calibrated electric field strength (in kV/m) inside the microwave cavity can be measured using a semi-rigid micro-coaxial probe, and this diagnostic technique is now described.

3.5.1 Theory and Design of the Micro-coaxial Probes

The simplest way to measure the electric field strength inside the microwave cavity is to sample a small part of the electric fields existing within it [Hop-90b]. This is done by using a semi-rigid micro-coaxial probe inserted into

the side of the cavity through tiny holes (of a diameter such that the probe fits snugly into them, but the microwave power does not radiate out of them). The power collected by the micro-coaxial probe is then read on a standard HP 435A power meter. Since the power being siphoned into the micro-coax comes from the total power resonating inside the cavity, this process can be very invasive, and care needs to be taken to minimize the perturbation of the EM modes inside the cavity. This is ensured by using a micro-coax with a small inner conductor diameter, and a very shallow insertion into the cavity wall. The dimensions of the micro-coaxial cable that was used to construct the probes for this experiment are: inner conductor diameter = 0.6 mm, outer conductor diameter = 2.25 mm., with a Teflon™ dielectric.

Figure 3.13 shows the two different probe designs that were used during the course of these experiments - these are hereafter called the penetrating probe, and the flush probe. In the former, the outer conductor and the Teflon dielectric is peeled back to expose the inner conductor. This probe is then inserted into the small hole made in the cavity such that the inner conductor is penetrating into the cavity, with the outer conductor level with the inner wall of the cavity. As mentioned above, the diameter of the hole drilled in the wall is just large enough so that the probe is a snug fit in the hole, with good electrical contact between the outer conductor of the probe and the cavity wall. The insertion of the inner conductor into the cavity wall creates a monopole over a semi-infinite plane effect, which then samples a fraction of the radial power of electric field existing at that position in the cavity. If a series of holes are drilled in the wall of the microwave cavity, a relative electric field pattern may be measured.

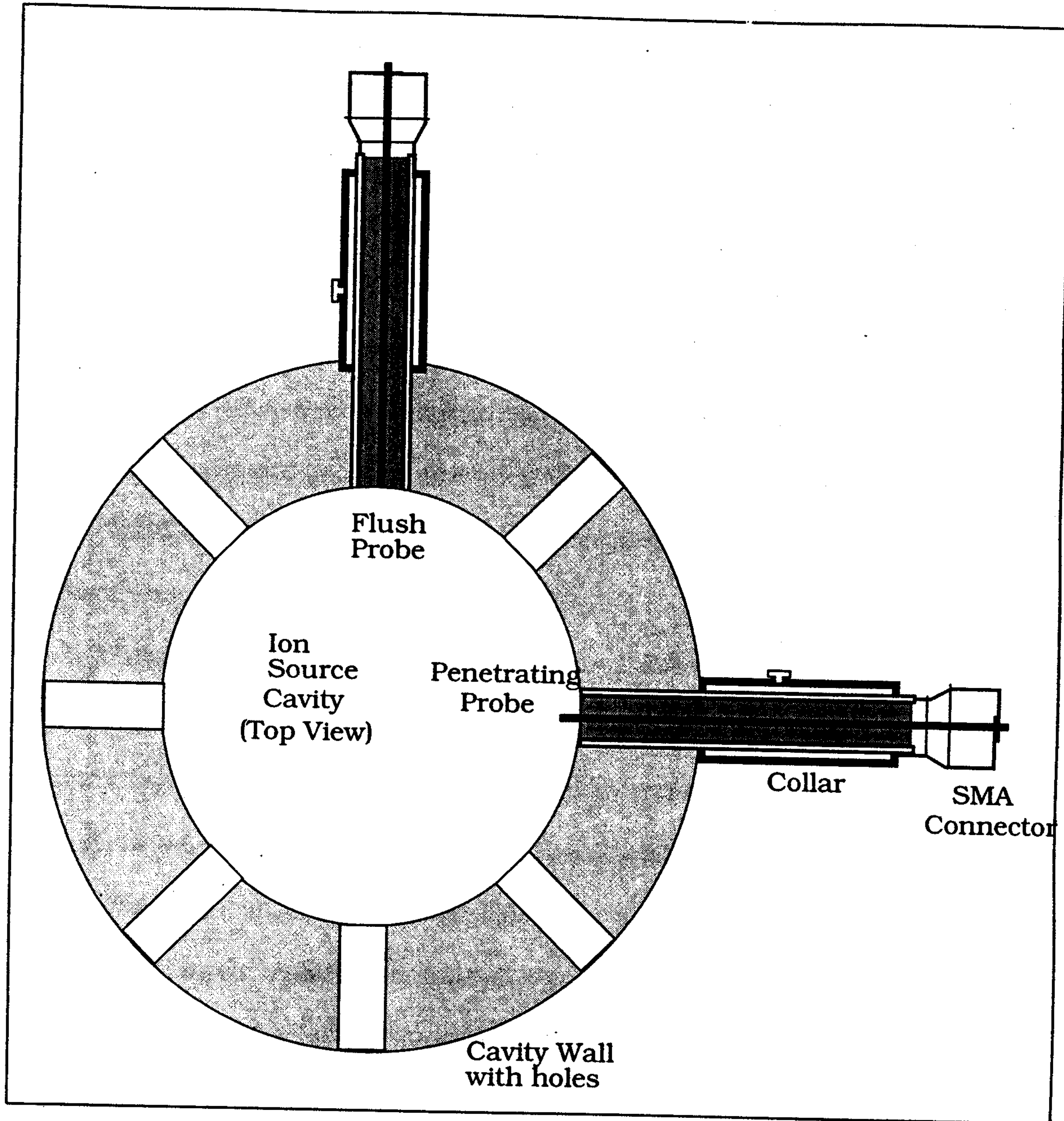

Figure 3.13 Design of the two micro-coaxial probes
These probes were used for measuring electric fields inside the microwave cavity. Note that the figure is not to scale.

For such a measurement however, it is *absolutely* imperative that the inner conductor protrude into the cavity the *exact same distance* for each hole to ensure an accurate relative measurement. This is because the power measured by the probe is extremely sensitive to the probe penetration depth inside the cavity. To make certain that the probe is inserted to the same depth at each hole, an adjustable collar is clamped on the outer conductor using a 4-40 screw. Once the desired penetration depth is set, this collar is secured firmly and this ensures that the probe penetration depth is constant throughout the experiment, assuming the cavity wall thickness remains constant. The penetration depth set for the probes used in Chapter Six was chosen to be 30/1000 of an inch (30 mils).

The penetrating probe of Figure 3.13 can only give a relative measurement of the radially directed electric field strength, which is proportional to the square root of the power measured by the probe. To calculate the absolute electric field strength, the power measurements need to be calibrated. This is done using the flush probe shown in Figure 3.13. For this probe, the inner conductor is not exposed, and the entire probe (inner conductor, Teflon dielectric and outer conductor) is inserted such that it are flush with the inner wall of the cavity. Then, the power measured by the probe is related to the electric field by [Bur-85]:

$$E_r = \left(\varepsilon_0 K_r \pi a^2 \omega\right)^{-1} \sqrt{2\frac{P}{Z_0}} \tag{3.24}$$

where, P is the measured power from the probe of Figure 3.12,

Z_0 is the coaxial probe's impedance (50 Ω),

ε_0 is the permittivity of free space,

a is the radius of the inner conductor of the coaxial probe,

ω is the microwave frequency (2.45 GHz), and

K_r = 3.846 - a constant (as indicated in Reference Bur-85).

During the experiments of Chapter Six, the penetrating probe was used to make the relative field pattern measurements inside the microwave cavity. Due to the penetration of the inner conductor, the signal to noise ratio of this probe was much better than the flush probe. Hence the data could be taken with greater accuracy. The flush probe measurement was then used to calibrate all the field data to give the exact radial electric field strength on the inner wall of the ion source involved in this study (on the 610-*a*). As will become apparent later in Chapter Six, there were in fact two penetrating probes that had to be built. This was because there were holes drilled through the magnet assembly of the 610-*a* also to allow for field measurement in the region where the magnets were present - known as the discharge region. It was imperative that the probe penetrating depth in this discharge region be the same as the depth elsewhere, and hence the necessity for the second penetrating probe. This will be discussed in greater detail later in Chapter Six.

3.5.2 Sources of Error with the Micro-coaxial Probes

As mentioned above, care must be taken to insert the penetrating probe only as far into the cavity as necessary. A deep insertion leads to a better signal to noise ratio since more power is captured by the micro-coax, but this may perturb the EM modes that are excited inside the resonating cavity to an extent

that would make the diagnostic tool prohibitively invasive and provide inaccurate field strength data. Also, the size of the probe insertion hole is crucial. A larger than necessary insertion hole could lead to several problems. First, the outer conductor of the probe must be in good electrical contact with the cavity walls. If the insertion hole is too large, the probe will not be snug and will move about inside the hole, making power measurements which are ambiguous and fluctuating, specially when measuring the relative field patterns. Second, the large hole may interrupt the surface currents flowing on the inner wall of the cavity to the extent that the cavity drops the EM mode that is being excited in it. Finally, a large hole may also lead to some microwave radiation specially when operating at high frequencies (low wavelengths) which is not only detrimental to health, but will also act as a secondary power loss mechanism.

3.6 Ion Beam Characterization

All characterization principles that have been discussed up to now assume that the quasi-neutral plasma diffuses freely out of the plasma source. However, as was observed in Chapter Two during the review of several compact sources, several of these sources have extraction grids attached to their output so that energetic ion beams may be extracted from them. This section briefly discusses some of the characterization techniques that are used to evaluate the properties of ion beams.

Once a plasma is ignited in the source, an ion beam may be extracted by using biased grids (or electrodes) that selectively impart a directed velocity (and hence energy) to the ions while retarding electrons. Several applications, like

high energy ion implantation or ion beam injection into particle accelerators, utilize these energetic ion beams. When discussing plasma/ion beam sources therefore, knowledge of ion beam technology is essential. One of the plasma sources studied during the research for this dissertation work (the MPDR 610) was also used as an ion beam source at the National Superconducting Cyclotron Laboratory (NSCL), as will be discussed in Chapters Eight and Nine. The diagnostic methods that were used at the NSCL to characterize the 610 ion beam are now discussed.

3.6.1 Charge State Distribution of the Ion Beam

It is important to know the exact charge state distribution (CSD) of the ion beam, specially for ion beam sources that generate multiply charged ions. This distribution plots a spectrum of the total particle current for each charge state as a function of the charge to mass ratio (Q/M), and hence can give a precise quantitative assessment on the ability of the ion source to produce the desired charge state. The CSD is obtained by bending the ion beam through a 90° analysis magnet, as shown in Figure 3.14. For a specific magnetic field strength that is perpendicular to the velocity of the charged particle, the degree of bending force created by the analysis magnet is specified by the Lorentz force equation: $\boldsymbol{F} = q(\boldsymbol{V} \, X \, \boldsymbol{B})$. This force is directly proportional to the charge state of the ion. Hence, a higher charge state will bend farther than a lower charge state in a give static magnetic field.

To obtain the CSD, the ion beam with all its extracted charge states is allowed to pass through the 90° bending magnet as the current through the coil

is ramped up. A Faraday cup is placed a few meters away at the focus of the ion optics. The Lorentz force selectively chooses the appropriate charge state to strike the Faraday cup. All other charge states are either bent too much, or not enough, and they strike the beam pipe. This is shown in Figure 3.14. A typical CSD of the multiple charge state producing Superconducting ECR (SCECR) ion source at the NSCL is shown in Figure 3.15 [Har-94]. The spectrum is that of a krypton-86 run, with oxygen used as the ballast gas (for super gas-mixing). It clearly indicates the amount of current at each peak, where the peaks represent some ionized species present in the ion beam. For example, the current for Kr^{19+} (at Q/M of about 4.5) is seen to be about 30 particle micro-amps (eμA). As can be seen, the exact current of each Q/M species (charge state) may be read and compared to other charge states.

An obvious advantage of the 90° bending magnet is that by setting the bending magnet's current to a specific value the researcher may choose any charge state from all the states that populate the initially extracted ion beam, while rejecting the other states. Only one charge state will then propagate beyond the Faraday cup (once the cup is removed from the beam line).

3.6.2 Emittance of the Ion Beam

The emittance diagram of an ion source gives an indication of the spatial distribution of the beam as it travels through a beamline. It is a measure of the beam volume in a six dimensional phase space defined by x, y, z, p_x, p_y, p_z, where the last three parameters are the three components of the momenta. For a beam travelling in the z direction, the phase volume characterizing the beam is

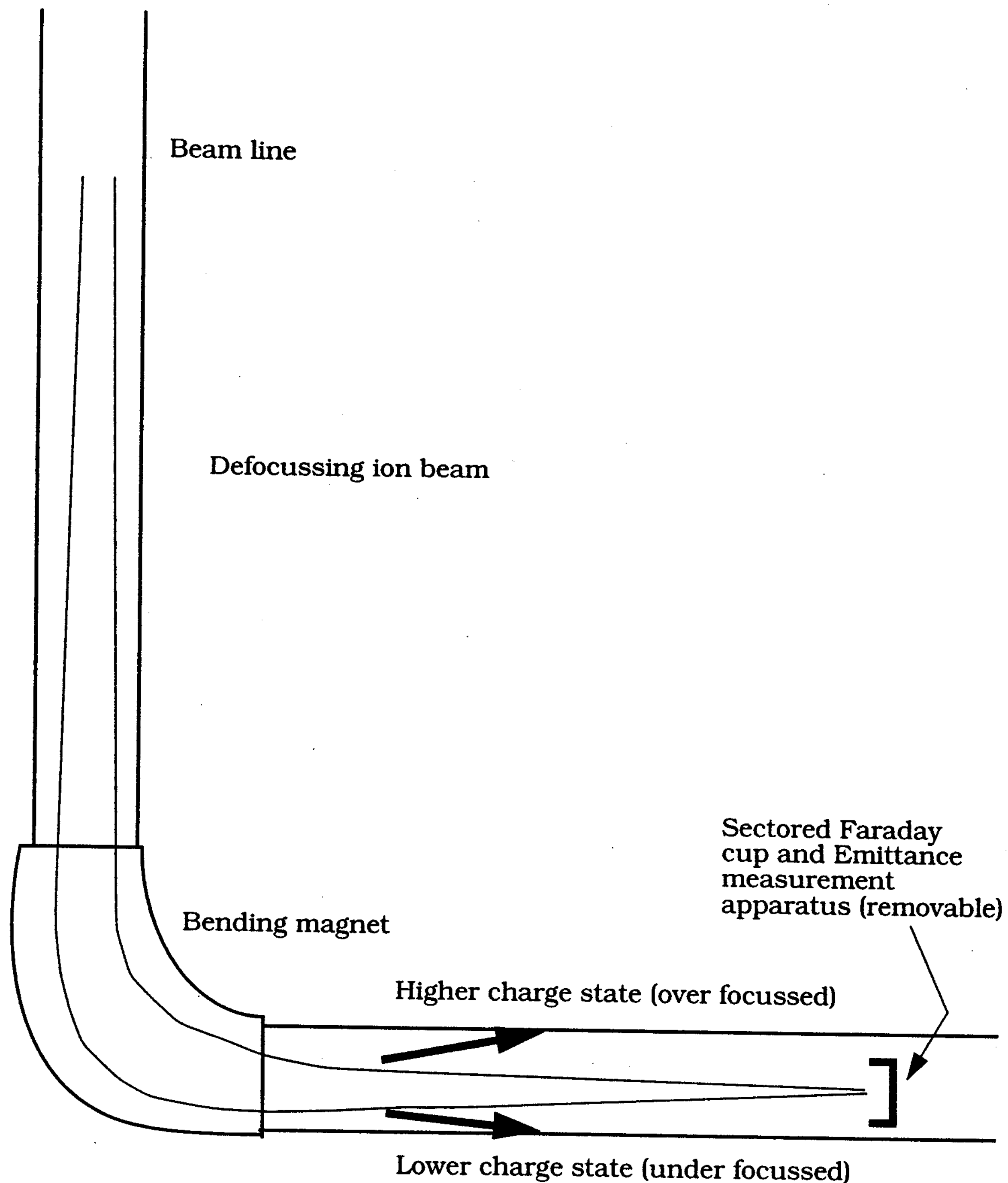

Figure 3.14 Charge state distribution measurement.
Beamline for an extracted ion beam, with a 90° analysis magnet and a removable sectored Faraday cup. Note that at a specific field strength of the analysis magnet, higher charge states are over focussed, and lower charge states are under focussed.

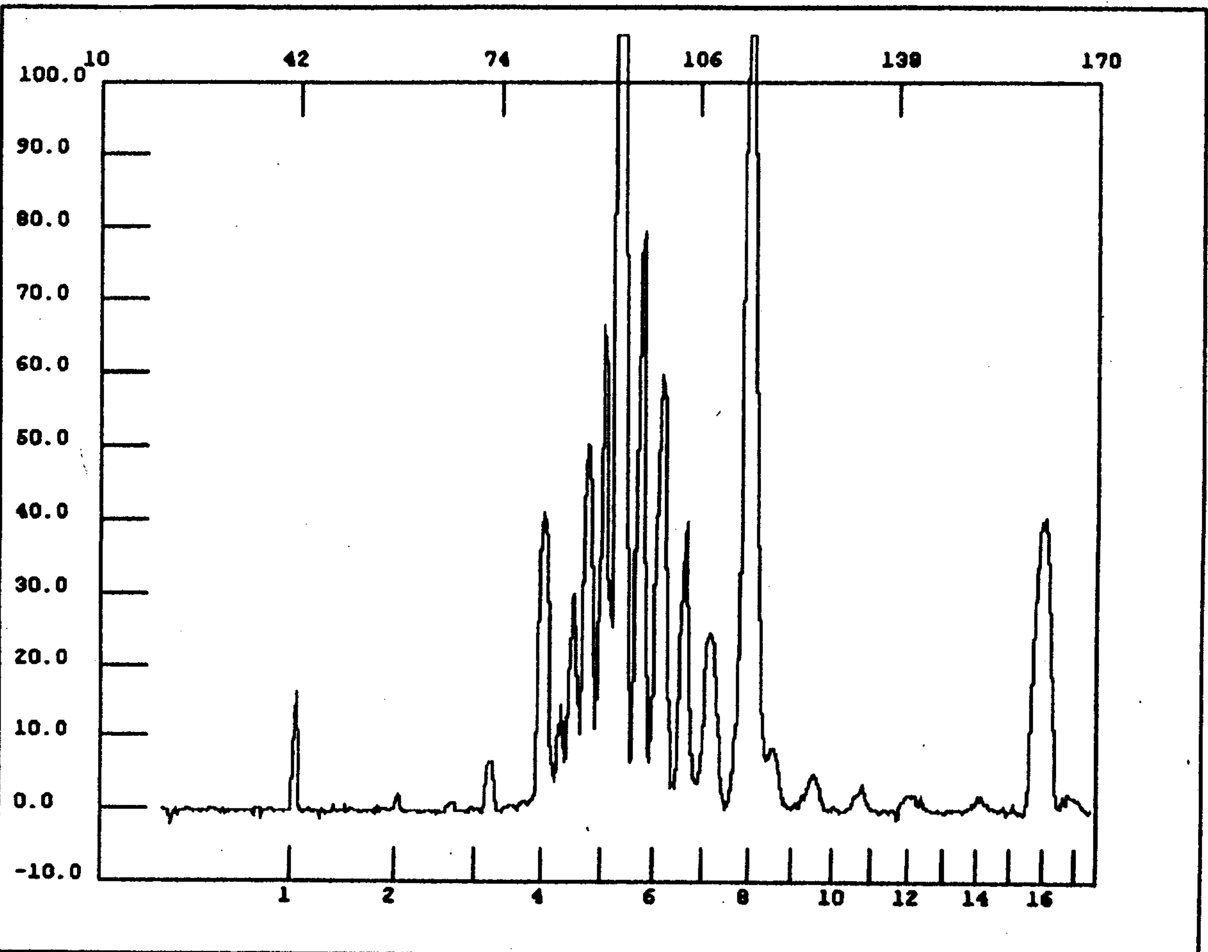

Figure 3.15 A typical charge state distribution of the SCECR at the NSCL.
The source is producing multiply charged states of krypton 86, with oxygen as the ballast gas. Note that the Kr^{19+} beam has 30 particle micro-amps of current.

given by the coordinates x, y, p_x, p_y. This phase volume is the emittance of the beam, and is usually measured in millimeter-milliradians (mm-mrad). In the case of cylindrical symmetry, the emittance may be further simplified and written terms of a 2-dimensional phase space with parameters r, p_r such that $p_r = p_z\alpha$ where α is the half angle of divergence of the ion beam from an axially parallel beam line. Note that a critical factor in beam divergence is that of space charge - the Coulombic radial force on the energetic ions that tends to make the beam diverge. Emittance data can provide information on the space charge effects that the beam is experiencing. For example, if by increasing the extraction bias, the emittance goes down, it may be because of an increase in the ratio of directed velocity to the radial velocity that the energetic ions experience due to space charge effects.

The exact derivation of the emittance formula is very complicated requiring knowledge of Hamiltonian mechanics, canonical momenta, etc., and need not be discussed here. Several references for the various emittance definitions and measurement techniques, and also for the derivation of the emittance formula may be cited for further study [Lej-80, Ste-67, Val-77, Kel-89, Wan-91].

Following Valyi [Val-77], the normalized beam has an ellipsoidal phase space, with its emittance given by: $\varepsilon = r\alpha\sqrt{2meV}$ (in mm-mRad). This equation takes into account the relativistic effects on a fast moving beam. It is to be noted that the net phase volume of the beam that comprises the emittance is not affected by any electric or magnetic fields, even if the beam diverges - emittance is a conserved quantity. Hence it is a useful beam parameter to evaluate the beam's characteristics, and also the extraction optics of the ion source. If the

area on the emittance plot of the beam is larger than the acceptance area of the beam pipe, the beam will diverge, and cannot be transported without substantial losses. Measuring emittance can therefore give an indication of the ion-optical system through which the beam of specific charge state is to be transported. Conversely, emittance data may also provide information on how certain charge states, with specific space charge forces would react to the beam optics.

Another widely used parameter to characterize the beam is its brightness. Defined as the ratio of the particle current (beam current divided by the particle charge) I, and the square of the radial emittance ε_r:

$$B = 2\frac{I}{\pi^2 \varepsilon_r^2} \tag{3.25}$$

The larger the brightness of the beam, the more focussed it is and the better it may be transported through the ion optics.

3.6.3 Emittance Measurement Techniques

Several methods exist for measuring the emittance of a beam, the principle of each method being to evaluate the angular deflection of the elementary fractions of the ion beam that have been created using appropriate slits, or a diaphragm with holes. Two such methods are briefly touched on here - the static, and the dynamic detection schemes. Both schemes require the beam to be broken up into tiny beamlets. The static system requires an image of the beamlets some known distance away from the slits (or apertures) - usually several centimeters. This image may be captured by burning a Kapton film, or

on a photographic paper, or even on vacuum grease. The divergence of each beamlet displayed on the image is then studied as a function of the distance separating the slits from the image capture device, and this gives an indication of the emittance of the total beam.

The dynamic method of emittance measurement also involves breaking up the beam into small beamlets, normally by using slits, or gridded diaphragms. A very thin conducting wire (a few mm diameter) is then swept in front of the beamlets measuring the currents of individual beamlets. The broadening of the beamlets as indicated by the ion current peaks then gives an indication of the beam's emittance. As shown in Figure 3.16, by measuring the beamlet's width at the base, and also the distance it travelled from source (the slits), the divergence angle of the beam may be determined, and the emittance then calculated from a phase space plot. Figure 3.17 shows a typical emittance diagram of the SCECR + 610 (see Chapter Eight) taken with the wire scanner method. A similar set of (r, α) measurements may be taken using the static method also, with the Kapton burns.

As may be seen in this figure (bottom sketch), the emittance diagram is generally elliptical. A gross classification of the ion beam may be made based on the shape of the emittance pattern [Kel-89]. If the pattern extends from the third to the first quadrant, the beam is generally divergent. If, on the other hand, it extends from the second to the fourth quadrant, the beam is generally convergent (see Figure 3.5, Reference Kel-89.). Indeed, as the beam travels through the beam pipe, initially focussing to its "minimum skirt," and then defocussing, the emittance ellipse rotates in phase space. However, as mentioned earlier, it is a conserved quantity, and so the total area enclosed by

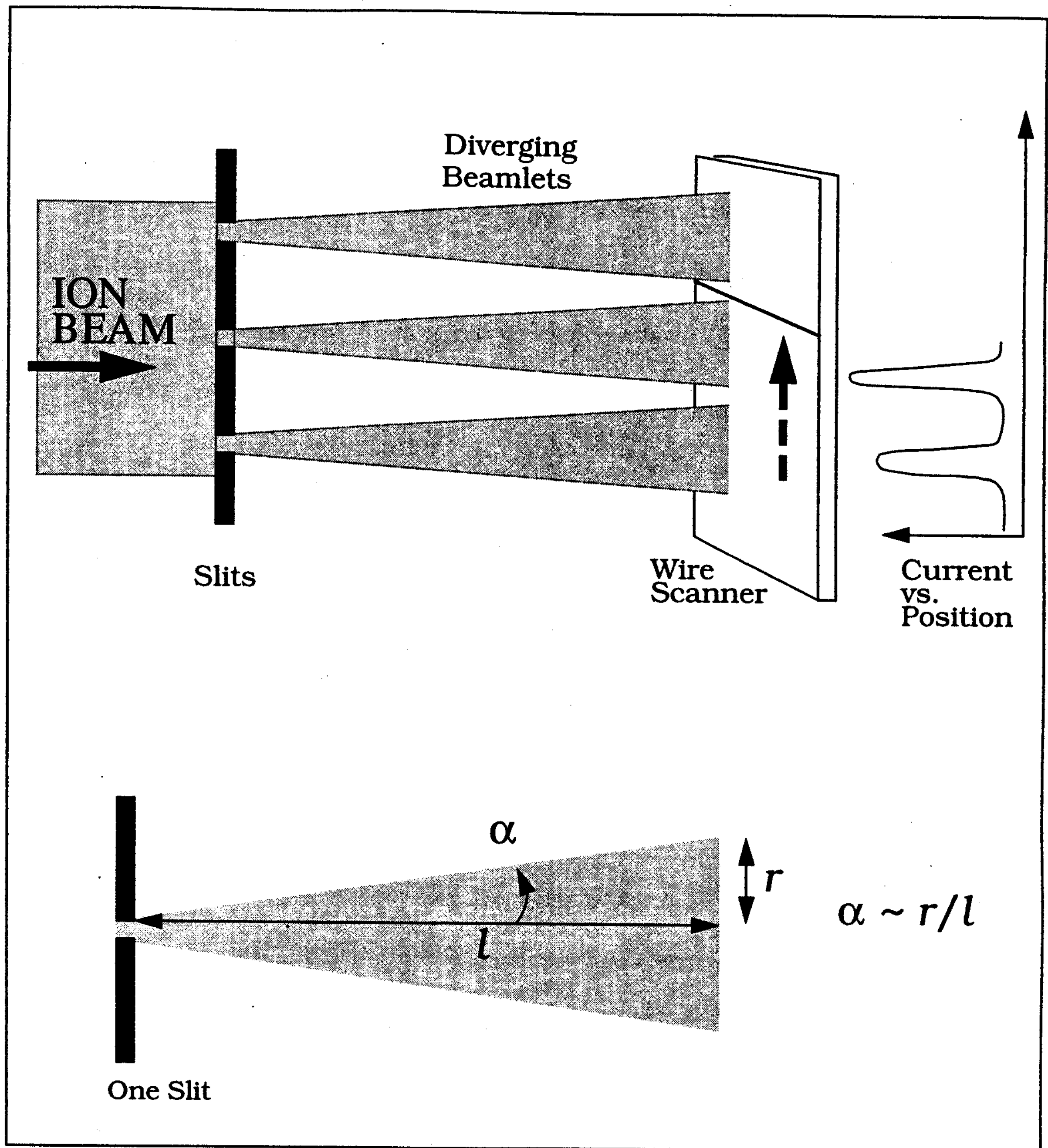

Figure 3.16 The dynamic emittance measurement technique
This method uses a wire scanner. Top sketch shows how wire is scanned across the beamlets, and the current vs. position plot acquired. Bottom sketch isolates one beamlet, and indicates the divergence half angle $\alpha \sim r/l$

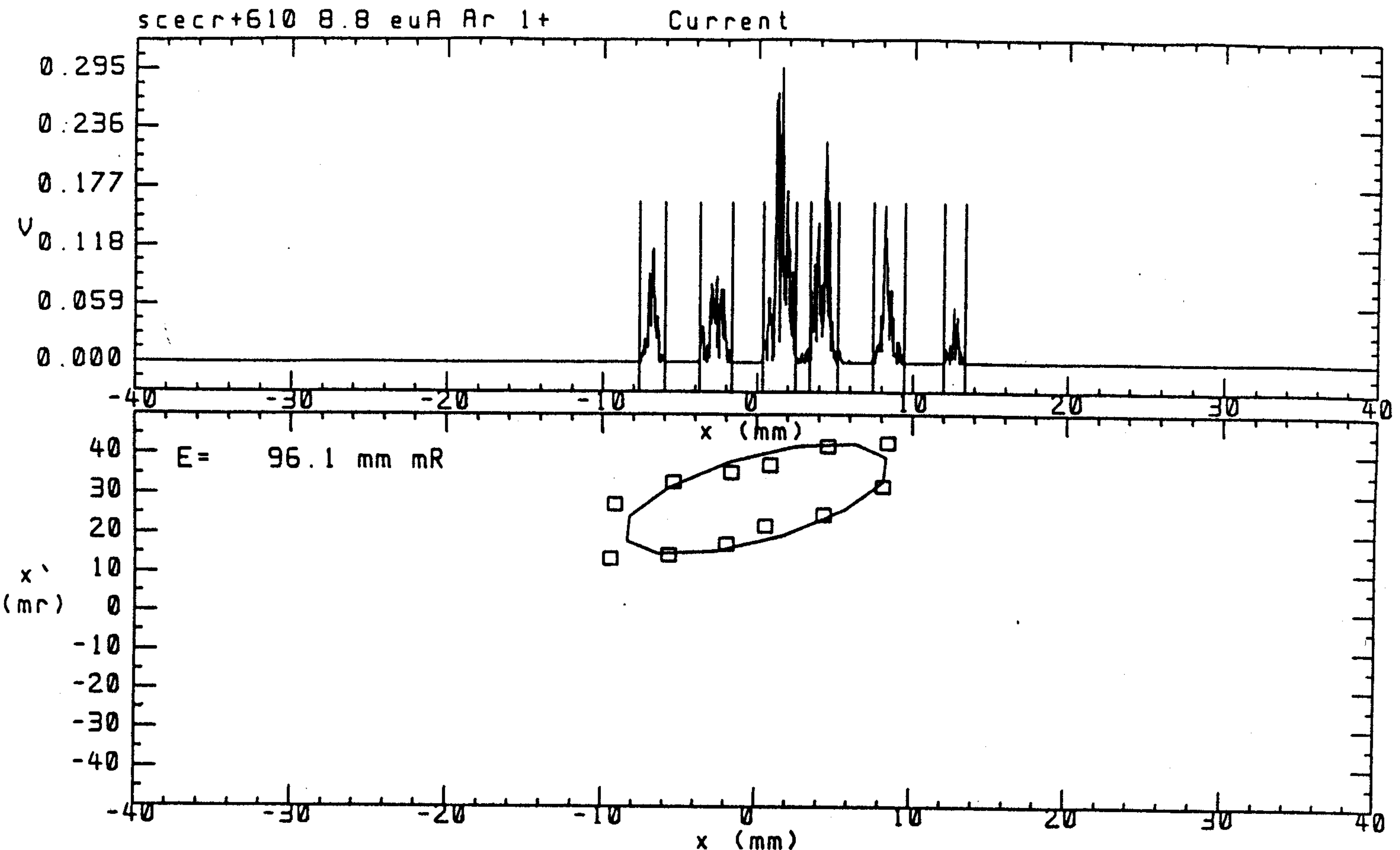

Figure 3.17 Typical emittance diagram of the SCECR+610.
The wire scanner method was used to obtain the relative currents of each beamlet, and the emittance calculated from this information. (Refer to Chapter Six.)

the ellipse does not change with the focussing-defocussing effects on the beam.

A very important aspect in ion beam characterization is the numerical simulation and modelling of the beam. Several codes exist to perform this simulation (like the BEAM3D developed at the NSCL, and PARMILA, among others). Most codes numerically solve the coupled Poisson-Vlasov equations for ions extracted from a plasma with an equilibrium electron density and for a give charge state distribution. Use of these codes can greatly simplify the design of the ion-optical system for beam transport. When used in conjunction with POISSON, and/or PANDIRA - codes that numerically simulate the magnetic fields, source specific extraction systems can be developed and tested on the computer before expensive models are constructed.

Both the static and dynamic systems were used to study the emittance of the MPDR 610 when it was used as an ion beam source. For the static case, the "pepper pot" method was employed where the beamlet image was captured on a Kapton film after the beam was allowed to pass through the tiny holes in a stainless steel membrane. The dynamic method, whose results are presented in later chapters, was utilized when the 610 was mounted on the beam line of the SCECR (see Chapters Eight and Nine).

3.7 Concluding Remarks

There are several characterization techniques mentioned in this chapter, and all were used to varying degrees for the performance evaluation of the four major ECR ion sources studied in the last five years. Characterization work is never complete, however - there is always more to learn, and techniques other

than those reviewed in this chapter were also attempted. Laser induced fluorescence (LIF) is an example, a complicated technique that was tested on the MPDR 610. For several reasons, the experiments were unsuccessful, and hence no further mention of this method is made in this dissertation. Optical emission spectroscopy (OES) was also used on a nitrogen plasma, but ambiguous results due to the enormous number of emission lines curtailed further experimentation with OES. A more concentrated effort for both LIF and OES needs to be made in the near future.

Other than LIF, several other characterization techniques may be used to further enhance the understanding of the ECR ion sources evaluated here. For example, quartz crystal microbalance (QCM) for measuring the reactive radical species (oxygen and hydrogen) concentration, Fabry-Perot interferometry for an accurate measurement of neutral species temperature, X-Ray analysis using a pin hole camera to further determine the exact location of ECR excitation, and energetic species bombardment on the plasma source walls. It is expected that as performance evaluation of the MPDR 610 and the MPDR 5 is carried further, some or all of the above recommended experiments will be conducted and the results then linked to those obtained using the techniques of this dissertation, ultimately leading to a better understanding of the sources.

Chapter 4

Evaluation: The MPDR 610 at 2.45 GHz.

4.1 Introduction

4.2 Description of the Plasma Source - the "MPDR 610"

4.3 Description of the Vacuum System - the "Yorktown T"

4.4 Description of the Microwave Apparatus

4.5 Discharge Ignition in the 610

4.6 Operational Performance of the 610 - ARGON

4.6.1 Argon Density Analysis

4.6.2 Argon Electron and Ion Energy Analysis

4.6.3 Comparison of Measured Data with Theoretical Predictions

4.6.4 Discussion of Theoretical and Measured Data

4.7 Operational Performance of the 610 - NITROGEN

4.7.1 Nitrogen Electron Energy Analysis

4.7.2 Nitrogen Ion Energy Analysis

4.7.3 A Summary of the Anomalies of a Nitrogen Discharge

4.8 Operational Performance of the 610 - HELIUM

4.9 Concluding Remarks